Tomas Bata University in Zlín
Faculty of Applied Informatics
Department of Electronics and Measurements

Ing. Jiří Pálka

Doctoral Thesis

EVALUATION OF THERMAL COMFORT OF A MAN ACCORDING TO PMV MATHEMATICAL MODEL

Study branch: Technical Cybernetics

Supervisor: Doc. Ing. František Hruška, Ph.D.

Consultant: Doc. RNDr. Vojtěch Křesálek, CSc.

Zlín, Czech Republic, 2011

ACKNOWLEDGEMENTS

I wish to thank to professors, assoc. professors and other colleagues at Tomas Bata University in Zlín who helped me with the completion of this thesis.

Namely I would like to thank to Assoc. Prof. František Hruška, my advisor, for the help and long-term guiding. I also appreciate the support and ideas provided by Assoc. Prof. Vojtěch Křesálek.

My special thanks belong to my colleague and friend Milan Navrátil, Ph. D., who revised my English and mainly for professional and mental support, without which I would have never finished this work.

Finally, I want to thank to my family, especially my wife for her understandings during my last busy times. Completely at the end I apologize to my 1 year old boy for not being with him as he needed and I wanted.

SUMMARY

This doctoral thesis deals with evaluation of thermal comfort of a man according to PMV mathematical model given by ISO 7730 and ASHRAE 55 standards. The thesis summarizes theoretical knowledge concerning thermal comfort and related themes.

At the beginning of the work, the problems concerning mean radiant temperature (MRT), which is the most difficult determinable factor, are solved. The thesis deals with integration of surface temperature of whole space and tries to eliminate problems arisen from MRT measurement on spherical surface. There are used Matlab simulations in this part.

Within this work, the PMV model was modified in order to provide more accurate results and be simpler applicable.

Further in experimental part, a software tool for PMV, PPD, DR indices assessment and also a tool computing these parameters in simplified model representing real room with corresponding problems are prepared.

Another important part of this work is optimizing of economic costs, energy saving and emission reduction with SOMA evolutionary algorithm.

The results of thesis led to design two thermal comfort evaluation systems – the laboratory and embedded version. At the end, the results of this work are discussed and suggestions for further research in this filed are given.

RESUMÉ

Tato doktorská práce se zabývá vyhodnocováním tepelné pohody člověka podle matematického modelu PMV, který je dán standardy ISO 7730 a ASHREAE 55. Disertační práce obsahuje souhrn teoretických znalostí týkající se tepelné pohody a s ní spojených témat.

V úvodní části je řešena problematika měření střední radiační teploty (SRT), která představuje největší problém při vyhodnocování ukazatelů tepelné pohody. Práce se zabývá integrací povrchové teploty celého prostoru a snahou je odstranit problémy vznikající při měření SRT na kulové ploše. V této části řešení jsou využity simulace v prostředí Matlab s využitím všech předností, včetně grafických.

V rámci této práce byl model PMV modifikován tak, aby poskytoval přesnější výsledky a byl jednodušeji aplikovatelný.

Dále v experimentální části byl připraven softwarový nástroj pro vyhodnocování ukazatelů PMV, PPD a DR a nástroj počítající tyto ukazatele ve zjednodušeném modelu odpovídající reálné místnosti a s tím souvisejících problémů.

Další významnou částí této práce je optimalizace, resp. hledání extrému ekonomických nákladů, úspory energie a snížení emisí a to pomocí evolučního algoritmu SOMA.

Výsledky disertační práce vyúsťují v návrh dvou typů vyhodnocovacích systémů tepelné pohody – laboratorní verze a embedded verze. V závěru jsou zhodnoceny výsledky této práce a jsou dány návrhy na další pokračování v tomto výzkumu.

CONTENTS

LIST OF FIGURES

LIST OF TABLES

LIST OF SYMBOLS

$\dot{V}$	dm^3s^{-1}	air breathing rate
F_{oi}	-	fraction of oxygen in the inhaled air
F_{oe}	-	fraction of oxygen in the exhaled air
α	-	absorptivity
β	deg	flat angle (declination)
ε	-	emissivity of surface
φ	-	view factor
ρ	-	reflectivity
σ	$Wm^{-2}K^{-4}$	Stefan Boltzmann constant for black radiation, $\sigma=5.6693\times10^{-8}\ Wm^{-2}K^{-4}$
τ	-	transmissivity
λ	m	wavelength
ω	sr	solid angle
v_r	ms^{-1}	relative velocity of the air
ε_β	-	directional emissivity of surface in direction determined by angle β
ρ_b	-	perfectly black reflectivity
ΔS	W	change of thermal capacity
A	m^2	surface area
a	$Jm^{-3}K^{-4}$	universal radiation constant, $a=7.764\times10^{-16}\ Jm^{-3}K^{-4}$
A_β	m^2	equivalent surface
A_D	m^2	surface of human body according Dubois equation
A_r	m^2	surface of the human body participating on radiant heat transfer
A_{TP}	-	gain of operational amplifier
c	ms^{-1}	speed of propagation of electromagnetic waves

C	W	convection heat flux
c_0	ms^{-1}	speed of propagation of electromagnetic waves in vacuum $c_0=2.9979\times10^{8}\ ms^{-1}$
c_1	Wm^2	the first Planck's constant, $c_1=3.74\times10^{-16}\ Wm^2$
c_2	mK	the second Planck's constant, $c_2=1.4388\times10^{-2}\ mK$
c_3	mK	the third Planck's constant, $c_3=2.8976\times10^{-3}\ mK$
c_4	$Wm^{-3}K^{-5}$	the fourth Planck's constant, $c_4=1.2866\times10^{-5}\ Wm^{-3}K^{-5}$
CLO	clo	thermal insulation of clothing [m^2KW]
D	m	diameter of black-globe thermometer
E	Wm^{-2}	evaporative heat loss
e_λ	Wm^{-3}	monochromatic emission density
E_{AB}	V	called the relative Seebeck emf
E_d	W	thermal loss via skin diffusion
e_g	-	emissivity of the black globe
E_{sw}	Wm^{-2}	heat loss via sweating
f_{cl}	-	ratio of the body surface covered
f_{pcl}	-	coefficient of moisture vapour transmission
$F_{p\text{-}N}$	-	angle factor between a person and surface
G	Vm^2W^{-1}	thermopile sensor constant
h	Js	Planck's constant, $h=6.625\times10^{-34}Js$
h_c	$Wm^{-2}K^{-1}$	coefficient of heat transfer via convection
h_{cg}	$Wm^{-2}K^{-1}$	coefficient of heat transfer by convection at the level of the globe
h_e	$Wm^{-2}Pa^{-1}$	coefficient of heat transfer at sweat evaporation
i	$Wm^{-2}sr^{-1}$	directional radiation intensity
J	W	radiosity
j	Wm^{-2}	radiosity density
k	JK^{-1}	Boltzmann constant, $k=1.3805\times10^{-23}JK^{-1}$

K	W	conduction heat flux
K	VW^{-1}	instrument sensitivity
L	W	heat balance of human with surroundings
LR	$°CkPa^{-1}$	Lewis ratio for common interior parameters
L_{res}	W	latent thermal loss via breathing
M	W	energy from metabolism
m	kg	weight of human body
MET	met	metabolic rate [met = $58Wm^2$]
n	-	refraction index
p_a	Pa	ambient water vapour pressure
P_b	Wm^{-2}	heat supply to the black sensor at two-sphere radiometer
PD	%	percentage dissatisfied
PMV	-	predicted mean vote index
P_p	Wm^{-2}	heat supply to the polished sensor at two-sphere radiometer
PPD	%	predicted percentage dissatisfied
p_{wa}	Pa	partial pressure of water vapour in the air
p_{ws}	Pa	partial pressure of saturated water vapour at skin temp
q_c	Wm^{-2}	heat exchange by convection between the air and the globe thermometer
q_r	Wm^{-2}	heat exchange by radiation between the walls of the enclosure and the globe thermometer
R	W	radiant heat flux
RH	%	relative humidity
R_i	m^2KW^{-1}	heat transfer coefficient
R_o	m^2KW^{-1}	construction heat resistence
S_{AB}	V/K	Seebeck coefficient
S_{PS}	m^2	surface of heating panel
S_{res}	W	thermal loss via breathing

S_s	m^2	sensitive area of sensor
T	K	absolute temperature
t_a	°C	interior air temperature, ambient air temperature
t_{cl}	°C	temperature of the clothing
T_g	K	temperature of the black globe
T_n	K	temperature of the net radiometer
t_{op}	°C	operative temperature
T_{pr}	K	plane radiant temperature
t_{psi}	°C	temperature of i-th heating panel surface
t_r	°C	mean radiant temperature
T_s	K	sensor temperature
T_u	%	local turbulence intensity
v_a	ms^{-1}	air velocity at the level of the globe thermometer
$v_{a,l}$	ms^{-1}	local mean air velocity
v_r	ms^{-1}	relative air velocity
W	W	mechanical work
WME	met	external work
$\Delta t_{a,v}$	°C	vertical air temperature difference between head and feet
Δt_{pr}	°C	radiant temperature asymmetry
η	-	efficiency of heating panel
Φ_e	W	radiant flux

LIST OF ABBREVIATIONS

ADC	Analog to Digital Converter
ADI	Analog/Digital Interface
ASC	Absolute Seebeck Coefficients
ASHRAE	American Society of Heating, Refrigerating and Air Conditioning Engineers
CMRR	Common-mode rejection ratio
DAC	Digital to Analog Converter
DR	Drought Rating
EA	Evolutionary algorithm
FOV	Field of View
GA	Genetic algorithm
GPIB	General Purpose Interface Bus
I^2C	Inter-Integrated Circuit
IO	Input/Output devices
IR	Infrared
ISO	International Organization for Standardization
LCD	Liquid Crystal Display
MRT	Mean Radiant Temperature
PD	Percentage dissatisfied
PGA	Programmable Gain Amplifier
PMV	Predicted Mean Vote
PPD	Predicted Percentage of Dissatisfied
RSE	Relative Seebeck emf
RTD	Resistance temperature detector
SOMA	Self-Organizing Migrating Algorithm

SPI	Serial Peripherial Interface
UART	Universal Aasynchronous Receiver/Transmitter
USB	Universal Serial Bus
WBGT	Wet Bulb Globe Temperature

1 INTRODUCTION

Thermal comfort describes a psychological person's state of mind concerning thermal sensation in given environment and is usually referred to terms of whether someone is feeling comfortably, hot or cold. This definition is easy to understand; on the other hand, it is difficult to express it in physical parameters because thermal comfort if a function of many parameters and not only the obvious one, the air temperature.The general approach in thermal comfort determination is based on thermoregulation of human body and heat balance with surroundings. Based on this approach, during the last century, there were developed dozens of models rating heat stress and strain of humans in given environment (the list of available models is also presented in Appendix A of this thesis). Out of these models and research works, the PMV-PPD model from (Fanger, 1970) has been most widely used. Also, the international organzations ASHRAE (American Society of Heating, Refrigerating and Air-Conditioning Engineers) and ISO (International Organization for Standardization) has adopted the PMV-PPD model in their standards ISO EN 7730 and ASHRAE 55 respectively. Both standards define thermal comfort as „the condition of mind which expresses satisfaction with the thermal environment and is assessed by subjective evaluation".

As mentioned before, the determination of thermal comfort is quite difficult because the evaluation takes into account various environmental factors such as air temperature, mean radiant temperature (MRT), relative humidity, relative air velocity and personal factors - insulative clothing and activity level.

As can be seen from ISO 7726 "Ergonomics of the thermal environment - Instruments for measuring", the most problematic measurable and discussed physical quantity is the mean radiant temperature, which is the uniform temperature of an imaginary enclosure in which radiant heat transfer from the human body is equal to the radiant heat transfer in the actual non-uniform enclosure. Mean radiant temperature can have a greater influence on loosing or gaining heat than any other parameter even the air temperature. This heat exchange by radiation between person and surroundings is high because of high skin absorptivity and emissivity (the relative ability to absorb and emit energy by radiation). The assessment of

mean radiant temperature is also standardized by ISO 7726 “Ergonomics of the thermal environment - Instruments for measuring physical quantities” but methods described in this standard have some limits and uncertainties discussed later in this book and also in (Alfano, 2011), (Hruška, 2003), (Health and Safety Executive, 2005).

2 STATE OF ART

People used to build various building to protect themselves against different weather conditions especially rain, cold, sun, thunderstorm and others. The problem of thermal comfort was recorded as early as Ancient Egypt times. Around 400 BC the classical Greek Athenian philosopher Socrates had thoughts on the climatic suitability of houses, on how to build to ensure thermal comfort. Vitruvius (1st century BC) also wrote about the need to consider climate in building design, for reasons of health and comfort. This however had very little influence on the practice of architecture (Auliciems, et al., 2007). The practical solution of thermal discomfort issues was minimal because of lack of appropriate tools and devices. There were used hand-held fans, ventilating towers, tunnels or wooden shutter on windows for cooling purposes and on the other hand there existed a fire to keep warm in cold conditions.

The progress in heating technology became from late 18th century and in cooling (mechanical) technology became from early 20th century. The study of thermal comfort as a relation to temperature we can date from 20th century second decade, especially in United States and England. In 1923 the American Society of Heating and Ventilating Engineers (ASHVE) has created a chart defining the comfort zone for most people in the United States, but the results of this study were applicable worldwide.

During thirties of 20th century brought some empirical studies, Vernon and Warner in 1932 and Bedford (1936) and analytical works from Winslow, Herrington and Gagge (1937).

The studies (Nevins, et al., 1966) and (McNall, et al., 1967) used participants that rated their thermal sensation in response to specified thermal environments and based on these studies and own research, (Fanger, 1970) derived comfort equation describing thermal comfort on six parameters (physical activity and clothing and environmental parameters: air temperature, mean radiant temperature, air velocity and air humidity). This equation linked thermal conditions to the seven-point thermal sensation scale defined by ASHRAE (earlier ASHVE) and became known as the Predicted Mean Vote (PMV) index. Then, Fanger developed Predicted Percentage Dissatisfied (PPD) index that predicts percentage of people dissatisfied with given thermal conditions.

The International Standards Organization (ISO) has adopted the PMV-PPD model in

thermal comfort as ISO 7730 standard in 1984.

Beside these indices of the thermal comfort, the evaluation of dissatisfaction due to draught should be taken in account. This dissatisfaction is caused by air velocity and turbulence intensity; thus, cooling is caused not only by air velocity, but also by fluctuation in the air stream. For people in thermal neutrality, the draught risk model was developed predicting the percentage of individuals dissatisfied due to draught (Fanger et al, 1988).

Basically we can divide thermal sensation models into two groups – physiologically based and non-physiologically based group; the former uses algorithm that produces a predicted physiological state and predicted thermal comfort vote for human exposed to an indoor environment using certain physical parameters of given environment and of the human as input while the latter are based on statistical fits to data relating comfort indices to the physiological environment.

Basically, physiological model uses heat balance of the human body. The heat is generated from metabolism and lost due to respiration and evaporation. In addition, human body gain or lose heat by conduction, convection and radiation. Most of the models use initial values for physiological constants and variables and then iterates. Within the iteration the thermoreceptor signals to the brain are established, physiological responses are determined, heat flows, core and skin temperatures are calculated. Iteration repeats usually with minute period. In addition to this, the Fanger's PMV-PPD model (and other modifications of this model) is based on iteration determining clothing surface temperature and the convective heat transfer coefficient in fixed heat flow.

Today, two versions are in general use:

- Two-node model from (Gagge, et al., 1986) - This treats first the heat transfer from the body core to the skin, then from the skin to the environment. In this model the sensible heat loss from the body surface calculates with convection and radiation, on the other hand these losses are considered as one loss depended on difference between skin temperature and ambient air temperature.
- Comfort equation (PMV model) from (Fanger, 1970) – Mode standardized by ASHRAE 55 and ISO 7730 standards. The PMV-PPD model uses a

steady-state heat balance for the human body and gives the relationship between human physiological processes (sweating, vasoconstriction, and vasodilation) and thermal comfort vote.

There are a large number of physical variables that influence thermal comfort. As can be seen, the biggest limitation of PMV thermal model, from the input information point of view, is the mean radiant temperature that is difficult to determine precisely. Measurements with globe thermometer recommended by ISO 7726 standard suffer from globe temperature dependency on convection and radiation, high time constants (20-30 min), non-uniform temperature distribution and the impossibility to measure asymmetric radiant temperature. Some problems can be solved with two-sphere radiometer method measurement that gives lower dependency on convection; on the other hand the emissivity of surrounding surfaces must be known.

The PMV-PPD model solves heat balance equations for the human body and is generally implemented on a computer. However; we suffer from the lack of user-friendly interfaces.

3 STATEMENT OF RESEARCH OBJECTIVES

- Processing of theoretical knowledge related to thermal comfort and mean radiant temperature
- Modification of PMV model to provide more accurate results and simpler deployment
- Creation of software tool used for computing PMV mathematical model
- Design and creation of simplified model of real room used for thermal comfort indices evaluation
- Optimize the costs for maintaining the thermal comfort in modelled room
- Determination of mean radiant temperature based on measurement with several thermopile sensors
- Thermal comfort evaluation systems design
    i. laboratory version – based on DataLab unit and personal computer
        - apparatus arrangement with connection to personal computer
        - implementation of sensory system for monitoring
        - software creation for thermal comfort indices evaluation
        - acquiring experimental data
    ii. embedded version – based on ADI (Analog/Digital Interface)
        - selection of appropriate ADI device
        - preparation of the evaluation system
        - programming modules
- Suggestion for further research in this field

4 THEORETICAL PART

This part describes theory related to this work. At the beginning the general term temperature is described. Then thermal radiation and physical laws are discussed. Middle part of this section is focused on thermal comfort and related standards. Next chapter describes mean radiant temperature as a specific parameter influencing thermal comfort. Finally IR thermometers and pyrometers are introduced and one chapter is devoted to thermopile sensors that are used in practical part of this work.

The final chapter presents possible modification of predicted mean vote mathematical model. This modification is convenient when using thermopile sensors in thermal comfort evaluation and simplifies the computation of thermal comfort indices.

4.1 Temperature

Temperature is a state parameter that determines ability for heat transfer. The temperature T' of a body is higher than the temperature T'' of another body if after contact between the bodies the first one transfers heat to the second one. However, if the heat transfer does not appear between these bodies when separated from their surroundings, then between these bodies there is a thermal equilibrium and the bodies have the same temperature ($T' = T''$). Maxwell formulated the following law regarding temperature, known as the zeroth law of thermodynamics. If three systems A, B, and C are in a state of respective internal thermal equilibrium, and systems A and B are in thermal equilibrium with system C, then systems A and B are in mutual thermal equilibrium, i.e., they have the same temperature. This law is the basis for using thermometers for the measurement of temperature. Thus, thermometers allow for different systems for measuring temperature. As a principle, in thermodynamic equations the absolute temperature is given in Kelvin (K). Another commonly used scale of temperature is the Celsius scale, where $t = T - 273.15$, where T is the absolute temperature. The value 273.15 is the absolute temperature for the triple point of water, which is the temperature at which the three phases (solid, liquid, and gas) of water can exist in equilibrium (Petela, 1983).

4.2 Thermal radiation

Radiation source

Thermal radiation can be considered from many different viewpoints. It is caused only by the fact that a radiating body has a temperature higher than absolute zero. According to its purpose, radiation can be considered to be electromagnetic waves or a collection of radiation energy quanta, i.e., photons, which are the matter particles.

The photons constitute a so-called photon gas. Therefore, analogously to a substance gas, a photon gas can be the subject of statistical (microscopic) or phenomenological (macroscopic) consideration. Energy supplied to a body, e.g., by heating, sustains oscillations of atoms in molecules that then become like the emitters of electromagnetic waves. At expend of internal energy or enthalpy of the body substance the energy propagates from the body via the waves in a process called thermal radiation. The terms radiation and emission are two homonyms and can be used not only for the process but also for the product of the radiation or emission process, respectively, i.e., the collection of emitted energy quanta or photon gas. The product of radiation is comprised of matter, the rest mass of which, in contrast to a substance, is equal to zero. According to the Prevost law, a body at a temperature greater than absolute zero radiates energy that can differ depending on different types of body substance, surface smoothness, and temperature. The energy of this radiation does not depend on the parameters, properties, or presence of neighbouring bodies. The different bodies also absorb oncoming radiation in different amount. Thus, energy exchange by radiation depends on the difference in emitted and absorbed radiation. For example, if the energy emitted is greater than the energy absorbed, and the energy of the body is not supplemented, then the temperature of the body decreases.

Phenomenologically, heat exchange by radiation is interpreted as a transformation of internal energy (or enthalpy) into the energy of electromagnetic waves of thermal radiation, which then travels through the surrounding medium to another body, at which point the radiation energy transforms again to internal energy (or enthalpy).

Statistically, heat exchange by radiation is defined as the transportation of energy by photons that emit from excited atoms and move until they are absorbed by other atoms.

Radiation energy is composed of electromagnetic waves of length theoretically from 0 to ∞. The length λ of the waves is correlated with the oscillation frequency ν and the speed of propagation c as follows:

$$\lambda \nu_o = c \tag{3.1}$$

The speed c_0 of the propagation of electromagnetic waves in a vacuum is largest: $c_0 = 2.9979 \times 10^8$ *m/s*. The ratio n of speed c_0 to the propagation speed c in a given medium

$$n = \frac{c_0}{\lambda} \tag{3.2}$$

is called the refractive index and is always larger than 1. For gases, n is close to 1, but, e.g., for glass it is about 1.5. In experimental investigations it is usually more convenient to measure the wavelength. In theoretical investigations, however, it is usually more convenient to use frequency, which does not change when radiation travels from one medium to another at different speeds.

The shorter are the wavelengths, the more penetrable are the waves. Fig. 4.1 shows approximately some characteristic regions of the wavelengths. As the wavelength decreases, i.e., the frequency increases, the penetration of the radiation within the matter grows deeper and deeper. For example, X-rays at $\sim 10^{17}$ Hz (Hz ≡ 1/s) travel through the human body, finding only slight difficulty in penetrating bones. Gamma rays at $\sim 10^{22}$ Hz have no problem penetrating most substances including metals. Shields used against gamma rays are made of dense metals, e.g., lead. However, natural cosmic waves have far greater penetrating power than manmade gamma radiation and can pass through a thickness even of 2 m of lead. With increasing radiation frequency, the wavelength becomes very short in comparison to even the densest metal lattices. For extremely large frequencies even the heaviest metals lose their shielding ability and are not able to reflect the radiation.

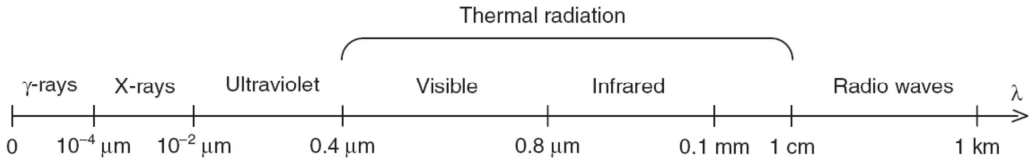

Fig. 4.1. Scheme of the characteristic wavelength regions (Petela, 2010)

With diminishing wavelengths the radiation energy decreases significantly. The shortest possible wavelength limit is equal to the so-called Planck's length, which corresponds to a frequency of 7.4×10^{42} Hz. All the regions shown in Fig. 4.1 overlap and, e.g., radiation of wavelength 10^{-3} m can be produced either by microwave techniques (microwave oscillators) or by infrared techniques (incandescent sources). All these waves are electromagnetic and propagate with the same speed c_0 in a vacuum. The properties of radiation depend on their wavelengths. From the viewpoint of heat transfer, most essential are the rays that, when absorbed by bodies, cause a noticeable increase of energy of these bodies. The rays that indicate such properties at practical temperature levels are called thermal radiation. An electromagnetic wave is said to be polarized if its electric field oscillates up and down along a single axis. For example, polarized radiation is comprised of the waves generated by radio broadcasting with a vertical antenna, which makes the electric field point either up or down, but never sideways. The light from an electric bulb is an example of non-polarized radiation: the radiating atoms are not organized. Such radiation arriving in the eyes can have, for a while a vertical electric field, but then it rotates around to horizontal, then back to vertical in random fashion. The radiation can be polarized, e.g., with use of a material such as Polaroid that absorbs radiation in one direction while transmitting radiation in the other direction. For example, Polaroid sunglasses can absorb horizontally polarized radiation emitted mostly from reflective surfaces such as glass, water and others. (Petela, 2010)

Radiant properties of surfaces

The principles of propagation, deflection, and refraction of visible rays are valid for all rays, thus also for all invisible rays. An energy portion E from any surface, striking the

considered body of finite thickness, splits into three parts as schematically shown in Fig. 4.2. Generally, part E_ρ is reflected, part E_α is absorbed, and part E_τ can be transmitted through the body. The energy conservation equation for the portion E comes in the following form:

$$E = E_\rho + E_\alpha + E_\tau \tag{3.3}$$

The parts can be expressed in relation to the portion E. Thus we have the definitions: reflectivity $\rho=E_\rho/E$, absorptivity $\alpha=E_\alpha/E$, and transmissivity $\tau=E_t/E$, where:

$$1 = \rho + \alpha + \tau \tag{3.4}$$

The magnitudes ρ, α, and τ are dimensionless and can vary for different bodies from 0 to 1.

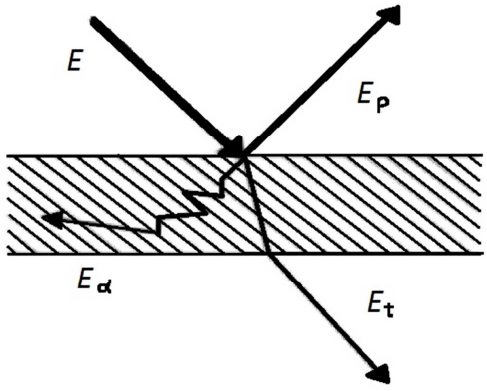

Fig. 4.2. Split of emission energy E arriving at the considered body (Petela, 2010)

In practice, there are some bodies with different specific properties that make the characteristic magnitudes of equation (3.4) take values very close to 1 or 0. In order to systemize considerations, some idealized body models with extreme values of radiation are introduced. If a body is able to totally absorb any radiation striking the body, i.e. $\alpha=1$, and thus from equation (3.4) has the result $\rho=\tau=0$, then such a perfectly absorbing body is called perfectly black (i.e., a blackbody). If a body is able to totally reflect any radiation striking the body, then in such a case $\rho=1$ and $\alpha=\tau=0$, and the body is called perfectly white. If, due to the perfect smoothness of the surface, the reflection is not dispersed, i.e.,

the incident and reflection angles are identical (specular reflection), then the body is additionally called a mirror. However, if reflected radiation is dispersed in many directions (diffuse reflection), then the surface is called dull. Monatomic gases (e.g., He, Ar) and diatomic gases (e.g., O_2, N_2) are examples of bodies that practically transmit total radiation. Such bodies can be considered as a model called perfectly transparent ($\tau=1$), and from equation (3.4) we get $\alpha=\rho=0$. Some bodies are permeable only for waves of a determined length. For example, a window glass transmits only visible radiation and almost entirely does not transmit other thermal radiation. Quartz glass is also practically non-transmittable for thermal radiation except for visible and ultraviolet radiation. Solid and liquid bodies, even of very small thickness, practically do not transmit thermal radiation. They can be considered as a model of perfectly radio-opaque body for which $\tau=0$ and:

$$\alpha + \rho = 1 \tag{3.5}$$

As the results from equation (3.5) show, the better a body reflects radiation, the worse it absorbs, and vice versa. The reflecting ability of thermal radiation can be significantly larger for smooth and polished surfaces in comparison to rough surfaces.

Definitions of the Radiation of Surfaces

Emission E of a surface is the energy radiated at the temperature of the surface and emitted into the front hemisphere. The emission expressed in watts (W), related to the emitting surface area A, is called the density of emission:

$$e = \frac{E}{A} \tag{3.6}$$

and is expressed in Wm^{-2}.

However, generally, the radiation propagating from a considered surface can be composed of both the emission from such a surface and the radiation from other surfaces that are reflected by the considered surface. The particular radiation components can differ depending on their temperature. In energetic consideration of radiation, the temperature of such components is not distinguished and the total radiation (emission and reflected

radiation) is called the radiosity, J. The radiosity is expressed in the same units as emission and, analogously, the radiosity density j is related also to the surface area:

$$j = \frac{J}{A} \tag{3.7}$$

For a blackbody, which does not reflect radiation, the radiosity equals the emission ($J=E$). Usually the general term radiation can mean either emission or radiosity. The exchange of radiation energy can occur between surfaces of different size and configuration. In calculations of the exchange between any two surfaces n and m, generally only a part of the radiation from surface n arrives at surface m. Therefore, one can use the view factor φ_{n-m}, which is defined as the ratio of the radiosity J_{n-m}, arriving from surface n at surface m, to the radiosity J_n leaving surface n:

$$\varphi_{n-m} = \frac{J_{n-m}}{J_n} \tag{3.8}$$

The factor value can be within the range from 0 to 1. If each of the considered surfaces is uniform in terms of temperature and radiative properties, i.e., the density of radiosity is constant at every point of the respective surfaces, then the factor depends only on the location of both the surfaces in space and is sometimes called the view factor. However, if j is not the same at any point of the considered surface area A, then the radiosity density has to be considered locally $(j=dJ/dA)$ as will be discussed later. The density of emission e consists of the energy emitted at the wavelength λ from zero to infinity. The very small part of the emission corresponds to the wavelength range $d\lambda$. Therefore, for the given wavelength, the monochromatic density e_λ of emission is defined as follows:

$$e_\lambda = \frac{de}{d\lambda} \tag{3.9}$$

The monochromatic emission density e_λ [$\mathrm{Wm^{-3}}$] depends on the wavelength, temperature, and radiative properties of the emitting surface. However, the model of a black surface has determined radiative properties and the monochromatic density $e_{b,\lambda}$ of emission of the black surface

$$e_{b,\lambda} = \frac{de_b}{d\lambda} \tag{3.10}$$

is only a function of temperature and wavelength.

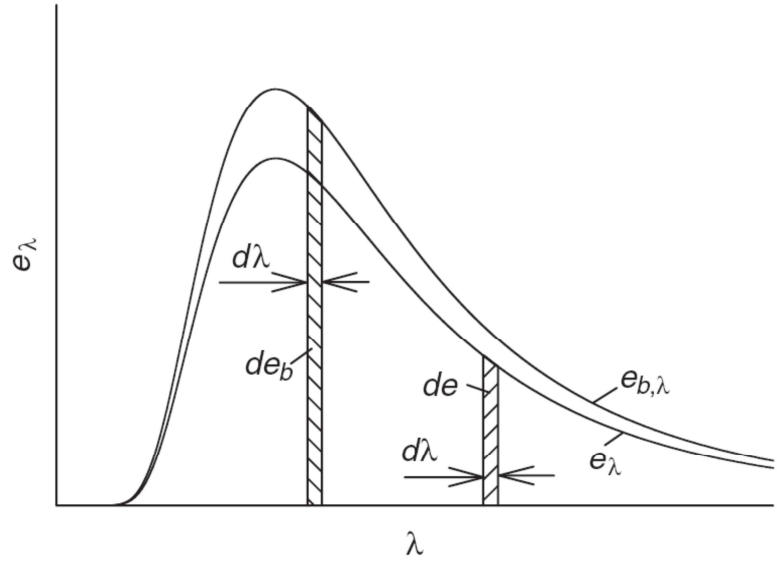

Fig. 4.3. The area representing the elemental energy of emission (Petela, 2010)

As shown in Fig. 4.3, the total, i.e. panchromatic (for all wavelengths), emission density e_b of the black surface is represented by the area under the $e_{b,\lambda}$ spectrum, whereas the total panchromatic emission of the gray surface corresponds to the smaller area, under the e_λ spectrum. The quantity e_b can be determined based on equation (3.10) by its integration over the whole range of wavelengths from 0 to ∞. (Petela, 2010)

Planck's law

Fig. 4.4 shows the theoretical model of a blackbody, called the cavity radiator, which has played an important role in the study of radiation. The analysis of the nascent radiation in the model led to the birth of modern quantum physics. The virtual model of the black surface (Fig. 4.4) appears as a small hole in the wall embracing a certain space. Any radiation portion *P* entering the space through the hole is the subject of successive multiple deflections. Each deflection attenuates the portion *P*, especially when the interior is lined up with material with high absorptivity. It can be assumed that the portion *P* is entirely absorbed by the hole; therefore the hole behaves like a perfect blackbody *(α=1).* The

radiosity of the hole does not contain any reflected radiation, but it represents the density of the emission e_b of a perfectly black surface. Thus, the density of black radiosity j_b of the hole is equal to the density of emission e_b of the black surface, $j_b = e_b$. The cavity space does not contain any substance; the refractive index $n=1$. The emission density e_b expresses radiation energy emitted from the hole into the front hemisphere, i.e., within the solid angle 2π sr.

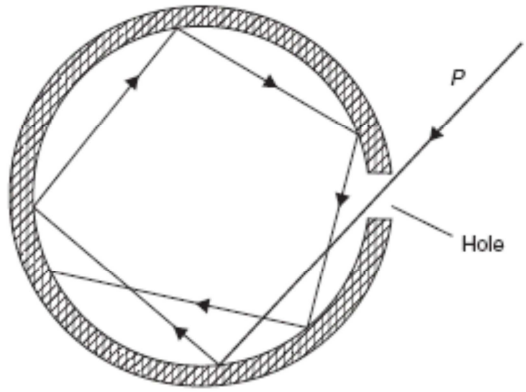

Fig. 4.4. Blackbody model (cavity radiator) (Petela, 2010)

In 1900, Planck announced his hypothesis with a detailed model of the atomic processes taking place at the wall of the cavity radiator. The atoms that make up the cavity wall behave like tiny electromagnetic oscillators. Each oscillator emits electromagnetic energy into the cavity and absorbs electromagnetic energy from the cavity. The oscillators do not exchange energy continuously, but only in jumps called quanta $h\nu$, where ν is the oscillator frequency and h is Planck's constant, $h = 6.625 \times 10^{-34}$ *Js*.

Thus, in radiation processes discrete quanta arise for which, if the principle of quantum-statistical thermodynamics is applied, the following expression can be derived for the energy density u_λ, Jm^{-4}, of radiation per unit volume and per unit wavelength:

$$u_\lambda = \frac{8\pi h c_0}{\lambda\left(e^{\frac{hc}{\lambda kT}} - 1\right)} \tag{3.11}$$

where $k=1.3805\times10^{-23}\ JK^{-1}$ is the Boltzmann constant.

In order to obtain the radiation energy flux, i.e., the energy emission $e_{b,\lambda}$, instead of the radiation energy remaining within a certain volume, the energy density u_λ should be multiplied by the factor $c_0/4$ resulting from the geometrical considerations discussed, e.g., by (Guggenheim, 1957). Thus, based on the quantum theory, initially empirically and later proven theoretically, the Planck's formula for the black monochromatic emission density $e_{b,\lambda}$, can be established as follows:

$$e_{b,\lambda} = \frac{c_1}{\lambda^5\left(e^{\frac{c_2}{\lambda T}}-1\right)} \tag{3.12}$$

where

$$c_1 = 2\pi h c_0^2 = 3.74\times10^{-16}\ Wm^2$$

$$c_2 = \frac{hc_0}{k} = 1.4388\times10^{-2}\ mK$$

are the first and the second, respectively, Planck's constants and T [K] is the absolute temperature of black radiation. Fig. 4.5 presents the curves of the black monochromatic density of emission $e_{b,\lambda}$ as a function of wavelength λ and for some different temperatures T. The higher is the temperature T, the larger is the area between the λ-axis and the respective curve.

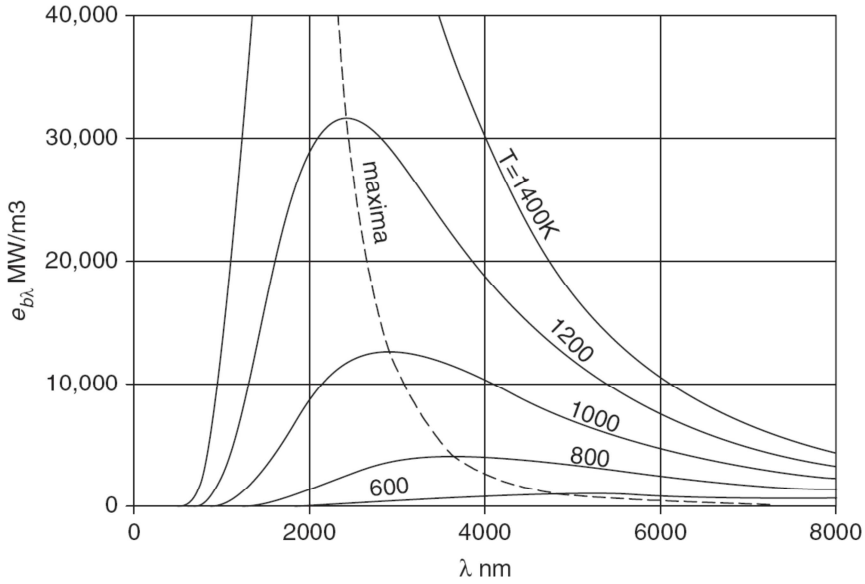

Fig. 4.5. Monochromatic density of emission as a function of temperature and wavelength (Petela, 2010)

The dashed line in Fig. 4.5 represents points of the maximum values of $e_{b,\lambda}$ and it shows that the higher is the temperature T the smaller is the wavelength λ_m corresponding to the maximum. For the model of a perfectly gray surface it is assumed that the panchromatic emissivity ε, defined later by Equation (3.29), is equal to the monochromatic emissivity ε_λ as follows:

$$\varepsilon = \frac{e}{e_b} = e_\lambda = \frac{e_\lambda}{e_{b,\lambda}} \tag{3.13}$$

For comparison, Fig. 4.6 presents four examples of the different surface spectra e_λ for the same temperature. The largest and always the maximum values of the spectrum appear for the black surface (dashed–dotted line). The real surfaces (solid line) have the smaller values of the monochromatic emission e_λ, (always $e_\lambda \leq e_{b,\lambda}$), which can be represented by the regular averaged curve (dashed line) corresponding to the appropriately selected model of a perfectly gray surface with a constant value of emissivity ε_λ. Thus, the spectra for the models of black and gray surfaces reach the maximum for the same wavelength. An

entirely different type of spectrum can appear for a gas. The gas spectrum can be irregular (e.g., dotted line) so that application of the gray model is too inexact.

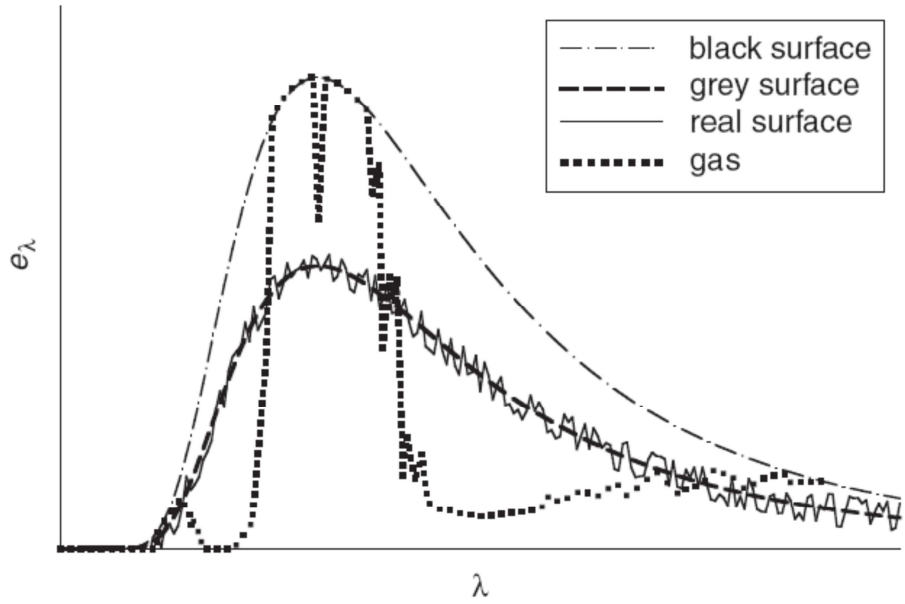

Fig. 4.6. Examples of spectra of three surfaces; black, gray (at ε = 0.6), and real, compared to the spectrum of gas (H_2O), at the same temperature. (Petela, 2010)

For some cases the Planck's formula (3.12) can be simplified to the two forms; each giving an error smaller than only 1%. First, if $\lambda \times T < 3000$ μm K, then $c_2/(\lambda T) >> 1$ and the following formula derived by Wien, is obtained:

$$e_{b,\lambda} = \frac{c_1}{\lambda^5} e^{-\frac{c_2}{\lambda T}} \tag{3.14}$$

Second, if $\lambda \times T >> c_2$, i.e., if $\lambda \times T > 7.8 \times 10^{-5}$ μm K, then expanding the expression in brackets in the denominator of equation (3.13) in series:

$$e^{\frac{c_2}{\lambda T}} - 1 = \frac{c_2}{\lambda T} + \frac{1}{2!}\left(\frac{c_2}{\lambda T}\right)^2 + \ldots \tag{3.15}$$

and neglecting further terms, the Rayleigh–Jeans formula can be applied:

$$e_{b,\lambda} = \frac{c_1}{c_2}\frac{T}{\lambda^4} \tag{3.16}$$

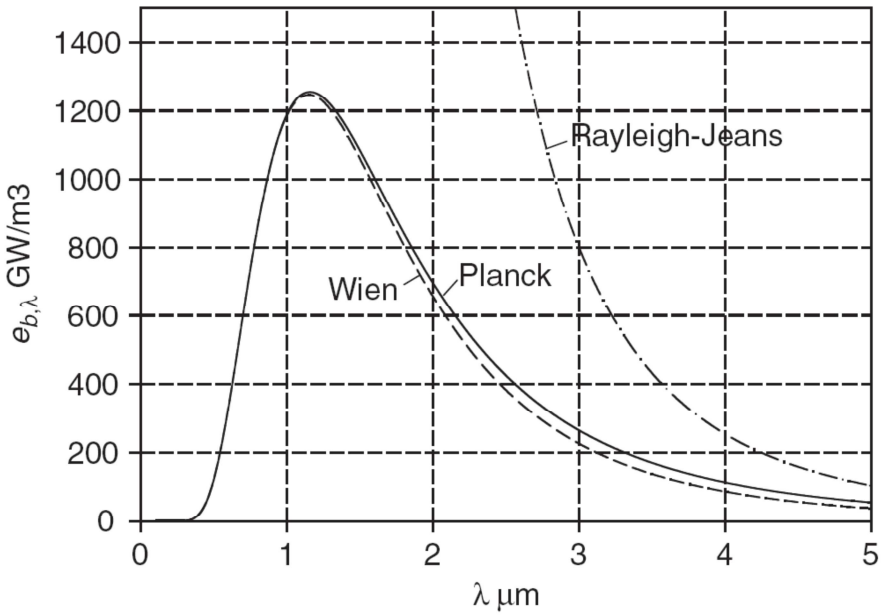

Fig. 4.7. Comparison of $e_{b,\lambda}$ values for 2500 K (Petela, 2010)

The precision of the Wien formula (3.14), in comparison to Planck's formula (3.12), is illustrated in Fig. 4.7. for *T = 2500 K*. The convergence for this temperature is better the smaller is the wavelength. The Rayleigh-Jeans formula (3.16) for the shown range of wavelength gives significantly inexact values. The precision of the Rayleigh–Jeans formula (3.16) in comparison to the Planck's formula (3.12) is illustrated in Fig. 4.7 for *T=1000 K*. The convergence for this temperature is better the larger is the wavelength.
The Wien formula (3.14) for the shown range of wavelength gives significantly inexact values. (Petela, 2010)

Wien's Displacement Law

The wavelength λ_m, for which the spectrum of black emission reaches maximum, can be determined by considering the derivative of equation (3.12) as equal to zero:

$$\frac{de_{b,\lambda}}{d\lambda} = 0 \tag{3.17}$$

Introducing a new variable *x* as follows:

$$\lambda = \frac{c_2}{Tx}, \qquad d\lambda = -\frac{c_2}{Tx^2}dx \tag{3.18}$$

it could be written as:

$$\frac{d}{dx}\left(\frac{x^5}{e^x - 1}\right) = 0 \tag{3.19}$$

which leads to the transcendental equation:

$$\frac{xe^x}{e^x - 1} = 5 \tag{3.20}$$

with only one real solution, *x=4.965*. Thus, the considered maximum value in the spectrum appears for the condition, called the Wien's displacement law:

$$\lambda_m T = c_3 \tag{3.21}$$

where $c_3 = c_2 / x = 2.8976 \times 10^{-3}\ mK$

Substituting (3.21) into (3.12), the value of the maximum of the monochromatic intensity of the blackbody emission is:

$$e_{b\lambda_m} = c_4 T^5 \tag{3.22}$$

where $c_4 = \frac{c_1}{c_3^5\left(e^{4.965} - 1\right)} = 1.2866 \times 10^{-5}\ \frac{W}{m^3 K^5}$

Equation (3.22) presents the hyperbole with asymptotes that are the axes of the coordination system *(λ, $e_{b,\lambda}$)* as shown in Fig. 4.5 (dashed line). (Petela, 2010)

Stefan–Boltzmann Law

In order to determine the emission density e_b of a black surface, equation (3.10) can be applied in integrated form:

$$e_b = \int_0^\infty e_{b,\lambda} d\lambda \tag{3.23}$$

Applying Planck's relation (3.12) into (3.23), with substitution $x \equiv c_2/(\lambda T)$, yields:

$$e_b = c_1 \left(\frac{T}{c_2} \right)^4 \int_0^\infty x^3 \frac{1}{e^x - 1} dx \tag{3.24}$$

The fraction in equation (3.24) can be represented as the sum of the infinite geometric series:

$$\frac{1}{e^x - 1} = \sum_{m=1}^{m=\infty} e^{-mx} \tag{3.25}$$

Using (3.25) in (3.24):

$$e_b = c_1 \left(\frac{T}{c_c} \right)^4 \sum_{m=1}^{\infty} \int_0^\infty x^3 e^{-mx} dx \tag{3.26}$$

Then, combining consecutively the integration solution

$$\int_0^\infty x^n e^{ax} dx = \frac{1}{a} x^n e^{ax} - \frac{n}{a} \int x^{n-1} e^{ax} dx \qquad (n > 0) \tag{3.27}$$

given, e.g., by (Korn, et al., 1968), and after substitution for the present considerations: $n=m$ and $a=-n$, integral (3.23) comes finally to the following Stefan–Boltzmann law:

$$e_b = \sigma T^4 = \frac{a c_0}{4} T^4 \tag{3.28}$$

where the Stefan-Boltzmann constant for black radiation

$$\sigma = \frac{\pi^4}{15} \frac{c_1}{c_2^4} = 5.6693 \times 10^{-8} \frac{W}{m^2 K^4}$$

and the universal constant

$$a = 7.564 \times 10^{-16} \frac{J}{m^3 K^4}$$

are determined theoretically.

From the assumption for the gray surface model, expressed by relations in equation (3.13), the emission density e_b of the black surface, given by equation (3.28), can be used for determination of the emission density e of the gray surface as follows:

$$e = \varepsilon \sigma T^4 \tag{3.29}$$

For convenience in practical calculations, equation (3.29) is sometimes applied in the form:

$$e = \varepsilon C_b \left(\frac{T}{100} \right)^4 \tag{3.30}$$

in which the radiation constant for a black surface $C_b = 10^8 \times \sigma$. The experimental value is $C_b = 5.729\ Wm^{-2} K^{-4}$, which is a little larger than $\sigma / 10^8 = 5.6693$.

In practice, the choice of a proper value of emissivity ε is difficult. Some averaged values of ε for different materials are shown in Table 4.1 and more values can be found in related literature, e.g., (Holman, 2009).

Table 4.1 Emissivity values of different materials (Petela, 2010)

Surface material	***Surface temperature [°C]***	***Emissivity*** $(\varepsilon)_{\beta=0}$	***Average emissivity ε***
Gold	*20*	*0.02-0.03*	-
Silver. polished	*20*	*0.02-0.03*	-
Copper. polished	*20*	*0.03*	-
Copper. oxidized	*130*	*0.76*	*0.725*
Aluminium	*170*	*0.039*	*0.049*
Steel. polished	*20*	*0.24*	-
Steel. red rust	*20*	*0.61*	-
Steel. scale	*130*	*0.60*	-
Zinc. oxidized	*20*	*0.23-0.28*	-
Lead. oxidized	*20*	*0.28*	-
Bismuth. shining	*80*	*0.34*	*0.366*

Clay. burnt	*70*	*0.91*	*0.86*
Brick	*20*	*0.93*	-
Ceramics	-	-	*0.85*
Porcelain	*20*	*0.91-0.94*	-
Glass	*90*	*0.94*	*0.876*
Ice. liquid water	*0*	*0.966*	-
Frost	*0*	*0.985*	-
Paper	*90*	*0.92*	*0.89*
Wood	*70*	*0.935*	*0.91*
Soot	-	-	*0.96*
Asbestos	*23*	-	*0.96*

Lambert's Cosine Law

The radiosity density *j* can be considered for a body surface or for any cross section in a space. The radiosity density *j* determines the total energy radiated in unit time, corresponding to the unit of surface area and in all directions into the front hemisphere, i.e., within the solid angle 2π sr:

$$j = \int_0^{2\pi} i_\beta d\omega \tag{3.31}$$

where i_β is the directional radiation intensity, $Wm^{-2}sr^{-1}$, expressing the total radiation propagating within solid angle $d\omega$ and along a direction determined by the flat angle β with the normal to the surface Fig. 4.8.

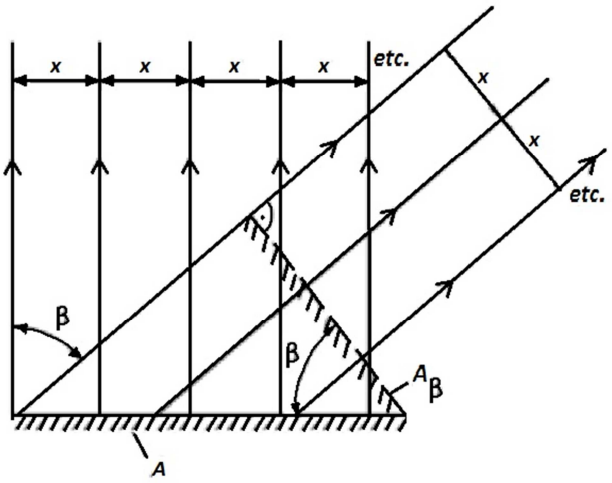

Fig. 4.8. Interpretation scheme of rays' density independent of direction (constant spacing *x* between imagined rays is independent on angle β). (Petela, 2010)

Usually, the practical observations motivate the assumption that a certain surface *A* (Fig. 4.8), is seen at the same brightness under any angle β. It means that for any direction determined by β the radiation intensity is the same as is schematically represented by equal spacing *"x"* of the normal rays *(at β=0)* and for the rays propagating from surface *A* under arbitrary angle β. Thus, the directional radiation intensity i_β of surface *A* along angle β can be replaced by the normal radiation intensity i_0 of equivalent surface A_β:

$$A_\beta = A\cos(\beta) \tag{3.32}$$

If the surfaces *A* and A_β have the same temperature and properties, then the energetic equivalence of radiation of both surfaces leads to the statement:

$$Ai_\beta = A_\beta i_0 \tag{3.33}$$

Substituting (3.32) into (3.33) the Lambert's cosine law is obtained which states that for the flat surface the radiation intensity i_β along a direction determined by angle β with the normal to the surface is:

$$i_\beta = i_0\cos(\beta) \tag{3.34}$$

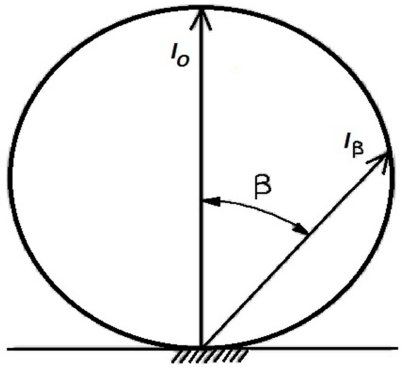

Fig. 4.9. Circular diagram of radiation intensity (Petela, 2010)

where i_0 is the normal radiation intensity. Equation (3.34) can be illustrated by a circular diagram shown in Fig. 4.9. With the growing angle β from 0 to $\pi/2$ deg, the intensity i_β decreases respectively from values i_0 to 0 deg. Based on Lambert's cosine law the following consideration can be developed.

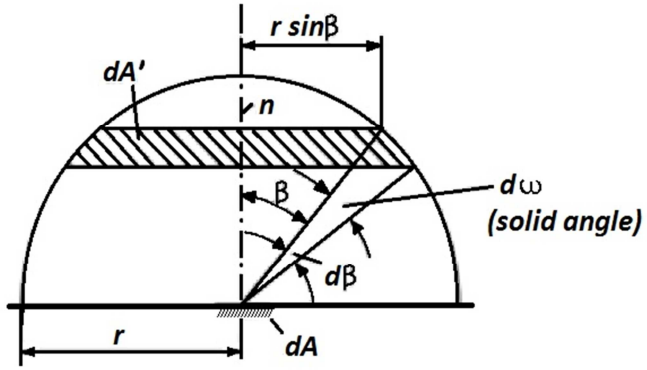

Fig. 4.10. Radiation of element *dA* on element *dA'* (Petela, 2010)

As shown in Fig. 4.10, the solid angle $d\omega$, under which a surface *dA'* is seen from surface *dA*, is measured as a surface area *dA* divided by the square of distance *r* of this surface from the observation point at surface *dA*:

$$d\omega = \frac{dA'}{r^2} \tag{3.35}$$

where

$$dA' = r\, d\beta\, 2\pi r \sin(\beta) \tag{3.36}$$

Substitute (3.34) (3.35) and (3.36) into (3.31)

$$j = \pi i_0 \int_0^{\pi/2} 2\sin(\beta)\cos(\beta)\, d\beta = \pi i_0 \int_0^{\pi/2} \sin(2\beta)\, d\beta = \pi i_0 \left[\frac{1}{2} - \cos(2\beta)\right]_0^{\pi/2} \tag{3.37}$$

and finally:

$$j = \pi i_0 \tag{3.38}$$

based on equation (3.34) and (3.38)

$$i_\beta = \frac{j}{\pi}\cos(\beta) \tag{3.39}$$

For given values of the radiosity density j and angle β, formula (3.39) allows for calculation of directional radiation intensity i_β. The result is that when Lambert's law is fulfilled, the surface emitting radiation has the same radiosity intensity regardless of the direction from which the surface is seen. For example, this is why heavenly bodies make an impression like shining flat walls and not like a lump body. (Petela, 2010)

Kirchhoff's Law

The relation between the absorptivity α and emissivity ε of the surface can be derived with use of the model of heat exchange shown in Fig. 4.11. There are two flat, infinite, and parallel surfaces facing each other; one is perfectly gray (with any constant values of emissivity ε and reflectivity ρ), the other is perfectly black ($\varepsilon_b=1$ and $\rho_b=0$). The same and uniform temperature T prevails over both surfaces. Emission $e = \varepsilon \times e_b$ of the gray surface is totally absorbed by the black surface. Emission e_b of the black surface is partly absorbed ($\alpha \times e_b$) and partly reflected ($\rho \times e_b$). The system boundary (the dashed line in Fig. 4.11) defines the considered system, which is the very thin layer next to the gray surface.

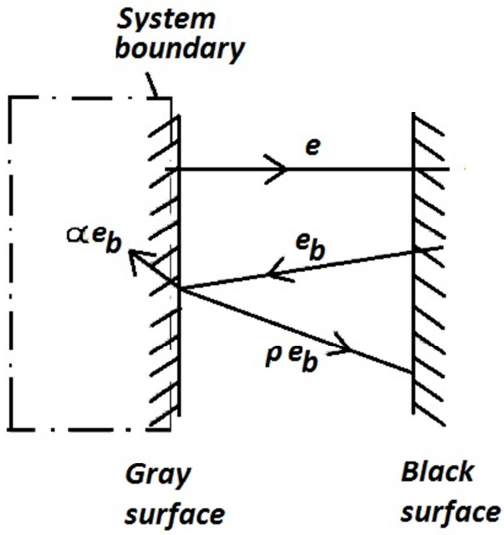

Fig. 4.11. Scheme of energy radiation balance (Petela, 2010)

The energy conservation equation, applied for the system, yields:

$$e_b - \rho e_b = e \tag{3.40}$$

After elimination of ρ and e from equation (3.40) by using, respectively, equations (3.5) and (3.13), one obtains:

$$\alpha = \varepsilon \tag{3.41}$$

which is Kirchhoff's law (also called Kirchhoff's identity); the surface emissivity is equal to the surface absorptivity at the same temperature. In practice, equation (3.41) can be applied if $\varepsilon > 0.5$. For smaller values of ε, Kirchhoff's law can be inexact. Derivation of the obtained result (3.41) did not require assumptions about any parameters, i.e., the result does not depend on the wavelength λ, temperature T, and the angle; thus, for any wavelength, temperature, or direction, we have also:

$$\alpha_{\lambda T \beta} = \varepsilon_{\lambda T \beta} \tag{3.42}$$

Emissivities of real materials differ from the values for discussed models, e.g., Lambert's cosine law, especially for polished surfaces. The directional emissivity ε_β, in a direction determined by angle β, is the following ratio of the respective directional radiation

intensities i_β and $i_{b,\beta}$, for gray and black surfaces:

$$\varepsilon_\beta = \frac{i_\beta}{i_{b\beta}} \tag{3.43}$$

For example, Fig. 4.12 shows the comparison of the directional emissivities ε_β for bronze and wood to the emissivity $\varepsilon_{b,\beta}$ for a black surface ($\varepsilon_{b,\beta} = 1$). There are different surfaces, e.g., bronze, for which, in the significant range of angle β, the emissivity ε_β can grow with the increased angle β. However, for all materials, with the angle β approaching 90°, the directional emissivity ε_β rapidly decreases to zero. Table 4.1 presents some illustrative data on emissivity of different surfaces, selected from data given by (McAdams, 1954) and (Schmidt, 1963).

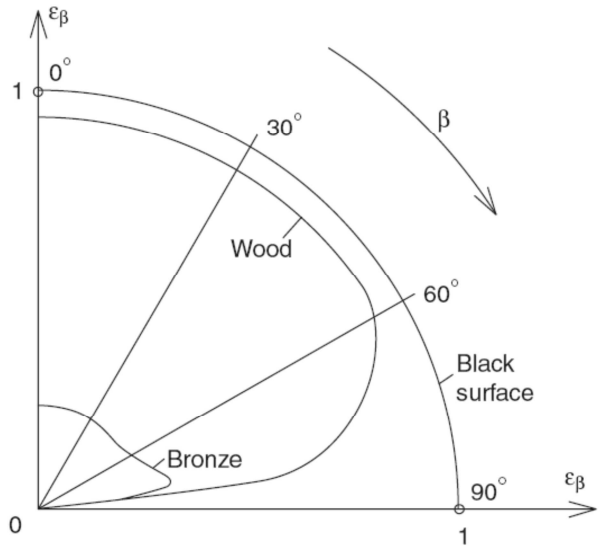

Fig. 4.12. Real directional emissivity ε_β of bronze and wood as a function of angle β (Petela, 2010)

4.3 Thermal comfort

The problem of thermal comfort and its solution has evolved thousands of years (see also State of art chapter). Many solutions and technical devices were developed during history but until the last century and the progress in heating technology the thermal comfort cannot be solved effectively. The last century also brought also progress in theoretical area and dozens on new thermal comfort models were developed. This thesis deals primarily with PMV-PPD thermal model declared in ISO and ASHRAE international standards.

Next subchapters describe standards related directly to the thermal comfort and thermal environment: ASHRAE 55, ISO 7730 standards and ISO 7243 (for extreme environmental conditions).

4.3.1 ISO 7730 Ergonomics of the thermal environment

Analytical determination and interpretation of thermal comfort using calculation of the PMV and PPD indices and local thermal comfort criteria

This International Standard (2005 revision) covering the evaluation of moderate thermal environments was developed in parallel with the revised ASHRAE standard 55 and is one of a series of ISO documents specifying methods for the measurement and evaluation of the moderate and extreme thermal environments to which human beings are exposed (ISO 7243, ISO 7933 and ISO 11079, all three dealing with extreme environmental conditions, are others in the series).

A human being's thermal sensation is mainly related to the thermal balance of his or her body as a whole. This balance is influenced by physical activity and clothing, as well as the environmental parameters: air temperature, mean radiant temperature, air velocity and air humidity. When these factors have been estimated or measured, the thermal sensation for the body as a whole can be predicted by calculating the predicted mean vote (PMV) that is described in Clause 4 of this standard.

The predicted percentage dissatisfied (PPD) index provides information on thermal discomfort or thermal dissatisfaction by predicting the percentage of people likely to feel

too warm or too cool in a given environment. The PPD can be obtained from the PMV and its definition is presented in Clause 5 of the standard.

Thermal discomfort can also be caused by unwanted local cooling or heating of the body. The most common local discomfort factors are radiant temperature asymmetry (cold or warm surfaces), draught (defined as a local cooling of the body caused by air movement), vertical air temperature difference, and cold or warm floors. Clause 6 specifies how to predict the percentage dissatisfied owing to local discomfort parameters. Dissatisfaction can be caused by hot or cold discomfort for the body as a whole. Comfort limits can in this case be expressed by the PMV and PPD indices. But thermal dissatisfaction can also be caused by local thermal discomfort parameters. Clause 7 deals with acceptable thermal environments for comfort.

Clauses 6 and 7 are based mainly on steady-state conditions. Means of evaluating non-steady-state conditions such as transients (temperature steps), cycling temperatures or temperature ramps are presented in Clause 8. The thermal environments in buildings or at workplaces will change over time and it might not always be possible to keep conditions within recommended limits. A method for long-term evaluation of thermal comfort is given in Clause 9.

Clause 10 gives recommendations on how to take into account the adaptation of people when evaluating and designing buildings and systems (ISO 7730, 2005).

4.3.2 ASHRAE 55 Thermal environmental conditions for human occupancy

ASHRAE 55 (2004 revision) is an American standard adopted by international organization ASHRAE (American Society of Heating, Refrigerating and Air-Conditioning Engineers). The purpose of this standard is to specify the combinations of indoor thermal environmental factors and personal factors that will produce thermal environmental conditions acceptable to a majority of the occupants within the space.

The scope of this standard is:

a) the environmental factors addressed in this standard are temperature, thermal radiation, humidity, and speed; the personal factors are those of activity and clothing;

b) all of the criteria in the standard must be applied together, since comfort in the space environment is complex and responds to the interaction of all the factors that are addressed;
c) the standard specifies thermal environment conditions acceptable for healthy people at atmospheric pressure equivalent to altitudes up to 3000 m in indoor spaces designated for human occupancy for periods not less than 15 minutes;
d) the standard does not address such non-thermal environmental factors as air quality, acoustics, and illumination nor other physical, chemical, or biological space contaminants that may affect comfort or health (ASHRAE 55, 2004).

The standard provides the list of definitions and determines the conditions that provide thermal comfort. The very short definition says that "thermal comfort is that condition of mind which expresses satisfaction with the thermal environment". There are six primary factors that must be addressed when defining conditions for thermal comfort. Other factors can affect thermal comfort in particular circumstances. Although the factors may vary in time, this standard describes steady state only. The standard defines comfort zone as a range of operative temperature that provide suitable thermal environmental conditions, where operative temperature is the uniform temperature of an imaginary black enclosure in which an occupant would exchange the same amount of heat by radiation plus convection as in the actual nonuniform environment.

The calculation of operative temperature based on air and mean-radiant temperature given by this form is

$$t_{op} = At_a + (1-A)t_r \tag{3.44}$$

Where t_{op} [°C] is an operative temperature, t_a [°C] is air temperature, t_r [°C] is mean radiant temperature and the value of A [-] can be found from the values in table 4.2 as a function of relative air speed v_r [ms^{-1}] (ASHRAE 55, 2004).

Table 4.2. Values used for operative temperature assessment (ASHRAE 55, 2004)

v_r	< 0.2 ms^{-1}	0.2 to 0.6 ms^{-1}	0.6 to 1.0 ms^{-1}
A	0.5	0.6	0.7

Under certain conditions described in Appendix D of ASHRAE 55 dry-bulb temperature may be used, where dry-bulb temperature is the temperature of air measured by a thermometer freely exposed to the air but shielded from radiation and moisture.

The comfort zone for typical application can be simply determined by graphical method presented in standard ASHRAE 55. The range of operative temperatures presented in this method is for 80% occupant acceptability. This is based on 10% dissatisfaction criteria for general (whole body) thermal comfort based on PMV-PPD index, plus an additional 10% dissatisfaction that may occur on average from local thermal discomfort. Appendix D of this standard provides a computer program for calculation of PMV-PPD indices. The definitions of PMV-PPD indices come from ISO 7730 and ASHRAE 55 standard adopted it in 2004 revision.

For wider range of applications a computer program based on a heat balance model is used. For given set of conditions, the results from the two methods are consistent, and either method may be used as long as the criteria outlined in respective section of the standard are met. (ASHRAE 55, 2004)

4.3.3 ISO 7243 Hot environments

Estimation of the heat stress on working man, based on the WBGT-index (wet bulb globe temperature)

This standard provides a simple convenient method, which can be easily used in industrial environments, and uses the wet bulb globe temperature (WBGT) index to assess heat stress of an individual in hot environments.

ISO 7243 is intended for heat stress assessment on the human body during his activity. However, this standard is neither suitable for heat stress assessment during very short time

periods nor for heat stress assessment which are very close to thermal comfort conditions (ISO 7243, 1989).

4.3.4 ISO 7933 Ergonomics of the thermal environment

Analytical determination and interpretation of heat stress using calculation of the predicted heat strain

This International Standard specifies a method for the analytical evaluation and interpretation of the thermal stress experienced by a subject in a hot environment. It describes a method for predicting the sweat rate and the internal core temperature that the human body will develop in response to the working conditions.

The various terms used in this prediction model, and in particular in the heat balance, show the influence of the different physical parameters of the environment on the thermal stress experienced by the subject. In this way, this International Standard makes it possible to determine which parameter or group of parameters should be modified, and to what extent, in order to reduce the risk of physiological strains.

The main objectives of this International Standard are the following:

a) the evaluation of the thermal stress in conditions likely to lead to excessive core temperature increase or water loss for the standard subject;
b) the determination of exposure times with which the physiological strain is acceptable (no physical damage is to be expected). In the context of this prediction mode, these exposure times are called “maximum allowable exposure times”.

This International Standard does not predict the physiological response of individual subjects, but only considers standard subjects in good health and fit for the work they perform. It is therefore intended to be used by ergonomists, industrial hygienists, etc., to evaluate working conditions (ISO 7933, 2004).

4.3.5 Thermal balance

Thermal balance of the human body and its surroundings is a state, when the thermal equality is kept between heat produced by the body and heat which is taken away from the body by surroundings. Thermal balance of the body can be expressed as follows:

$$M - W = \pm R \pm C \pm K \pm E_d \pm E_{sw} \pm L_{res} \pm S_{res} \pm \Delta D \ [W] \qquad (3.45)$$

where M [W] is the metabolism value; W [W] is the mechanical work; R [W] is the radiant heat flux; C [W] is the convection heat flux; K [W] is the conduction heat flux; E_d is the thermal loss via skin diffusion; E_{sw} [W] is the thermal loss via common sweating; L_{res} [W] is the latent thermal loss via breathing; S_{res} [W] is the appreciable thermal loss via breathing; ΔS [W] is the change of thermal capacity. (Auliciems, et al., 2007)

If ΔS is positive, the temperature of the human body is increasing; if it is negative the temperature is decreasing. In case $\Delta S = 0$ human body is in equilibrium with its surroundings.

Individual components in Equation (3.45) are described in following subchapters. These components are expressed for unit body surface area.

4.3.6 Metabolism M [Wm^{-2}]

This is the body heat production rate resulting from the oxidation of food. Its value for every person depends upon their diet and level of activity and may be estimated using the equation below:

$$M = 2,06 \times 10^4 \dot{V} (F_{oi} - F_{oe}) \quad [W] \qquad (3.46)$$

where $\dot{V}$ [dm^{3}s^{-1}] is air breathing rate; F_{oi} [-] and F_{oe} [-] are the fraction of oxygen in the inhaled end exhaled air, respectively. The value of F_{oi} is normally 0.206 but F_{oe} varies with the composition of food used in metabolism; for fat diet $F_{oe} \approx 0.159$ and for carbohydrates $F_{oe} \approx 0.163$ (Awbi, 1991).

4.3.7 Radiant heat flux *R* [Wm^{-2}]

Radiant heat flux arises between human body surface (clothing and skin) and surfaces of surroundings places including heat sources. In most cases the mean radiant temperature is lower than temperature of human clothing so it is mostly thermal loss.

$$R = A_{eff}\,\varepsilon\sigma\left[\left(t_{cl}+273\right)^4-\left(t_r+273\right)^4\right] \tag{3.47}$$

$$A_{eff} = f_{cl}\,\frac{A_r}{A_D} \tag{3.48}$$

$$A_D = 0.202m^{0.425}h^{0.725} \tag{3.49}$$

$$f_{cl}\begin{cases} 1.00+0.290I_{cl} & for\ I_{cl}\le 0.078\ m^2KW^{-1} \\ 1.05+0.645I_{cl} & for\ I_{cl}> 0.078\ m^2KW^{-1} \end{cases} \tag{3.50}$$

where f_{cl} [-] is the ratio of the body surface covered with clothing and naked body; t_{cl} [°C] is the temperature of the clothing; t_r [°C] is mean radiant temperature; ε [-] is emissivity of the clothing (for common clothing ε = 0.95); σ [Wm^{-2}K^{-4}] is the Stefan-Boltzmann constant $\sigma = 5.6693\times10^{-8}$ Wm^{-2}K^{-4}; A_r [m^2] is the surface of the human body participating on radiant heat transfer (for sitting persons A_r/A_D = 0.70 and for staying persons A_r/A_D = 0.73; A_D [m^2] is the surface of human body – according Dubois equation (3.49); m [kg] is the weight of human body; h [m] is the height of human body; I_{cl} [clo] is the thermal insulation of clothing (Auliciems, et al., 2007) (Centnerová, 2001).

4.3.8 Convection heat flux *C* [Wm^{-2}]

Thermal flow between human body and surroundings air is caused by airflow around human body. Two types of airflow can be distinguished – free and forced convection.

$$C = h_c\,f_{cl}\left(t_{cl}-t_a\right) \tag{3.51}$$

$$h_c = 2.38\left(t_{cl}-t_a\right)^{0.25} \tag{3.52}$$

$$h_c = 12.1\sqrt{v} \tag{3.53}$$

where v_r [ms^{-1}] is the relative velocity of the air, it is final air velocity on the surface of human body which is influenced by movements of the body; h_c [Wm^{-2}K^{-1}] is the coefficient of heat transfer via convection; for natural ventilation (v_r < 0.1ms^{-1}) – see equation (3.52), for forced ventilation (v_r < 0.25ms^{-1}) – see Equation (3.53); t_a [°C] is air temperature (Centnerová, 2001).

4.3.9 Conduction heat flux *K* [Wm^{-2}]

Conduction heat flux from human body to solid bodies is very low in contrast to other heat flows and in most cases it is neglected (Auliciems, et al., 2007).

4.3.10 Evaporative heat loss *E* [Wm^{-2}]

Evaporative heat loss from human body consists of heat loss via diffusion of skin E_d [Wm^{-2}] and heat loss via sweating E_{sw} [Wm^{-2}].

Evaporating via skin diffusion is invisible and continuous sweat evaporation which occurs all the time even in cold surroundings. On the contrary, visible sweating occurs only if the human body is in warm surroundings or during higher activity. Maximal heat loss via sweating can be reached when the skin is completely wet. Acceptable humidification is about 25% of skin surface for moderately active persons.

$$E_d = 3.05\times10^{-3}\left(p_{ws} - p_{wa}\right) \tag{3.54}$$

$$p_{ws} = 256t_s - 3373 \tag{3.55}$$

$$\left(E_{sw}\right)_{\max} = f_{pcl}h_e\left(p_{ws} - p_{wa}\right) \tag{3.56}$$

$$f_{pcl} = \frac{1}{1+0.143\frac{h_c}{h_{cl}}} \tag{3.57}$$

$$h_e = LRh_c \tag{3.58}$$

$$E_{sw} = 0.42\left(M - W - 58.15\right) \tag{3.59}$$

where p_{ws} [Pa] partial pressure of saturated water vapour at skin temperature, for 27 °C < t_s < 37 °C is valid equation (3.55); p_{wa} [Pa] is the partial pressure of water vapour in the air; f_{pcl} [-] is the coefficient of moisture vapour transmission through clothing, for porous clothing the equation (3.57) is valid; h_e [$Wm^{-2}Pa^{-1}$] is the coefficient of heat transfer at sweat evaporation; LR [$°CkPa^{-1}$] is the Lewis ratio for common interior parameters LR = 16.5 $°CkPa^{-1}$.

Equation (3.59) is valid for 1 met < M < 3 met. If the skin is completely wet, heat loss via skin diffusion is not considered and heat loss via sweating is calculated according (3.56) (Centnerová, 2001).

4.3.11 Heat loss via breathing [Wm^{-2}]

Heat loss via breathing arises due to warming and moistening of inhaled air in respiratory tract. Two types of loss can be distinguished, sensible S_{res} [Wm^{-2}] and latent L_{res} [Wm^2] thermal loss.

$$S_{res} = 0,0014M\left(34 - t_a\right) \tag{3.60}$$

$$L_{res} = 1.72\times10^{-5}M\left(5867 - p_a\right) \tag{3.61}$$

where t_a [°C] is ambient air temperature; p_a [Pa] is the ambient water vapour pressure.

S_{res} is a small quantity in comparison with the latent loss. And in total, the sum of sensible and respiration heat loss is only significant at high activity and under normal sedentary it is less than 6 Wm^{-2} and can be neglected (Awbi, 1991).

4.3.12 Predicted mean vote (PMV)

The PMV is an index that predicts the mean value of the votes of a large group of persons according 7-point thermal sensation scale (see Table 4.3.).

Table 4.3. Seven-point thermal sensation scale (ISO 7730, 2005)

Degree	***Thermal sensation***
+3	Hot
+2	warm
+1	slightly warm
0	neutral
-1	slightly cool
-2	cool
-3	cold

This index is based on the heat balance of the human body. Thermal balance is obtained when the internal heat production in the body is equal to the loss of heat to the environment. In a moderate environment, the human thermoregulatory system will automatically attempt to modify skin temperature and sweat secretion to maintain heat balance (ISO 7730, 2005).

The mean vote (PMV) from a large number of laboratory studies has been correlated with the thermal load L and produced the following equation

$$\frac{\delta PMV}{\delta L} = 0.303e^{-0.036M} + 0.028 \tag{3.62}$$

Then, the calculation of PMV can be written as

$$PMV = \left[0.303e^{-0.036M} + 0.028\right]L \tag{3.63}$$

where L [W] is the heat balance of human with surroundings, i.e., difference between heat flow produced by organism and heat flow taken away from surroundings (see (3.64))

$$
\begin{aligned}
L = {} & (M - W) - 3.05\times10^{-3}\left[5733 - 6.99(M - W) - p_a\right] \\
& -0.42\left[(M - W) - 58.15\right] - 1.7\times10^{-5} M (5867 - p_a) \\
& -0.0014M (34 - t_a) - 3.96\times10^{-8} f_{cl}\left[(t_{cl} + 273)^4 - (\overline{t_r} + 273)^4\right] \\
& - f_{cl} h_c (t_{cl} - t_a)
\end{aligned}
\tag{3.64}
$$

$$
\begin{aligned}
t_{cl} = {} & 35.7 - 0.028(M - W) \\
& -I_{cl}\left\{3.96.10^{-8} f_{cl}\left[(t_{cl} + 273)^4 - (\overline{t_r} + 273)^4\right] + f_{cl} h_c (t_{cl} - t_a)\right\}
\end{aligned}
\tag{3.65}
$$

where M [W] is metabolism value; W [W] is mechanical work; p_w [Pa] is partial pressure of water vapor in the air; t_a [°C] is the air temperature; f_{cl} [-] is ratio of the body surface covered with clothing and naked body; t_{cl} [°C] is the temperature of the clothing; $\overline{t_r}$ [°C] is the mean radiant temperature; h_c [$Wm^{-2}K^{-1}$] is the coefficient of flux heat transfer; I_{cl} [clo] is the thermal insulation of clothing.

Equation (3.65) is implicit and may be solved via iteration methods (Auliciems, et al., 2007), (ISO 7730, 2005).

4.3.13 Predicted percentage dissatisfied (PPD)

The PMV predicts the mean value of the thermal votes of a large group of people exposed to the same environment. But individual votes are scattered around this mean value and it is useful to be able to predict the number of people likely to feel uncomfortably warm or cool.

The PPD is an index that establishes a quantitative prediction of the percentage of thermally dissatisfied people who feel too cool or too warm. For the purposes, thermally dissatisfied people are those who will vote hot, warm, cool or cold on the 7-point thermal sensation scale given in Table 4.3.

With the PMV value determined, calculate the PPD using Equation (3.66), see Fig. 4.13.:

$$PPD = 100 - 95\,\mathrm{e}^{\left(-0.03353PMV^4 - 0.2179PMV^2\right)} \tag{3.66}$$

where *PMV* [-] is predicted mean vote index.

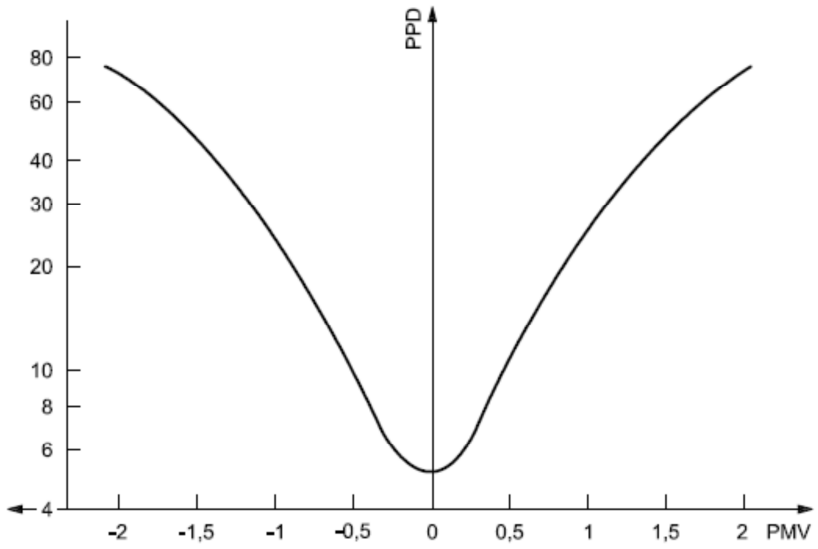

Fig. 4.13. PPD as function of PMV (ISO 7730, 2005)

The PPD predicts the number of thermally dissatisfied persons among a large group of people. The rest of the group will feel thermally neutral, slightly warm or slightly cool. (ISO 7730, 2005)

4.3.14 Local thermal discomfort

Draught

The discomfort due to draught may be expressed as the percentage of people predicted to be bothered by draught. Calculate the draught rate (*DR*) using Equation (3.67) (model of draught):

$$DR = \left(34 - t_{a,l}\right)\left(\overline{v}_{a,l} - 0.05\right)^{0.62}\left(0.37\overline{v}_{a,l}Tu + 3.14\right) \tag{3.67}$$

where $t_{a,l}$ [°C] is the local air temperature; $v_{a,l}$ [ms^{-1}] is the local mean air velocity (< 0.5 ms^{-1}); T_u [%] is the local turbulence intensity, 10 % to 60 % (if unknown, 40 % may be used). For $v_{a,l}$ < 0,05 ms^{-1} use $v_{a,l}$ = 0.05 ms^{-1}. For DR > 100% use DR = 100 %.

The model applies to people at light, mainly sedentary activity with a thermal sensation for the whole body close to neutral and for prediction of draught at the neck. At the level of arms and feet, the model could overestimate the predicted draught rate. The sensation of draught is lower at activities higher than sedentary (> 1.2 met) and for people feeling warmer than neutral. (ISO 7730, 2005)

Vertical air temperature difference

A high vertical air temperature difference between head and ankles can cause discomfort. The percentage dissatisfied (PD) is a function of the vertical air temperature difference between head and ankles. People are less sensitive under decreasing temperatures. Determine the PD using Equation

$$PD = \frac{100}{1 + e^{5.76 - 0.856 \Delta t_{a,v}}} \tag{3.68}$$

where PD [%] is percentage dissatisfied, $\Delta t_{a,v}$ [°C] is vertical air temperature difference between head and feet. (ISO 7730, 2005)

Warm or cool floors

If the floor is too warm or too cool, the occupants could feel uncomfortable owing to thermal sensation of their feet. For people wearing light indoor shoes, it is the temperature of the floor rather than the material of the floor covering which is important for comfort.

For people sitting or lying on the floor, similar values may be used. Determine the PD using Equation (3.69)

$$PD = 100 - 94 e^{-1.387 + 0.118 t_f - 0.0025 t_f^2} \tag{3.69}$$

where PD [%] is percentage dissatisfied; t_f [°C] is floor temperature. (ISO 7730, 2005)

Radiant asymmetry

Radiant asymmetry Δt_{pr} can also cause discomfort. People are most sensitive to radiant asymmetry caused by warm ceilings or cool walls (windows). Determine the predicted dissatisfied (*PD*) using Equations (3.70) to (3.73)

a) Warm ceiling

$$PD = \frac{100}{1 + e^{2.84 - 0.174\Delta t_{pr}}} - 5.5 \qquad (3.70)$$

where PD [%] is percentage dissatisfied, Δt_{pr} [°C] is radiant temperature asymmetry and should be $\Delta t_{pr} < 23$°C.

b) Cool wall

$$PD = \frac{100}{1 + e^{6.61 - 0.345\Delta t_{pr}}} \qquad (3.71)$$

where PD [%] is percentage dissatisfied, Δt_{pr} [°C] is radiant temperature asymmetry and should be $\Delta t_{pr} < 15$°C.

c) Cool ceiling

$$PD = \frac{100}{1 + e^{9.93 - 0.5\Delta t_{pr}}} \qquad (3.72)$$

where PD [%] is percentage dissatisfied, Δt_{pr} [°C] is radiant temperature asymmetry and should be $\Delta t_{pr} < 15$°C.

d) Warm wall

$$PD = \frac{100}{1 + e^{3.72 - 0.052\Delta t_{pr}}} - 3.5 \qquad (3.73)$$

where PD [%] is percentage dissatisfied, Δt_{pr} [°C] is radiant temperature asymmetry and should be $\Delta t_{pr} < 35$°C. (ISO 7730, 2005)

4.4 Mean radiant temperature (MRT)

The mean radiant temperature is the uniform temperature of an imaginary enclosure in which radiant heat transfer from the human body is equal to the radiant heat transfer in the actual non-uniform enclosure. The mean radiant temperature can be measured by instruments which allow the generally heterogeneous radiation from the walls of an actual enclosure to be "integrated" into a mean value such as black-globe thermometer, two-sphere radiometer or constant-air-temperature sensor (all instruments are discussed further in this chapter). The black globe thermometer is a device frequently used in order to derive an approximate value of the mean radiant temperature from the observed simultaneous values of the globe temperature, t_g, and the temperature and the velocity of the air surrounding the globe.

The accuracy of measurement of the mean radiant temperature obtained using this appliance varies considerably according to the type of environment being considered and the accuracy of measurement of the temperatures of the globe and the air and the velocity of the air. The actual measuring accuracy shall be indicated wherever it exceeds the tolerances specified in ISO 7726.

The mean radiant temperature is defined in relation to the human body. The spherical shape of the globe thermometer can give a reasonable approximation of the shape of the body in the case of a seated person. An ellipsoid-shaped sensor gives a closer approximation to the human shape both in the upright position and the seated position. The mean radiant temperature can also be calculated from measured values of the temperature of the surrounding walls and the size of these walls and their position in relation to a person (calculation of geometrical shape factors).

The mean radiant temperature may also be estimated for the plane radiant temperature in six opposite directions weighted according to the projected area factors for a person. Similarly, it can be estimated from the measurement of the radiant flux from different directions. Any other measuring device or calculation method which allows the mean radiant temperature to be determined with the accuracy specified in ISO 7726 may be used. (ISO 7726, 1998)

The **plane radiant temperature** is the uniform temperature of an enclosure where the radiance on one side of a small plane element is the same as in the non-uniform actual environment. The so-called "net" radiometer is an instrument which is often used to measure this quantity. With this it is possible to determine the plane radiant temperature from the net radiation exchanged between the environment and the surface element and the surface temperature of the radiometer.

A radiometer with a sensor consisting of a reflective disc (polished) and an absorbent disc (painted black) can also be used.

The plane radiant temperature can also be calculated from the surface temperatures of the environment and the shape factors between the surfaces and the plane element.

The radiant temperature asymmetry is the difference between the plane radiant temperatures of the two opposite sides of a small plane element. The concept of radiant temperature asymmetry is used when the mean radiant temperature does not completely describe the radiative environment, for instance when the radiation is coming from opposite parts of the space with appreciable thermal heterogeneities. The asymmetric radiant field is defined in relation to the position of the plane element used as a reference. It is, however, necessary to specify exactly the position of the latter by means of the direction of the normal to this element. The radiant temperature asymmetry is measured or calculated from the measured value of the plane radiant temperature in the two opposing directions.

Any other device or method which allows the radiant temperature asymmetry or the plane radiant temperature to be measured or calculated with the same accuracy as indicated below may be used (ISO 7726, 1998).

Instruments for measurement of the mean radiant temperature

Mean radiant temperature can be calculated from radiant fluxes incident to the human body. It is possible to calculate radiant fluxes from knowing the locations, dimensions, temperature of surrounding surfaces and each surface emissivity. While it is possible to calculate these fluxes, this method becomes very complex in case of real environment containing large number of surfaces with different shapes and temperatures. Instead of this

calculating method it is preferable to use a device that can measure mean radiant temperature indirectly but easily.

The ISO 7726 uses so-called **black-globe thermometer** consisting of a black globe in the centre of which is placed a temperature sensor; for instance a thermocouple, resistant probe or semiconductor thermometer. Black-globe thermometer has usually 15 cm in diameter and its surface is coated with matt black layer to absorb the radiation from surroundings. (ISO 7726, 1998)

Principle of black-globe thermometer measurement

The black globe shall be placed in the actual enclosure where the mean radiant temperature T_r, is to be measured. The globe tends towards a thermal balance under the effect of the exchanges due to the radiation coming from the different heat sources of the enclosure and under the effect of the exchanges by convection. The temperature of the globe at the thermal balance allows T_r to be determined. The temperature sensor placed inside the globe allows the mean temperature of the latter to be measured. In fact, the temperature of the inner surface of the globe (thin) and the temperature of the air outside the globe (closed space) are practically equal to the mean external temperature of the globe.

The balance of the thermal exchanges between the globe and the environment is given by the equation

$$q_r + q_c = 0 \tag{3.74}$$

where q_r [Wm^{-2}] is the heat exchange by radiation between the walls of the enclosure and the globe; q_c [Wm^{-2}] is the heat exchange by convection between the air and the globe.

The heat transfer by radiation between the walls of the enclosure, characterized by the mean radiant temperature, and the globe is expressed as follows:

$$q_r = \varepsilon_g \sigma \left(\overline{T}_r^4 - \overline{T}_g^4 \right) \tag{3.75}$$

Where e_g [-] is the emissivity of the black globe; σ [$Wm^{-2}K^{-4}$] is the Stefan-Boltzmann constant $\sigma = 5.6693 \times 10^{-8}$ $Wm^{-2}K^{-4}$; T_r [K] is the mean radiant temperature; T_g [K] is the temperature of the black globe.

The heat transfer by convection between the air contained in the enclosure and the globe is given by the equation:

$$q_c = h_{cg}\left(T_a - T_g\right) \tag{3.76}$$

where h_{cg} [$Wm^{-2}K^{-1}$] is the coefficient of heat transfer by convection at the level of the globe. In the case of natural convection

$$h_{cg} = 1.4\left(\frac{\Delta T}{D}\right)^{1/4} \tag{3.77}$$

and in the case of forced convection

$$h_{cg} = 6.3\left(\frac{v_a^{0.6}}{D^{0.4}}\right) \tag{3.78}$$

where D [m] is the diameter of the globe; v_a [ms^{-1}] is the air velocity at the level of the globe.

The thermal balance of the black globe is expressed as follows:

$$\varepsilon_g \sigma\left(\overline{T}_r^4 - \overline{T}_g^4\right) + h_{cg}\left(T_a - T_g\right) = 0 \tag{3.79}$$

The mean radiant temperature is given by

$$\overline{T}_r = \sqrt[4]{T_g^4 + \frac{h_{cg}}{\varepsilon_g \sigma}\left(T_g - T_a\right)} \tag{3.80}$$

By natural convection, one obtains:

$$\overline{t}_r = \left[\left(t_g + 273\right)^4 + \frac{0.25\times10^8}{\varepsilon_g}\left(\frac{\left|t_g - t_a\right|}{D}\right)^{1/4} \times\left(t_g - t_a\right)\right]^{1/4} - 273 \tag{3.81}$$

In the case of the standard globe D = 0.15 m, ε_g = 0.95 (matt black paint) and Equation (3.81) becomes

$$\overline{t}_r = \left[\left(t_g + 273\right)^4 + 0.4\times10^8\left|t_g - t_a\right|^{1/4} \times\left(t_g - t_a\right)\right]^{1/4} - 273 \tag{3.82}$$

By forced convection, one obtains

$$\overline{t_r} = \left[\left(t_g + 273 \right)^4 + \frac{1.1 \times 10^8 \times v_a^{0.6}}{\varepsilon_g \times D^{0.4}} \left(t_g - t_a \right) \right]^{1/4} - 273 \qquad (3.83)$$

or for the standard globe

$$\overline{t_r} = \left[\left(t_g + 273 \right)^4 + 2.5 \times 10^8 \times v_a^{0.6} \left(t_g - t_a \right) \right]^{1/4} - 273 \qquad (3.84)$$

In practice, it is this expression which will be most frequently used to calculate the mean radiant temperature. It is valid only for a standard globe by forced convection. (ISO 7726, 1998)

Black globe thermometer has some precautions that must be taken:

- In case of heterogeneous radiation, the black-globe thermometer measurement in single point is insufficient and three black globes must be used (places at the level of the head, the abdomen and ankles of occupant).
- The response time of black-globe thermometer is about 20 min to 30 min.
- Black-globe thermometer represents only approximation between occupant and a globe.
- When using globe thermometer exposed to effect of the short-wave radiation (sun), the surface absorptivity must be adjusted according to cloths.

Two-sphere radiometer

In this method, two spheres with different emissivities (one black and one polished) are used. As the two spheres are heated to the same temperature, they will be exposed to the same convective heat loss. As the emittance of the black sphere is higher than the polished one, there is a difference in the heat supply to the two spheres and this is a measure of the radiation.

To estimate the mean radiant temperature, the emissivity and temperature of the sensors are required.

The mean radiant temperature is calculated from the equation:

$$\bar{T}_r^4 = T_s^4 + \frac{P_p - P_b}{\sigma\left(\varepsilon_b - \varepsilon_p\right)} \tag{3.85}$$

where T_r [K] is the mean radiant temperature; T_s [K] is the sensor temperature; P_p [Wm^{-2}] is the heat supply to the polished sensor; P_b [Wm^{-2}] is the heat supply to the black sensor; e_p is the emissivity of the polished sensor; ε_b [-] is the emissivity of the black sensor; σ [$Wm^{-2}K^{-4}$] is the Stefan-Boltzmann constant $\sigma = 5.6693\times10^{-8}$ $Wm^{-2}K^{-4}$.

Instead of a sphere, an ellipsoid shaped sensor, which is closer to the shape of the human body, can be used (ISO 7726, 1998).

Constant-air-temperature sensor

In this method, a sensor (sphere, ellipsoid) is controlled at the same temperature as the surrounding air temperature; there being no convection heat loss and the necessary heat supply (cooling supply) to the sensor being equal to the radiant heat loss (or gain).

The mean radiant temperature is calculated by equation (3.86):

$$\bar{T}_r^4 = T_s^4 - \frac{P_s}{\sigma\varepsilon_s} \tag{3.86}$$

where T_r [K] is the mean radiant temperature; T_s [K] is the sensor temperature; P_s [Wm^{-2}] is the heat supply (cooling supply) to the sensor; ε_s [-] is the emissivity of the sensor; σ [$Wm^{-2}K^{-4}$] is the Stefan-Boltzmann constant $\sigma = 5.6693\times10^{-8}$ $Wm^{-2}K^{-4}$ (ISO 7726, 1998).

Net radiometer

The net radiometer consists of a small black plane element with a heat flow meter (thermopile) between the two sides of the element. The net heat flow between the two sides is equal to the difference between the radiant heat transfers at the level of the two sides of the element. The measuring elements are usually covered by a thin polyethylene sphere to decrease the effect of air velocity. Occasionally the net radiometer is equipped with an adaptor for unidirectional measurement. The net radiation is given by the

following equation:

$$P = \sigma\left(T_{pr1}^4 - T_{pr2}^4\right) \tag{3.87}$$

where P [Wm^2] is the net radiation measured; T_{pr1} [K] is the plane radiant temperature, side 1; T_{pr2} [K] is the plane radiant temperature, side 2; σ [Wm^{-2}K^{-4}] is the Stefan-Boltzmann constant $\sigma = 5.6693\times10^{-8}$ Wm^{-2}K^{-4}.

The radiant temperature asymmetry is equal to:

$$\Delta t_{pr} = T_{pr1} - T_{pr2} \tag{3.88}$$

where Δt_{pr} [K] is the radiant temperature asymmetry.

This quantity is not measured directly by a net radiometer but has to be calculated.

Equation (3.87) can be written as:

$$P = 4\sigma T_n^3\left(T_{pr1} - T_{pr2}\right) \tag{3.89}$$

In the linear radiant heat transfer coefficient $\left(4\sigma T_n^3\right), T_n = 0.5\left(T_{pr1} - T_{pr2}\right)$, or with a closer approximation equal to the temperature of the net radiometer. On most net radiometers, T_n is easily measured. Thus the radiant temperature asymmetry is equal to:

$$\Delta t_{pr} = \frac{P}{4\sigma T_n^3} \tag{3.90}$$

where Δt_{pr} [K] is the radiant temperature asymmetry.

The linear radiant heat transfer coefficient is influenced by the temperature level given by T_n [K]. At a temperature level equal to 20 °C the coefficient is equal to 5.7 Wm^{-2}K^{-1} and for a temperature level equal to 50 °C the coefficient is equal to 7.6 Wm^{2}K^{-1}.
The following equation is valid only when the radiation heat transfer on one side of the net radiometer (P_1) is measured.

$$P_1 = \sigma T_{pr1}^4 - \sigma\varepsilon_s T_n^4 \tag{3.91}$$

where P_1 [Wm^{-2}] is the radiation measured at side 1; T_{pr1} [K] is the plane radiant

temperature, side 1; T_n [K] is the temperature of the net radiometer; ε_s is the emissivity of the sensor; σ [$Wm^{-2}K^{-4}$] is the Stefan-Boltzmann constant $\sigma = 5.6693 \times 10^{-8}$ $Wm^{-2}K^{-4}$.

For a black painted surface, the emissivity may be estimated to approximately 0.95.
The plane radiant temperature is then equal to

$$T_{pr1} = \sqrt[4]{0.95T_n^4 + \frac{P_1}{\sigma}} \tag{3.92}$$

To determine the radiant temperature asymmetry, it is also necessary to measure in the opposite direction and to calculate the corresponding plane radiant temperature (ISO 7726, 1998).

4.5 IR thermometers and pyrometers

Pyrometer is derived from the Greek root pyro, meaning fire. The term pyrometer was originally used to denote a device capable of measuring temperatures of objects above incandescence, objects bright to the human eye. The original pyrometers were non-contacting optical devices which intercepted and evaluated the visible radiation emitted by glowing objects. A modern and more correct definition would be any non-contacting device intercepting and measuring thermal radiation emitted from an object to determine surface temperature. Thermometer, also from a Greek root thermos, signifying hot, is used to describe a wide assortment of devices used to measure temperature. Thus a pyrometer is a type of thermometer. The designation radiation thermometer has evolved over the past decade as an alternative to pyrometer. Therefore the terms pyrometer and radiation thermometer are used interchangeably by many references. A radiation thermometer, in very simple terms, consists of an optical system and detector. The optical system focuses the energy emitted by an object onto the detector, which is sensitive to the radiation. The output of the detector is proportional to the amount of energy radiated by the target object (less the amount absorbed by the optical system), and the response of the detector to the specific radiation wavelengths. This output can be used to infer the objects temperature. The emittivity, or emittance, of the object is an important variable in converting the detector output into an accurate temperature signal.

Infrared radiation thermometers / pyrometers, by specifically measuring the energy being radiated from an object in the 0.7 to 20 μm wavelength range, are a subset of radiation thermometers. These devices can measure this radiation from a distance. There is no need for direct contact between the radiation thermometer and the object, as there is with thermocouples and resistance temperature detectors (RTDs). Radiation thermometers are suited especially to the measurement of moving objects or any surfaces that cannot be reached or cannot be touched. But the benefits of radiation thermometry have a price. Even the simplest of devices is more expensive than a standard thermocouple or resistance temperature detector (RTD) assembly, and installation cost can exceed that of a standard thermowell. The devices are rugged, but do require routine maintenance to keep the sighting path clear, and to keep the optical elements clean. Radiation thermometers used

for more difficult applications may have more complicated optics, possibly rotating or moving parts, and microprocessor-based electronics. There are no industry accepted calibration curves for radiation thermometers, as there are for thermocouples and RTDs. In addition, the user may need to seriously investigate the application, to select the optimum technology, method of installation, and compensation needed for the measured signal, to achieve the performance desired (Omega, 2008).

Emittance, emissivity, and the N Factor

In an earlier chapter, emittance was identified as a critical parameter in accurately converting the output of the detector used in a radiation thermometer into a value representing object temperature. The terms emittance and emissivity are often used interchangeably. There is, however, a technical distinction. Emissivity refers to the properties of a material; emittance to the properties of a particular object. In this latter sense, emissivity is only one component in determining emittance. Other factors, including shape of the object, oxidation and surface finish must be taken into account. The apparent emittance of a material also depends on the temperature at which it is determined, and the wavelength at which the measurement is taken. Surface condition affects the value of an object's emittance, with lower values for polished surfaces, and higher values for rough or matte surfaces. In addition, as materials oxidize, emittance tends to increase, and the surface condition dependence decreases. Representative emissivity values for a range of common metals and non-metals are given in Table 4.1. The basic equation used to describe the output of a radiation thermometer is:

$$V(T) = \varepsilon K T^N \tag{3.93}$$

where ε [-] is emittance, V [V] is thermometer output with temperature, K is constant, T [K] is object temperature, N [-] is factor ($N = 14388/(\lambda T)$), λ [m] is equivalent wavelength. A radiation thermometer with the highest value of N (shortest possible equivalent wavelength) should be selected to obtain the least dependence on target emittance changes. The benefits of a device with a high value of N extend to any parameter that affects the output V. A dirty optical system, or absorption of energy by gases in the sighting path, has less effect on an indicated temperature if N has a high value. The values for the

emissivities of almost all substances are known and published in reference literature. However, the emissivity determined under laboratory conditions seldom agrees with actual emittance of an object under real operating conditions. For this reason, one is likely to use published emissivity data when the values are high. As a rule of thumb, most opaque non-metallic materials have a high and stable emissivity (0.85 to 0.90). Most unoxidized, metallic materials have a low to medium emissivity value (0.2 to 0.5). Gold, silver and aluminium are exceptions, with emissivity values in the 0.02 to 0.04 range. The temperature of these metals is very difficult to measure with a radiation thermometer. One way to determine emissivity experimentally is by comparing the radiation thermometer measurement of a target with the simultaneous measurement obtained using a thermocouple or RTD. The difference in readings is due to the emissivity, which is, of course, less than one. For temperatures up to 260 °C emissivity values can be determined experimentally by putting a piece of black masking tape on the target surface. Using a radiation pyrometer set for an emissivity of 0.95, measure the temperature of the tape surface (allowing time for it to gain thermal equilibrium). Then measure the temperature of the target surface without the tape. The difference in readings determines the actual value for the target emissivity. Many instruments now have calibrated emissivity adjustments. The adjustment may be set to a value of emissivity determined from tables or experimentally, as described in the preceding paragraph. For highest accuracy, independent determination of emissivity in a lab at the wavelength at which the thermometer measures, and possibly at the expected temperature of the target, may be necessary. Emissivity values in tables have been determined by a pyrometer sighted perpendicular to the target. If the actual sighting angle is more than 30 or 40 degrees from the normal to the target, lab measurement of emissivity may be required. In addition, if the radiation pyrometer sights through a window, emissivity correction must be provided for energy lost by reflection from the two surfaces of the window, as well as absorption in the window. For example, about 4 % of radiation is reflected from glass surfaces in the infrared ranges, so the effective transmittance is 0.92. The loss through other materials can be determined from the index of refraction of the material at the wavelength of measurement. The uncertainties concerning emittance can be reduced using short wavelength or ratio radiation

thermometers. Short wavelengths, around 0.7 μm, are useful because the signal gain is high in this region. The higher response output at short wavelengths tends to swamp the effects of emittance variations. The high gain of the radiated energy also tends to swamp the absorption effects of steam, dust or water vapour in the sight path to the target. For example, setting the wavelength at such a band will cause the sensor to read within ±5 to ±10 degrees of absolute temperature when the material has an emissivity of 0.9 (±0.05). This represents about 1 % to 2 % accuracy (Omega, 2008).

Types of Radiation Thermometers

Historically, as shown in Fig. 4.14, a radiation thermometer consisted of an optical system to collect the energy emitted by the target; a detector to convert this energy to an electrical signal; an emittance adjustment to match the thermometer calibration to the specific emitting characteristics of the target, and ambient temperature compensation circuit, to ensure that temperature variations inside the thermometer due to ambient conditions did not affect accuracy.

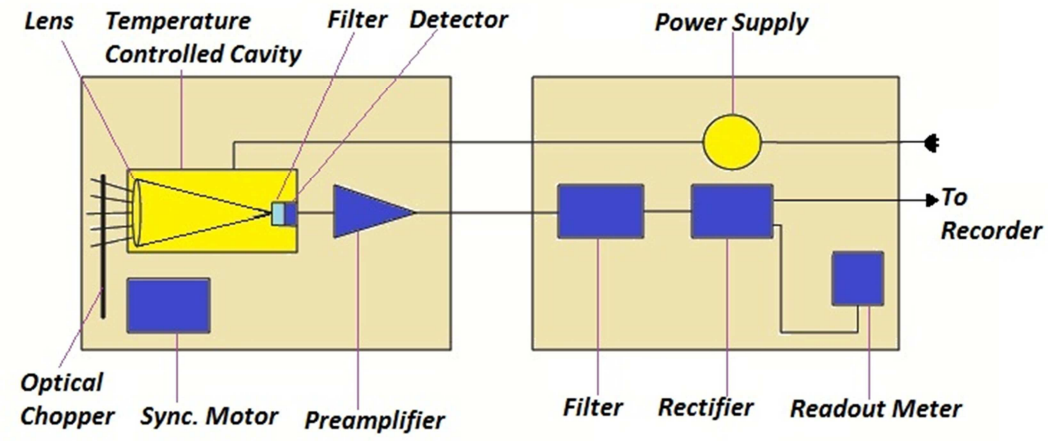

Fig. 4.14. Traditional infrared thermometer (Omega, 2008)

The modern radiation thermometer is still based on this concept. However the technology has become more sophisticated to widen the scope of the applications that can be handled. For example, the number of available detectors has greatly increased, and, thanks to

selective filtering capabilities, these detectors can more efficiently be matched to specific applications, improving measurement performance. Microprocessor-based electronics can use complex algorithms to provide real time linearization and compensation of the detector output for higher precision of measured target temperature. Microprocessors can display instantaneous measurements of several variables (such as current temperature, minimum temperature measured, maximum temperature measured, average temperature or temperature differences) on integral LCD display screens. A convenient classification of radiation thermometers is as follows:

- broadband radiation thermometers/pyrometers;
- narrow band radiation thermometers/pyrometers;
- ratio radiation thermometers/pyrometers;
- optical pyrometers;
- fibre optic radiation thermometers/pyrometers.

These classifications are not rigid. For example, optical pyrometers can be considered a subset of narrow band devices. Fibre optic radiation thermometers, to be discussed in detail in another section, can be classified as wide band, narrow band, or ratio devices. Likewise, infrared radiation thermometers can be considered subsets of several of these classes. (Omega, 2008)

Broadband Radiation

Broadband radiation thermometers typically are the simplest devices, cost the least, and can have a response from 0.3 μm wavelength to an upper limit of 2.5 to 20 μm. The low and high cut-offs of the broadband thermometer are a function of the specific optical system being used. They are termed broadband because they measure a significant fraction of the thermal radiation emitted by the object, in the temperature ranges of normal use. Broadband thermometers are dependent on the total emittance of the surface being measured.

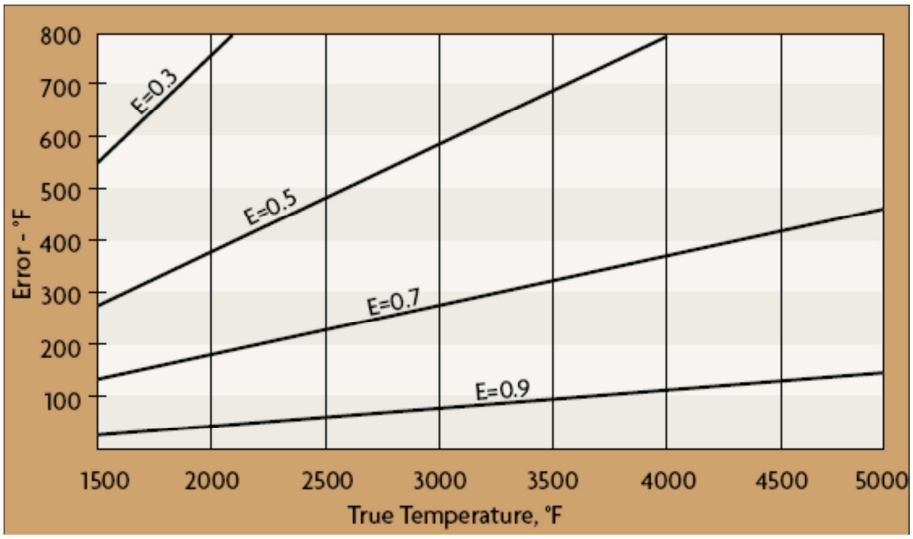

Fig. 4.15. Effect of non-blackbody emissivity on IR thermometer error (Omega, 2008)

Fig. 4.15 shows the error in reading for various emissivities and temperatures when a broadband device is calibrated for a blackbody. An emissivity control allows the user to compensate for these errors, so long as the emittance does not change. The path to the target must be unobstructed. Water vapour, dust, smoke, steam and radiation absorptive gases present in the atmosphere can attenuate emitted radiation from the target and cause the thermometer to read low. The optical system must be kept clean, and the sighting window protected against any corrosives in the environment. Standard ranges include 0 to 1000 °C, and 500 to 900 °C. Typical accuracy is 0.5 to 1 % full scale. (Omega, 2008)

Narrow Band Radiation

As the name indicates, narrow band radiation thermometers operate over a narrow range of wavelengths. Narrow band devices can also be referred to as single colour thermometers/pyrometers. The specific detector used determines the spectral response of the particular device. For example, a thermometer using a silicon cell detector will have a response that peaks at approximately 0.9 μm, with the upper limit of usefulness being about 1.1 μm. Such a device is useful for measuring temperatures above 600 °C. Narrow band thermometers routinely have a spectral response of less than 1 μm. Narrow band

thermometers use filters to restrict response to a selected wavelength. Probably the most important advance in radiation thermometry has been the introduction of selective filtering of the incoming radiation, which allows an instrument to be matched to a particular application to achieve higher measurement accuracy. This was made possible by the availability of more sensitive detectors and advances in signal amplifiers. Common examples of selective spectral responses are 8 to 14 μm, which avoids interference from atmospheric moisture over long paths; 7.9 μm, used for the measurement of some thin film plastics; 5 μm, used for the measurement of glass surfaces; and 3.86 μm, which avoids interference from car bon dioxide and water vapour in flames and combustion gases. The choice of shorter or longer wavelength response is also dictated by the temperature range. The peaks of radiation intensity curves move towards shorter wavelengths as temperature increases, as shown in Fig. 4.16. (Omega, 2008)

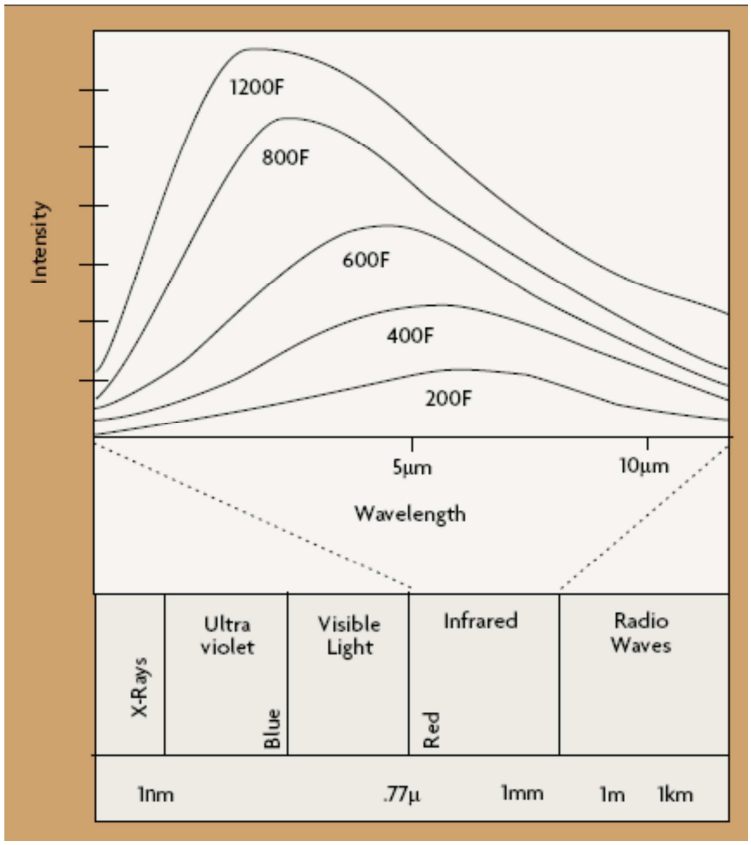

Fig. 4.16. Blackbody radiation in the infrared (Omega, 2008)

Applications that don't involve such considerations may still benefit from a narrow spectral response around 0.7 µm. While emissivity doesn't vary as much as you decrease the wavelength, the thermometer will lose sensitivity because of the reduced energy available. Narrow band thermometers with short wavelengths are used to measure high temperatures, greater than 500 °C, because radiation energy content increases as wavelengths get shorter. Long wavelengths are used for low temperatures -45.5 °C. Narrow band thermometers range from simple hand-held devices, to sophisticated portables with simultaneous viewing of target and temperature, memory and printout capability, to online, fixed mounted sensors with remote electronics having PID control. Typical accuracy is 0.25 % to 2 % of full scale. (Omega, 2008)

Ratio Radiation

Also called two-colour radiation thermometers, these devices measure the radiated energy of an object between two narrow wavelength bands, and calculate the ratio of the two energies, which is a function of the temperature of the object. Originally, these were called two colour pyrometers, because the two wavelengths corresponded to different colours in the visible spectrum (for example, red and green). Many people still use the term two-colour pyrometers today, broadening the term to include wavelengths in the infrared. The temperature measurement is dependent only on the ratio of the two energies measured, and not their absolute values as shown in Fig. 4.17.

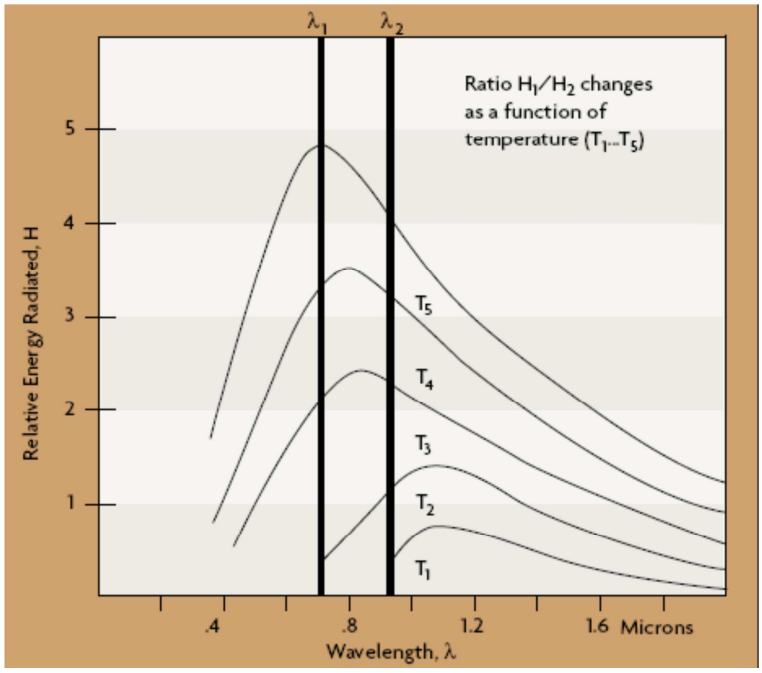

Fig. 4.17. The two-color IR thermometer (Omega, 2008)

Any parameter, such as target size, which affects the amount of energy in each band by an equal percentage, has no effect on the temperature indication. This makes a ratio thermometer inherently more accurate. The ratio technique may eliminate, or reduce, errors in temperature measurement caused by changes in emissivity, surface finish, and energy absorbing materials, such as water vapour, between the thermometer and the target.

These dynamic changes must be seen identically by the detector at the two wavelengths being used. Emissivity of all materials does not change equally at different wavelengths. Materials for which emissivity does change equally at different wavelengths are called gray bodies. Materials for which this is not true are called non-gray bodies. In addition, not all forms of sight path obstruction attenuate the ratio wavelengths equally. For example, if there are particles in the sight path that have the same size as one of the wavelengths, the ratio can become unbalanced. Phenomena which are non-dynamic in nature, such as the non-gray bodiness of materials, can be dealt with by biasing the ratio of the wavelengths accordingly. This adjustment is called slope. The appropriate slope setting must be determined experimentally. Fig. 4.18 shows a schematic diagram of a simple ratio radiation thermometer.

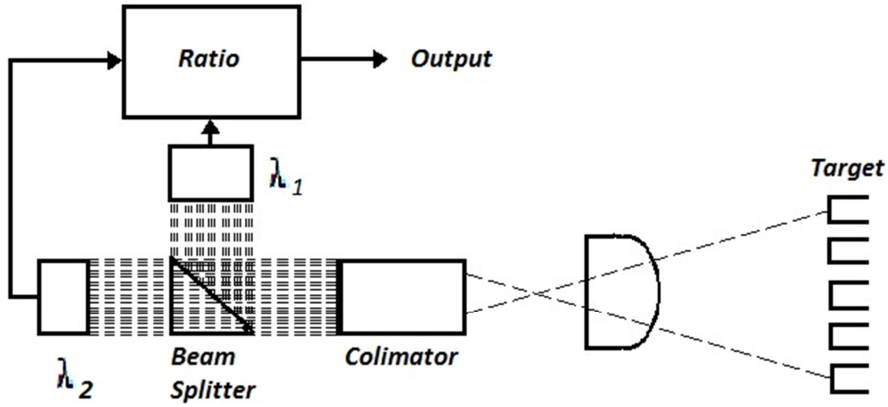

Fig. 4.18. Beam-splitting in the ratio IR thermometer (Omega, 2008)

A multi-wavelength device is schematically represented in Fig. 4.19. These devices employ a detailed analysis of the target's surface characteristics regarding emissivity with regard to wavelength, temperature, and surface chemistry. With such data, a computer can use complex algorithms to relate and compensate for emissivity changes at various conditions.

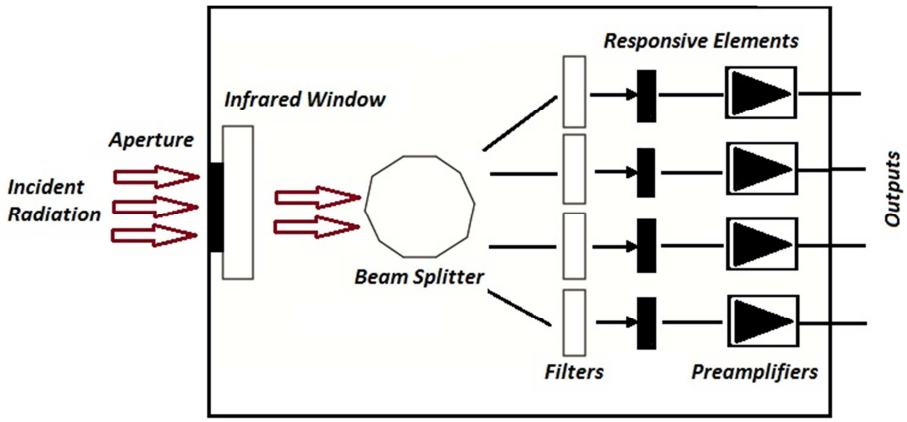

Fig. 4.19. Schematic of a multispectral IR thermometer (Omega, 2008)

The system described in Fig. 4.19 makes parallel measurement possible in four spectral channels in the range from 1 to 25 μm. The detector in this device consists of an optical system with a beam splitter, and interference filters for the spectral dispersion of the incident radiation. This uncooled thermometer was developed for gas analysis (Norkus, et al., 1966).

Optical Pyrometers

Optical pyrometers measure the radiation from the target in a narrow band of wavelengths of the thermal spectrum. The oldest devices use the principle of optical brightness in the visible red spectrum around 0.65 μm. These instruments are also called single color pyrometers. Optical pyrometers are now available for measuring energy wavelengths that extend into the infrared region. The term single color pyrometers has been broadened by some authors to include narrow band radiation thermometers as well. Some optical designs are manually operated as shown in Fig. 4.20.

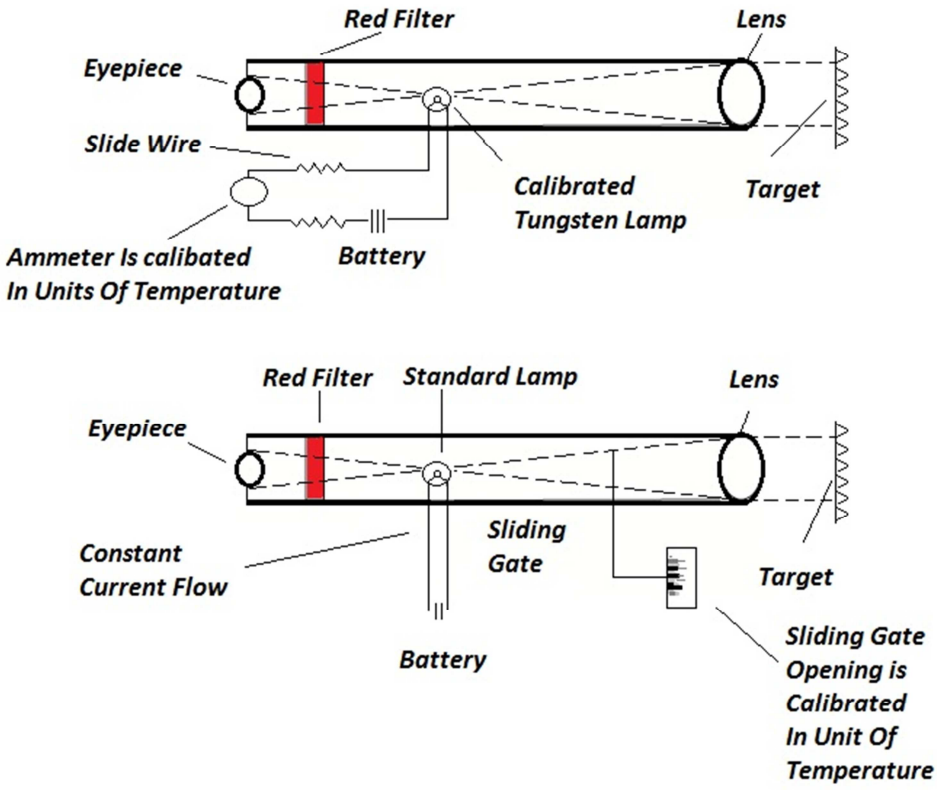

Fig. 4.20. Optical pyrometer by visual comparison (Omega, 2008)

The operator sights the pyrometer on target. At the same time he/she can see the image of an internal lamp filament in the eyepiece. In one design, the operator adjusts the power to the filament, changing its color, until it matches the color of the target. The temperature of the target is measured based upon power being used by the internal filament. Another design maintains a constant current to the filament and changes the brightness of the target by means of a rotatable energy-absorbing optical wedge. The object temperature is related to the amount of energy absorbed by the wedge, which is a function of its annular position. Automatic optical pyrometers, sensitized to measure in the infrared region, also are available. These instruments use an electrical radiation detector, rather than the human eye. This device operates by comparing the amount of radiation emitted by the target with that emitted by an internally controlled reference source. The instrument output is proportional to the difference in radiation between the target and the reference. A chopper, driven by a

motor, is used to alternately expose the detector to incoming radiation and reference radiation. In some models, the human eye is used to adjust the focus. In Fig. 4.21 there is a schematic of an automatic optical pyrometer with a dichroic mirror.

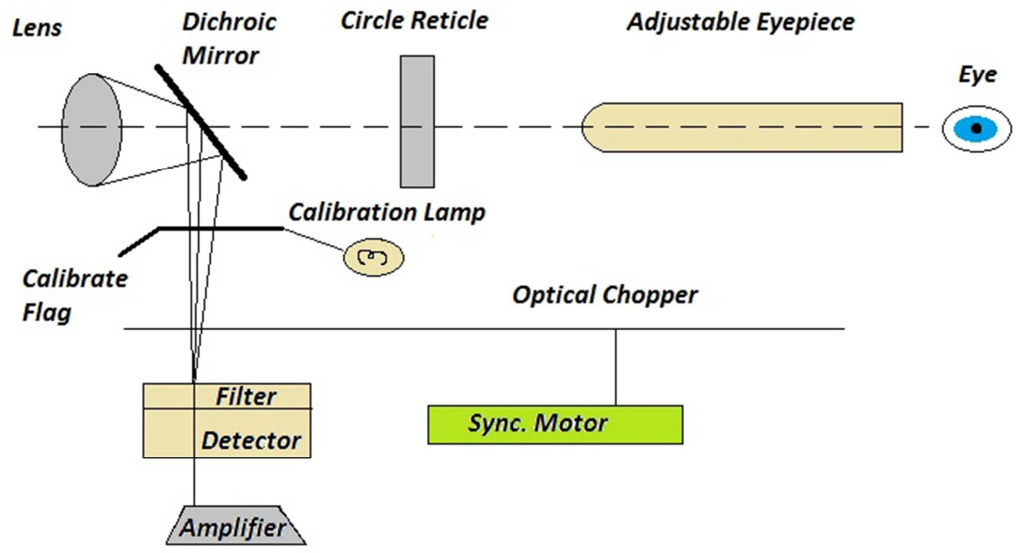

Fig. 4.21. An automatic optical pyrometer (Omega, 2008)

Radiant energy passes through the lens into the mirror, which reflects infrared radiation to the detector, but allows visible light to pass through to an adjustable eyepiece. The calibrate flap is solenoid-operated from the amplifier, and when actuated, cuts off the radiation coming through the lens, and focuses the calibrate lamp on to the detector. The instrument may have a wide or narrow field of view. All the components can be packaged into a gun-shaped, hand-held instrument. Activating the trigger energizes the reference standard and read-out indicator. Optical pyrometers have typical accuracy in the 1 % to 2 % of full scale range. (Omega, 2008)

Fiber Optic Radiation

Although not strictly a class unto themselves, these devices use a light guide, such as a flexible transparent fiber, to direct radiation to the detector. The spectral response of these fibers extends to about 2 μm, and can be useful in measuring object temperatures to as low

as 100 °C. Obviously, these devices are particularly useful when it is difficult or impossible to obtain a clear sighting path to the target, as in a pressure chamber. (Omega, 2008)

Design and Construction

The manufacturer of the radiation thermometer selects the detector and optical elements to yield the optimum compromise based upon the conflicting parameters of cost, accuracy, speed of response, and usable temperature range. The user should be cognizant of how the different detectors and optical elements affect the range of wavelengths over which a thermometer responds. The spectral response of a pyrometer will determine whether a usable measurement is possible, given the presence of atmospheric absorption, or reflections from other objects, or trying to measure the temperature of materials like glass or plastics. (Omega, 2008)

Detectors

Thermal, photon, and pyroelectric detectors are typically used in radiation pyrometers. Radiation detectors are strongly affected by ambient temperature changes. High accuracy requires compensation for this ambient drift. The responsivity of a radiation detector may be specified in terms of either the intensity of radiation, or the total radiant power incident upon the detector. When the image formed by the target surface area is larger than the exposed area of the detector, the entire detector surface is subjected to a radiation intensity proportional to the brightness of the target. The total radiant power absorbed by the detector then depends on the area of its sensitive surface. The actual size of the effective target area is determined by the magnification of the optical system. Sensitivity typically is not uniform over the surface of a detector, but this has no effect if the target brightness is uniform. If substantial temperature differences occur on the target surface within the patch imaged on the detector, an ambiguously weighted average will result. In the case of total radiant power, the area of the target surface imaged on the detector is limited by a stop optically conjugate to the detector. This area can be made arbitrarily small. As a result, local temperatures can be measured on the target body surface. The responsivity of the

detector may depend on the location of this target source image on the detector surface. Constancy of calibration will depend on maintaining the element in a fixed position with respect to the optical system.

Thermal detectors are the most commonly used radiation thermometer detectors. Thermal detectors generate an output because they are heated by the energy they absorb. These detectors have lower sensitivity compared to other detector types, and their outputs are less affected by changes in the radiated wavelengths. The speed of response of thermal detectors is limited by their mass. Thermal detectors are blackened so that they will respond to radiation over a wide spectrum (broadband detectors). They are relatively slow, because they must reach thermal equilibrium whenever the target temperature changes. They can have time constants of a second or more, although deposited detectors respond much faster.

A **thermopile** consists of one or more thermocouples in series, usually arranged in a radial pattern so the hot junctions form a small circle, and the cold junctions are maintained at the local ambient temperature. Advanced thin film thermopiles achieve response times in the 10 to 15 millisecond range. Thermopiles also increase the output signal strength and are the best choice for broadband thermometers. Ambient temperature compensation is required when thermopile detectors are used. A thermostatically controlled thermometer housing is used to avoid ambient temperature fluctuations for low temperature work.

Bolometers are essentially resistance thermometers arranged for response to radiation. A sensing element with a thermistor, metal film, or metal wire transducer is often called a bolometer.

Photon detectors release electric charges in response to incident radiation. In lead sulfide and lead selenide detectors, the release of charge is measured as a change in resistance. In silicon, germanium, and indium antimonide, the release of charge is measured as a voltage output. Photon detectors have a maximum wavelength beyond which they will not respond. The peak response is usually at a wavelength a little shorter than the cutoff wavelength. Many radiation thermometers use photon detectors rather than thermal detectors, even though they measure over a narrower band of wavelength. This is because within the range of useful wavelengths, the photon detectors have a sensitivity 1000 to

100,000 times that of the thermal detector. Response time of these detectors is in microseconds. They are instable at longer wavelengths and higher temperatures. They are often used in narrow band thermometers, or broadband thermometers at medium temperatures (93 to 427 °C), and often provided with cooling.

Pyroelectric detectors change surface charge in response to received radiation. The detector need not reach thermal equilibrium when the target temperature changes, since it responds to changes in incoming radiation. The incoming radiation must be chopped, and the detector output cannot be used directly. A chopper is a rotating or oscillating shutter employed to provide AC rather than DC output from the sensor. Relatively weak AC signals are more conveniently handled by conditioning circuitry. The detector change can be likened to a change in charge of a capacitor, which must be read with a high impedance circuit. Pyroelectric detectors have radiation absorbent coatings so they can be broadband detectors. Response can be restricted by selecting the coating material with appropriate characteristics. Photon and pyroelectric detectors have thermal drift that can be overcome by temperature compensation (thermistor) circuitry, temperature regulation, auto null circuitry, chopping and isothermal protection.

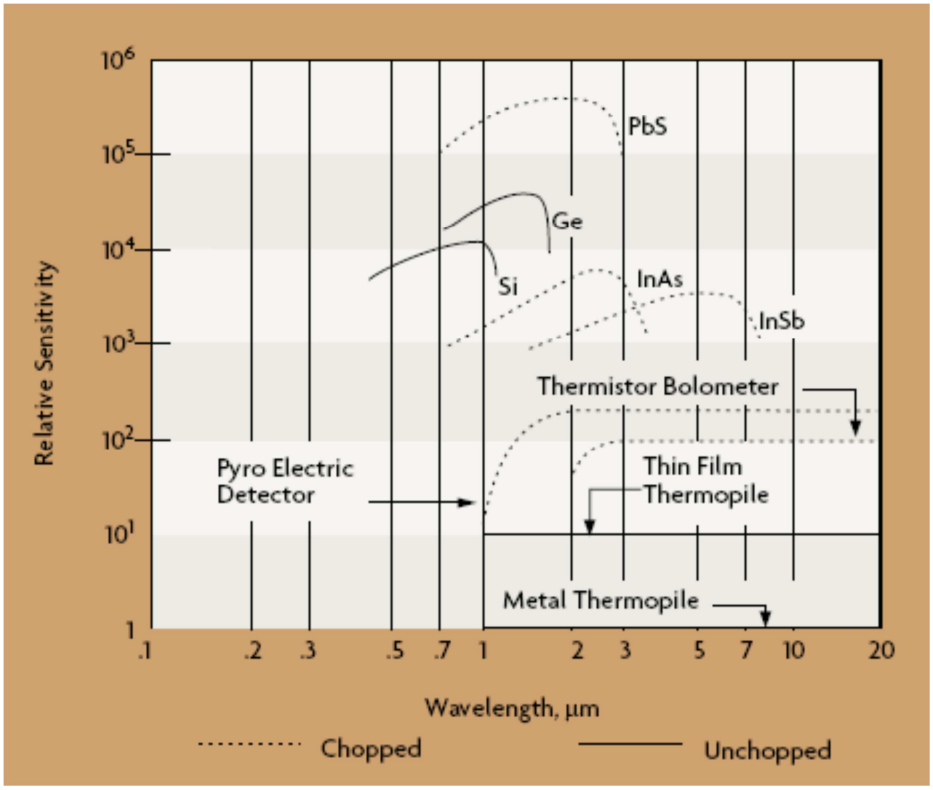

Fig. 4.22. Relative sensitivity of IR detectors (Omega, 2008)

Fig. 4.22 shows the different sensitivity for various radiation detectors. PbS has the greatest sensitivity, and the thermopile the least. (Omega, 2008)

Optical Systems

As shown in Fig. 4.23, the optical system of a radiation pyrometer may be composed of lenses, mirrors, or combinations of both. Mirror systems do not generally determine the spectral response of the instrument, as the reflectivity is not dependent on wavelength over the range used for industrial temperature measurement.

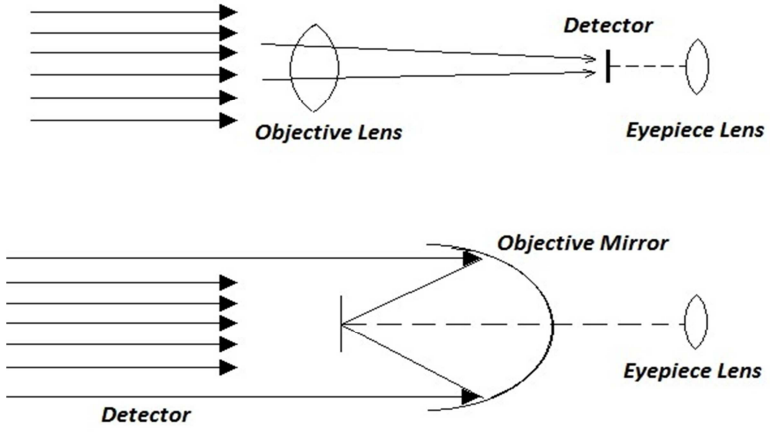

Fig. 4.23. Typical optical systems (Omega, 2008)

A mirror system must be protected from dirt and damage by a window. Copper, silver and gold are the best materials for mirrors in the infrared range. Silver and copper surfaces should be protected against tarnish by a protective film. The characteristics of the window material will affect the band of wavelengths over which the thermometer will respond. Glass does not transmit well beyond 2.5 μm, and is suited only for higher temperatures. Quartz (fused silica) transmits to 4 μm, crystalline calcium fluoride to 10 μm, germanium and zinc sulfide can transmit into the 8 to 14 μm range. More expensive materials will increase the transmission capability even more, as shown in Fig. 4.24.

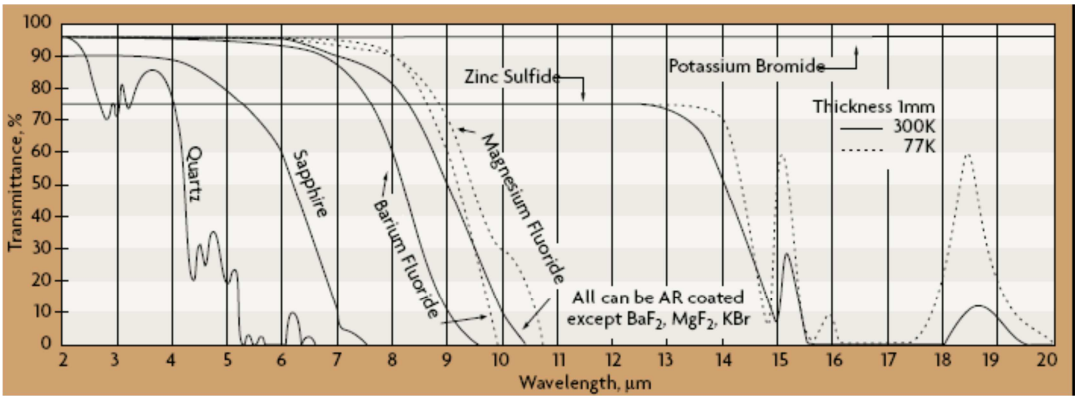

Fig. 4.24. IR transmission optical materials (Omega, 2008)

Windows and filters, placed in front of or behind the optical system, and which are opaque outside a given wavelength range, can alter the transmission properties greatly, and prevent unwanted wavelengths from reaching the detector. Mirror systems are generally used in fixed focus optical instruments.

Varying the focus of the instrument requires moving parts, which is less complicated in a lens system. The selection of lens and window material is a compromise between the optical and physical properties of the material, and the desired wavelength response of the instrument. The essential design characteristics of materials suitable for lenses, prisms, and windows include approximate reflection loss, and short and long wavelength cut-offs. Fig. 4.25. shows the transmittance of some common materials as a function of wavelength.

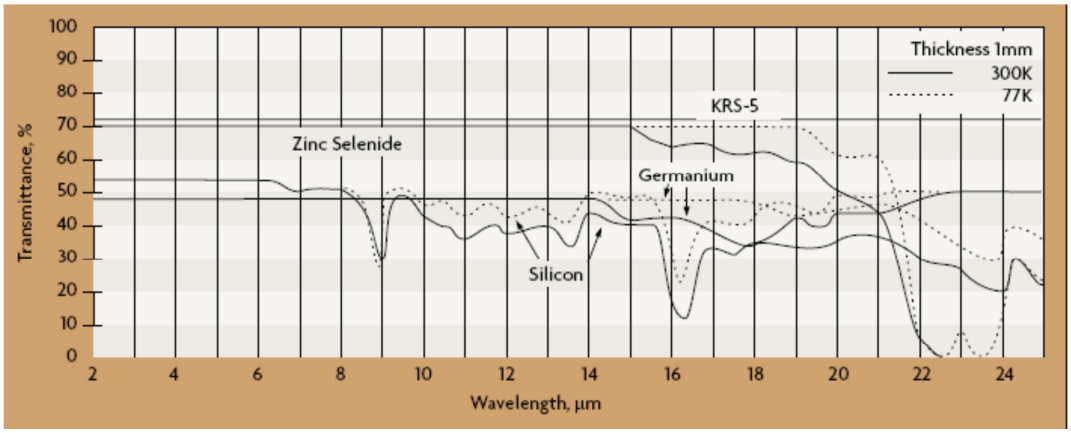

Fig. 4.25. IR transmission characteristics (Omega, 2008)

Chemical and physical properties may dictate choice of material to meet given operating conditions. The aberrations present in a single lens system may not permit precise image formation on the detector. A corrected lens, comprised of two or more elements of different material, may be required. The physical shape of the optical system, and its mounting in the housing, controls the sighting path. For many designs, the optical system is aligned to surface and measures surface temperature. This is satisfactory for sizable targets. Visual aiming accessories may be required for sighting very small targets, or for sighting distant targets. A variety of aiming techniques are available which include: simple bead and groove gun sights, integrated or detachable optical viewing finders, through-lens

sighting, and integrated or detachable light beam markers. (Omega, 2008)

Field of View

The field of view of a radiation thermometer essentially defines the size of the target at a specified distance from the instrument. Field of view can be stated in the form of a diagram (Fig. 4.26), a table of target sizes versus distance, as the target size at the focal distance, or as an angular field of view. (Omega, 2008)

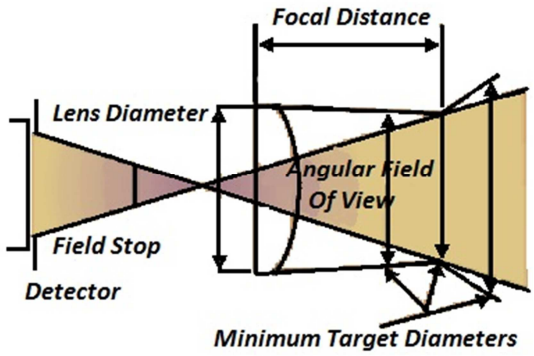

Fig. 4.26. Field of view (Omega, 2008)

Electronics

Today, microprocessors easily permit signals to be linearized very cost effectively. Microprocessor-based electronics (Fig. 4.27) are superior to conventional analog electronics because in situ computing can be used to correct detector imperfections, provide emissivity compensation, and provide digital outputs for two way communications between the thermometer and a PC or a control system workstation.

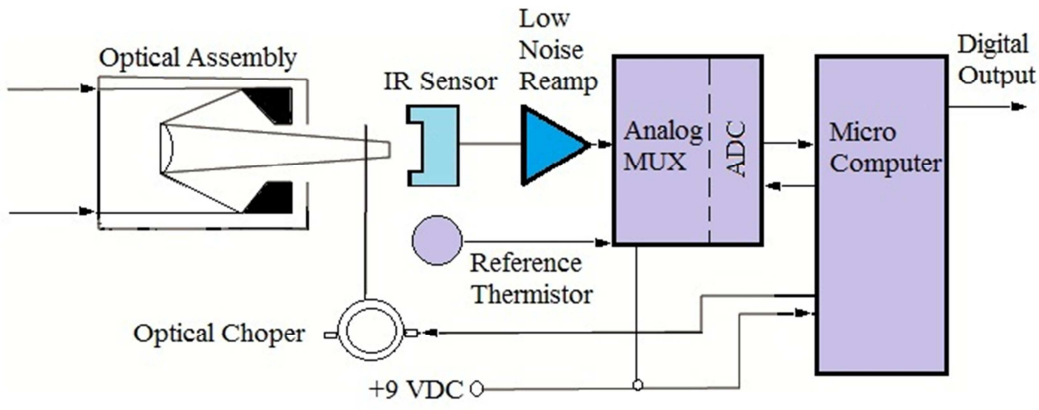

Fig. 4.27. Microprocessor-based IR thermometer (Omega, 2008)

Many of the shortcomings of thermal type detectors can be handled by sophisticated data processing techniques available in digital computers. The target temperature is an exponential function of the detector temperature. The output signal from the detector is a small voltage proportional to the difference in temperature between the target and the detector itself. To get the target temperature, it is necessary to accurately measure the detector temperature. Detector body temperatures span the range of the environment, from -50 to 100 °C. Over this range, the most precise and accurate temperature transducer is the thermistor. However, thermistor outputs are highly non-linear and vary widely from unit to unit. Analog devices must abandon use of the thermistor for a less accurate and easier to use element, such as an integrated circuit, which has a linear output. But highly non-linear responses are no problem for a computer, and units with microprocessors can employ thermistors. Detector responsivity is also a non-linear function of the detector body temperature. It is typically grossly corrected in analog devices with a simple linear gain correction produced by a temperature sensitive resistor in the preamplifier feedback network. A microprocessor can use a complex algorithm for the detection body temperature to correct for changes in detector responsivity. The net radiant target signal power impinging on the detector is highly non-linear with the target temperature, and for temperatures under 538 °C, it is also dependent on the detector temperature itself. Again, a microprocessor can make accurate compensation for both these effects. There is a fourth power relationship between the detector output voltage and target temperature. Analog

devices typically use linear approximation techniques to characterize this relationship. A computer can solve, in real time, a complex algorithm, with as many as seven terms, instead of linear approximation, for higher accuracy. Detector zero drift due to ambient temperature conditions can also be corrected using a microprocessor. This avoids errors of several degrees when you move an instrument from one room to another having a different temperature. Precise emissivity corrections can be called up, either from as many as 10 values stored in EEPROM, or from a complex real-time algorithm dependent on target time-temperature relationships. An example is a program to compensate for the emissivity of a piece of steel, which oxidizes as it heats to higher temperatures. Preprocessing by an onboard microprocessor may allow extraction of only the pertinent data needed by control systems. For example, only out of range data, determined by setpoints programmed into the microprocessor, may be desired for data transmission. This data can be transmitted digitally, on a priority interrupt basis. This is more efficient than having the user transmit all measured data to the host system, only to have the pertinent information sorted there. An intelligent radiation thermometer can be programmed to run preprogrammed internal calibration procedures during gaps, or windows in measurement activity. This prevents internal calibration checks from taking the device off-line at a critical moment in the process. A thermometer reading the temperature of cans on a conveyor belt can run an internal calibration program whenever a gap between successive cans is sensed. An internal microprocessor can also perform external control functions on external loop elements, using contact closure or relay outputs provided as options, and based on the incoming temperature data. In addition, intelligent devices can accept auxiliary inputs from thermocouples, RTDs or other radiation thermometers, and then use this data to support internal functions. For example, a high temperature setpoint could be continuously, and automatically reset by the microprocessor in response to input variable history. A sample-and-hold function is useful when a selected event serves to trigger the temperature measurement of an object. The thermometer measures temperature at that instant, disregarding earlier or later measurements. Analog circuitry exhibited a slow drift of the measurement during the hold period, but modern digital instruments hold the value without degradation for indefinite periods. Sometimes, the highest temperature within the field of

view is of interest during a given period. Intelligent electronics can be programmed to store into memory the highest temperature it saw in a sampling period. This is called peak picking. Valley picking, when the lowest temperature measured over a given period is of interest, also is possible. Averaging is used to prevent rapid excursions of the object temperature from the average value from causing noise in the control system. A common way to accomplish this is to slow down the response of the instrument via software in the microprocessor-based electronics. (Omega, 2008)

4.6 Thermopiles

Radiometry is the science of measuring thermal radiation. The atoms and molecules that compose real materials are in motion, and the interactions among them (collisions and boxing forces) produce displacements in the elementary charges within them. The resulting accelerating charges and changing electrical dipole moments produce thermal radiation. The electromagnetic spectrum is depicted in Fig. 4.28.

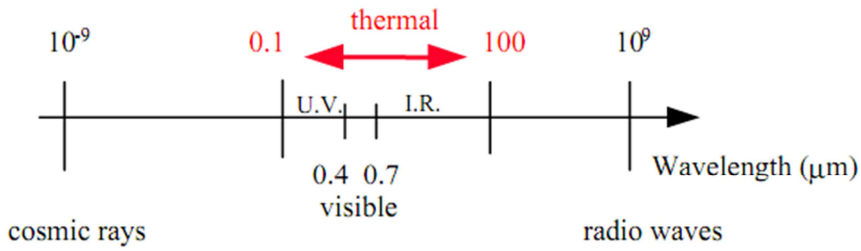

Fig. 4.28. Electromagnetic spectrum (Weckmann, 1997)

Based on the thermoelectric effect, the thermopile can be used as a heat sensor to measure thermal radiation. A thermopile is made of thermocouple junction pairs connected electrically in series. The absorption of thermal radiation by one of the thermocouple junctions, called the active junction, increases its temperature. The differential temperature between the active junction and a reference junction kept at a fixed temperature produces an electromotive force directly proportional to the differential temperature created. This effect is called a thermoelectric effect.

This chapter presents the background in thermoelectricity essential to understand the operation of a thermopile. It also presents the thermodynamics of the three effects in thermoelectricity: the Seebeck effect, the Peltier effect and the Thomson effect. The thermodynamics of thermoelectricity provides a means for describing the observed thermoelectric properties (Weckmann, 1997).

Nowadays the thermopile sensor allows measurement resolution up to 0.01°C, because of new inventions in Seebeck-coefficient materials used in thermopiles (www.melexis.com, 2007)

4.6.1 Background and Theory

This chapter presents some concepts of thermoelectricity and solid-state physics related to thermoelectric effects.

The thermoelectric effects

Any phenomenon involving an interconversion of heat and electrical energy may be termed a thermoelectric effect. We differentiate between reversible and irreversible energy conversion (Jaumont, 1960). The best known irreversible thermoelectric effect is the Joule effect, where an electric current I (A) is transformed irreversibly into heat P (W) according to

$$P = RI^2 \tag{3.94}$$

where R [Ω] is the electrical resistance of the conductor.

The Seebeck, Peltier and Thomson effects are three related reversible thermoelectric effects. The thermocouple is well known and has been used extensively over the last 100 years for measurement of temperature and process control. The principle governing the operation of thermocouple devices is the Seebeck effect.

In 1821, Thomas Johann Seebeck (1770-1831), a German scientist, discovered that a small electric current will flow in a closed circuit composed of two dissimilar metallic conductors when their junctions are kept at different temperatures. A thermocouple consists of two such dissimilar metals connected in series. The electromotive force or emf [V], that appears in an open circuit is the emf developed by the thermocouple to block the flow of electric current.

If the circuit is opened the emf created, E_{AB} [V] is called the relative Seebeck emf (RSE), or Seebeck voltage. The emf E_{AB} [V] created is directly proportional to the differential

temperature ΔT [K] between the two junctions

$$E_{AB} = S_{AB}\Delta T \tag{3.95}$$

where S_{AB} [V/K] is called the Seebeck coefficient.

This effect and is illustrated in Fig. 4.29. The pair A-B of conductors, or thermoelements, creates the circuit which forms the thermocouple. The thermoelement A is the positive conductor with respect to B if the current flows from A to B in the cold junction.

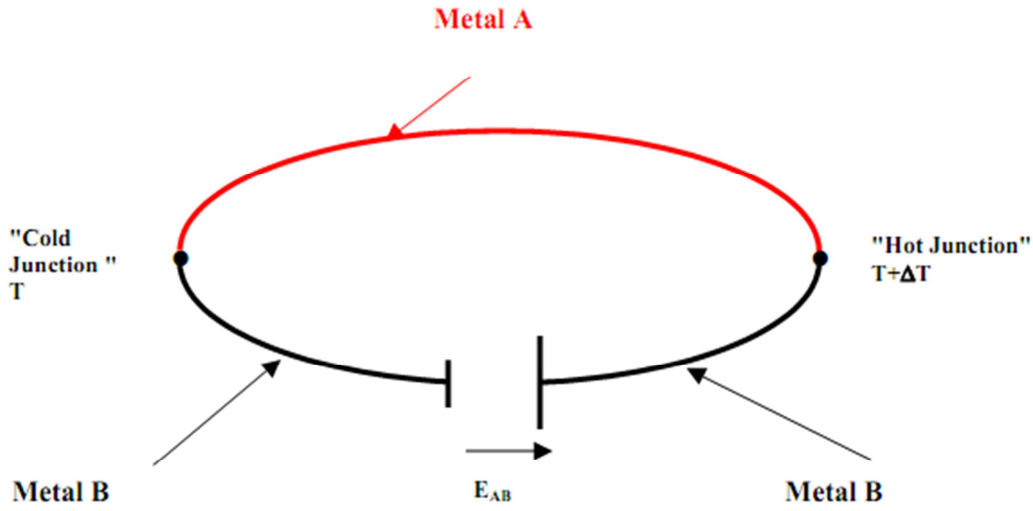

Fig. 4.29. Illustration of the Seebeck effect (Weckmann, 1997)

In 1834, Jean Charles Athanase Peltier (1785-1845), a French watchmaker-turned-physicist, discovered that when an electric current flows across a junction of two dissimilar metals, heat is liberated or absorbed depending on the direction of this electric current compared to the Seebeck current. The rate of heat liberated or absorbed P [W] is proportional to the electric current I [A] flowing in the conductor, that is

$$P = P_{AB}(T)\, I \tag{3.96}$$

where P_{AB} [V] is called the relative Peltier coefficient. This effect is the basis of thermoelectric refrigeration or heating. The Peltier effect is illustrated in Fig. 4.30.

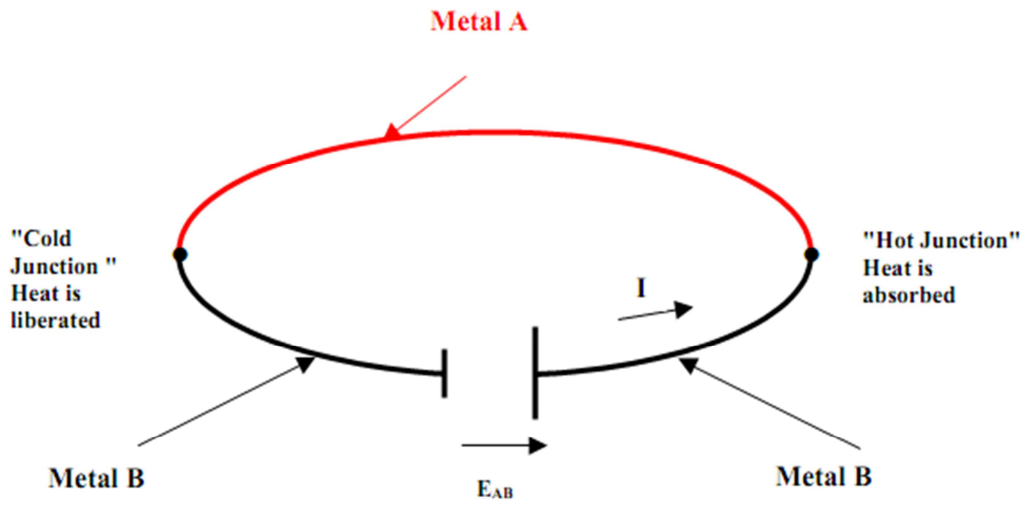

Fig. 4.30. Illustration of the Peltier effect (Weckmann, 1997)

In 1852, Thomson discovered that if an electric current flows along a single conductor while a temperature gradient exists in the conductor, an energy interaction takes place in which power is either absorbed or rejected, depending on the relative direction of the current and gradient. More specifically heat is liberated if an electric current flows in the same direction as the heat flows; otherwise it is absorbed. Fig. 4.31 illustrates the Thomson effect.

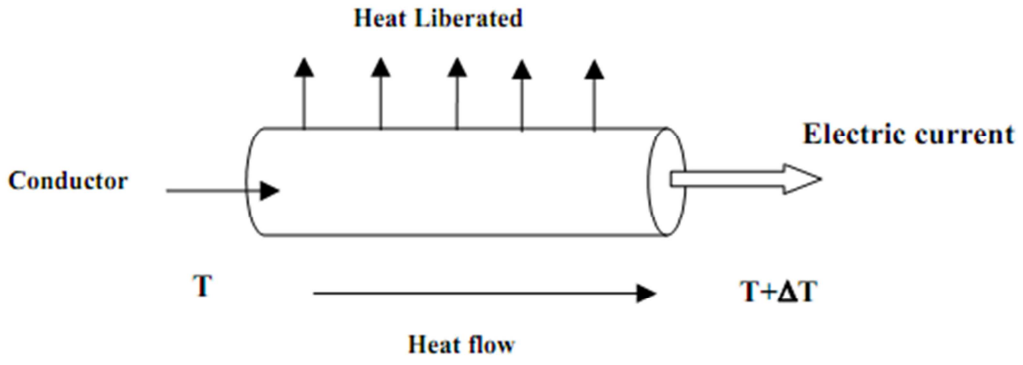

Fig. 4.31. Thomson effect (Weckmann, 1997)

The power P' absorbed or rejected per unit length [W/m] is proportional to the product of the electric current I [A] and the temperature gradient $\frac{dT}{dx}$ [K/m], that is

$$P' = \sigma(T)\, I \frac{dT}{dx} \tag{3.97}$$

where $\sigma(T)$ [VK^{-1}] is the Thomson coefficient.

While practical applications of the Thomson effect are few, the Seebeck effect is widely used in thermocouples to measure temperature and the Peltier effect is occasionally used for air conditioning and refrigeration units. Power generation is possible but because of the low thermal efficiency of the Peltier effect its commercial exploitation is of limited interest. Commercial exploitation of the Peltier effect has generally been limited to areas where quick heat and refrigeration is needed and where efficiency is not of utmost importance (Weckmann, 1997).

4.6.2 Thermodynamics of thermoelectricity

An understanding of the thermodynamic interdependency among the three reversible thermoelectric effects is critical. The thermodynamic theories presented here are essentially from the work of (Pollock, 1971). Let us consider a thermoelectric circuit where Joule heating is neglected. This system can then be considered a reversible heat engine. Consider the circuit in Fig. 4.29, where the cold junction is maintained at temperature T and the hotter junction at temperature $T+\Delta T$ by heat sinks and sources. If the emf generated in this circuit is E_{AB} [V], the thermoelectric power is defined as the change in emf per degree Kelvin, dE_{AB} / dT [VK^{-1}], such that the electrical voltage is given by

$$E_{AB} = (dE_{AB} / dT)\Delta T \tag{3.98}$$

It should be noted that although dE_{AB} / dT is called the thermoelectric power its dimensions are not power [W] but volts per kelvin [VK^{-1}] (Weckmann, 1997).

Taking into account the heat absorbed and liberated at the junctions (Peltier effects) and the heat absorbed and liberated within the conductors (Thomson effects), the conservation

of energy in the system, considered as a reversible heat engine, in which a current I [A] flows, can be written as

$$\left(dE_{AB}/dT\right)\Delta TI = P_{AB}\left(T+\Delta T\right)I - P_{AB}\left(T\right)I + \left(\sigma_B - \sigma_A\right)\Delta TI \qquad (3.99)$$

where $P_{AB}\left(T+\Delta T\right)I$ [W] is the heat absorbed at the hot junction, $P_{AB}\left(T\right)I$ [W], is the heat liberated at the cold junction, $\sigma_B \Delta TI$ [W] is the heat absorbed in conductor B, and $\sigma_A \Delta TI$ [W] is the heat absorbed in conductor A.

If we simplify Equation (3.99) by dividing through by I and ΔT and then taking the limit as ΔT approaches zero, we obtain the fundamental theorem of thermoelectricity,

$$\underset{[V/K]}{dE_{AB}/dT} = \underset{[V/K]}{\left(dP_{AB}/dT\right)} + \underset{[V/K]}{\left(\sigma_B - \sigma_A\right)} \qquad (3.100)$$

This equation, which is homogenous in VK^{-1}, gives the electrical Seebeck effect as the sum of the thermal Peltier and Thomson effects. This proves the relationship between the three effects and is the basis of the statement that the Seebeck effect is the result of both the Peltier and Thomson effects (Pollock, 1971). Let us now use the assumption that the thermoelectric interactions are thermodynamically reversible, and add heat sinks at temperature $T+\Delta T/2$ at the midpoints of the two conductors. The net change of entropy [kJK^{-1}], of the heat sinks at the junctions and along the conductors is zero so for a unit time we can write

$$\underset{[kJ/K]}{\frac{-P_{AB}(T+\Delta T)I}{T+\Delta T}} + \underset{[kJ/K]}{\frac{P_{AB}(T)I}{T}} - \underset{[kJ/K]}{\frac{\sigma_B \Delta T\ I}{T+(\Delta T/2)}} + \underset{[kJ/K]}{\frac{\sigma_A \Delta T\ I}{T+(\Delta T/2)}} = 0 \qquad (3.101)$$

After dividing through by the current I, if we multiply the first two terms by $\Delta T/\Delta T$ and then take the limit as ΔT approaches zero, Equation (3.101) becomes

$$-\frac{d}{dT}\left(\frac{P_{AB}}{T}\right)\Delta T - \frac{\sigma_B \Delta T}{T+(\Delta T/2)} + \frac{\sigma_A \Delta T}{T+(\Delta T/2)} = 0 \qquad (3.102)$$

If we now define the Thomson effect as the energy change for a temperature difference of 1 K, that is ΔT =1 K, then since T generally is much greater than 1 K, we can assume that $T+\Delta T/2$ is essentially equal to T. We then have from Equation (3.102)

$$\frac{d}{dT}\left(\frac{P_{AB}}{T}\right)=\frac{\sigma_A}{T}-\frac{\sigma_B}{T} \tag{3.103}$$

Carrying out the indicated differentiation in Equation (3.103) and multiplying each term of the resulting equation by T, we obtain

$$\frac{P_{AB}}{T}=\left(\frac{dP_{AB}}{dT}\right)+\sigma_A-\sigma_B \tag{3.104}$$

which gives the change in entropy per unit charge of the junction at a given temperature and relates the Peltier and Thomson effects. Equation (3.104) can be simplified using the theorem of thermoelectricity, Equation (3.100) yielding

$$P_{AB}=\left(\frac{dE_{AB}}{dT}\right)T \tag{3.105}$$

Where P_{AB} [V] is the Peltier coefficient and is described with respect to the thermoelectric power, dE_{AB}/dT [VK^{-1}].

If we differentiate Equation (3.105) with respect to T, we obtain

$$\frac{dP_{AB}}{dT}=\frac{dE_{AB}}{dT}+T\frac{d^2E_{AB}}{dT^2} \tag{3.106}$$

and if we substitute this result into the theorem of thermoelectricity, Equation (3.100), Equation (3.106) becomes

$$\frac{d^2E_{AB}}{dT^2}=\frac{\sigma_A-\sigma_B}{T} \tag{3.107}$$

Upon integration Equation (3.107) becomes, for closed thermoelectric circuits,

$$\frac{dE_{AB}}{dT}=\oint\frac{\sigma_A-\sigma_B}{T}dT=\oint\frac{\sigma_A}{T}dT-\oint\frac{\sigma_B}{T}dT \tag{3.108}$$

Equation (3.108) shows that the thermoelectric power of a thermocouple can be expressed in terms of the Thomson coefficients of its components. In other words, the thermoelectric power is the algebraic sum of the absolute thermoelectric powers of its components:

$$\frac{dE_{AB}}{dT}=S_A-S_B=S_{AB} \tag{3.109}$$

Where $S_A = \int_0^T \frac{\sigma_A}{T} dT \, [V/K]$ and $S_B = \int_0^T \frac{\sigma_B}{T} dT \, [V/K]$ are the absolute Seebeck coefficients (ASC) of each of the components of the thermocouple materials, or thermoelements, A and B. The symbol *S* denotes the rate of change with temperature of the Thomson voltage in a single conductor.

The concept of the ASC is very important because it allows the study of the properties of individual thermoelements. If the ASC of one thermoelement is known and the thermoelectric power of the couple is determined experimentally, the ASC of the unknown element can be calculated using Equation (3.108).

After a second integration over a closed thermoelectric circuit, Equation (3.109) becomes

$$E_{AB} = \oint S_A dT - \oint S_B dT = \oint S_{AB} dT \tag{3.110}$$

where the integrals of the Seebeck coefficients are the absolute Seebeck effects. The flow of current in this circuit is induced by the relative Seebeck coefficient (RSE) which is a consequence of the temperature difference between the two junctions of conductors A and B. Because the Thomson effect is present only when a current passes along the conductor, the Thomson coefficients (σ_A, σ_B) are nonzero only in closed circuits. This means that Equation (3.108) can account for thermoelectric properties only in a closed circuit. In contrast to this, the electrical potential (emf) within conductors is always present as long as a temperature difference is maintained between the two junctions, regardless of whether the circuit is open or closed. Hence Equations (3.109) and (3.110) are valid for both open and closed circuits. Usually the RSE is measured in open circuits to eliminate the Thomson and Peltier effects, which cause extraneous thermal variations. From Equation (3.108) the three laws of thermoelectric circuits may be inferred:

1. The law of homogeneous conductors.
2. The law of intermediate conductors.
3. The law of successive temperatures.

The law of homogeneous conductors states that a thermoelectric current cannot be maintained solely by application of heat to a single homogeneous conductor, regardless of any cross-sectional variations. In other words, if a thermoelectric circuit is formed of two

conductors of the same homogeneous material ($S_A = S_B$), no emf exists in this circuit. The law of intermediate conductors states that the sum of the absolute Seebeck coefficients of dissimilar conductors is zero when no temperature difference exists between the junctions. In other words no extraneous emf will be produced in a circuit made of intermediate materials if no temperature differences exist between the two ends of the materials. This law demonstrates that the contribution of a common thermoelement C to a pair of thermoelements A and B vanishes if the junctions A-C and C-B are at the same temperature. The law of successive temperatures states that the emf of a thermocouple composed of homogeneous conductors can be measured or expressed as the sum of its properties over successive intervals of temperature. Mathematically this may be stated (Weckmann, 1997)

$$E_{AB} = \int_{T_0}^{T_1} (S_A - S_B)\, dT + \int_{T_1}^{T_2} (S_A - S_B)\, dT + \int_{T_2}^{T_3} (S_A - S_B)\, dT = \int_{T_0}^{T_3} (S_A - S_B)\, dT \quad (3.111)$$

4.6.3 Description of the device

This section is aimed at describing the thermoelectric sensor proposed for use as a thermal radiation detector. The motivation behind the choice of such a device is developed, as are detailed descriptions of its operation, specifications and expected performance.

Thermocouple operation is based on the Seebeck effect; thus, the amount of electrical potential produced can be interpolated as a measure of temperature difference. But what is the relationship is there between the emf produced in the open circuit and the temperature difference between the two junctions? It all depends on the pair of thermoelements used: some pairs of thermocouple elements give a Seebeck voltage which varies in an anticipated way with temperature. Thermocouples in common use have nearly linear temperature-emf characteristics. Once the thermocouple calibration curve is obtained, by maintaining one of the junctions at a known fixed temperature, the other junction is used as the measuring junction and is held at the temperature to be determined. The junction maintained at a known temperature is called the reference junction while the other is called the active junction.

For an ideal thermocouple, the open-circuit voltage obtained is proportional to the temperature difference between the junctions constructed of conductors A and B,

$$\Delta V = S_{AB}(T)\Delta T \tag{3.112}$$

where S_{AB} is the relative Seebeck coefficient, expressed in μVK^{-1}. This coefficient depends not only on the temperature, but also on the choice of the two materials used in the thermocouple. A sign is assigned to the Seebeck coefficient according to the sign of the potential difference related to the temperature difference. However, it is much more convenient to work with absolute values: the magnitude of the Seebeck coefficient of a junction is then calculated as the absolute value of the difference between the Seebeck coefficient of each metal; that is,

$$S_{AB} = |S_A - S_B| \tag{3.113}$$

Because a voltage is produced when a temperature difference exists between the two junctions of the thermocouple junction pair shown in Fig. 4.29, the thermocouple can be used as a detector of incident radiation. In open-circuit operation the emf produced is usually low, on the order of a tenth of a microvolt per degree Celsius of temperature difference for a single junction pair. In order to increase the output voltage, several junction pairs may be connected in series. The responsivity is then increased by n if n thermocouple junction pairs are placed in series; that is,

$$\Delta V = nS(T)\Delta T \tag{3.114}$$

Such a device is called a thermopile. As shown in Fig. 4.32, based on the description by (Dereniak, 1984), elements of a series of thermocouples of alternate material A and B are placed between a heat source and a heat sink. The hot junction comes into thermal equilibrium with the high temperature surroundings producing an emf at the leads. If a current flow results, thermal energy is converted into electrical energy. The remaining energy absorbed at the hot junction is rejected to the heat sink at the cold junction.

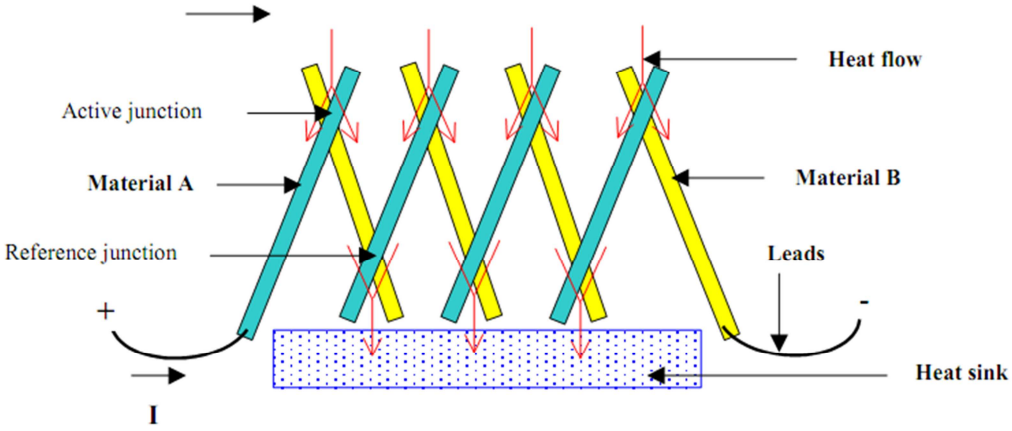

Fig. 4.32. Example of a thermopile (Weckmann, 1997)

We now turn our attention to thermal radiation detectors. The two most important parts of all thermal radiation detectors are the absorber and the temperature transducer. When a thermopile is used, the radiant energy is absorbed into a layer coated on the active junction which acts as the heat source, and the difference of temperature between the active and the reference junctions is translated into an output voltage through the Seebeck effect. In most practical implementations we can neglect the Joule, Thomson and Peltier effects because the input impedance of the signal-conditioning circuit is sufficiently high to ensure that a negligible current flows through the thermopile (Weckmann, 1997).

4.7 Predicted Mean Vote modification

This thesis deals with evaluation of thermal comfort according to the PMV model. First concept of this work was based on evaluation of PMV model from (Fanger, 1970) that is also given by standards ISO 7730 and ASHRAE 55. The biggest limitation of standardized PMV model is the measurement of mean radiant temperature (MRT) as ncessary parameter in PMV determination. The original objective of this research was the design of mean radiant temperature sensor based on thermopiles as a replacement of globe thermometer (dry bulb thermometer encased in a 150 mm diameter matte-black copper sphere whose absorptivity is similar to the skin) used as standard measurement device according to ISO 7726. This replacement solves the known shortcomings of globe thermometer

a) air movement influence
b) ambient temperature influence
c) impossibility to assess asymmetric thermal radiation

   The projection factors must be taken into account. The influences of radiation fluxes from above and below of person are different from radiant fluxes from east, south, west and north direction. To calculate mean radiant temperature correctly we have to multiply radiant fluxes with corresponding weighting factors which are derived from the projection factors.

d) long response time (20-30min)

These shortcomings are described in ISO 7726 and detailed research concerning the cases c) and d) are described in (Hruška, 2003). Hruška also did analysis of globe thermometer in COMSOL Multiphysics (formerly FEMLAB) and also experimentally verified his simulations. COMSOL Multiphysics is an engineering, design, finite element analysis, solver and simulation software environment for the modeling and simulation of any physics-based system.

The next objective of this research is to modify the PMV model. Basically, in evaluation of PMV, we have to determine mean radiant temperature as the necessary input parameter of PMV model. The MRT is either obtained directly, i.e. with globe thermometer or indirectly

with measurement of radiant fluxes (net radiometer) and then the heat fluxes are recalculated to MRT. Finally, PMV model uses MRT, calculates the heat transfer from human body through radiation and finally predicts mean response of a larger group of people with the PMV index. In case of thermopiles used in thermal comfort evaluation, it would be more convenient to evaluate the PMV directly from radiation fluxes measured with thermopile. The radiation component R [Wm^{-2}] in heat balance of human body (unit body surface) with surroundings in PMV model is given with equation (3.47)

$$R = A_{eff}\varepsilon\sigma\left[\left(t_{cl}+273\right)^4-\left(t_r+273\right)^4\right]$$

After substitution of the appropriate numerical values (see Chapter 4.3.7) and expression it we get

$$R = 3.96\times10^{-8}\, f_{cl}\left[\left(t_{cl}+273\right)^4-\left(t_r+273\right)^4\right]$$

which, as can be seen, is one term of heat balance of human with surroundings (3.64).

$$\begin{aligned}L = {} & \left(M-W\right)\\ & -3.05\times10^{-3}\left[5733-6.99\left(M-W\right)-p_a\right]\\ & -0.42\left[\left(M-W\right)-58.15\right]\\ & -1.7\times10^{-5}M\left(5867-p_a\right)\\ & -0.0014M\left(34-t_a\right)\\ & -3.96\times10^{-8}\, f_{cl}\left[\left(t_{cl}+273\right)^4-\left(\overline{t_r}+273\right)^4\right]\\ & -f_{cl}h_c\left(t_{cl}-t_a\right)\end{aligned}$$

To obtain the radiation component, we can use thermopile voltage U_{TP} [V]:

$$U_{TP} = G\Phi_e = KS_s\Phi_e \tag{3.115}$$

where G [Vm^{2}W^{-1}] is sensor constant, Φ_e [W] is the incident radiant flux; K [VW^{-1}] instrument sensitivity and S_s [m^2] is sensitive area of detector.

The radiation component R can be written as

$$R = \frac{A_r}{A_D}\, f_{cl}\Phi_e = \frac{A_r}{A_D}\, f_{cl}\,\frac{U_{TP}}{G} \tag{3.116}$$

where G [Vm^2W^{-1}] is sensor constant, Φ_e [W] is the incident radiant flux; A_r [m^2] is the surface of the human body participating on radiant heat transfer (for sitting persons $A_r/A_D = 0.70$ and for staying persons $A_r/A_D = 0.73$; A_D [m^2] is the surface of human body according Dubois equation (3.49).

Substitution of the appropriate numerical values gives:

$$R = 4.6938 \times 10^4 U_{TP} \tag{3.117}$$

And the full PMV equation (3.64) will be

$$PMV = \left[0.303e^{-0.036M} + 0.028\right] \times \left\{ \begin{array}{l} (M - W) \\ -3.05 \times 10^{-3}\left[5733 - 6.99(M - W) - p_a\right] \\ -0.42\left[(M - W) - 58.15\right] \\ -1.7 \times 10^{-5} M (5867 - p_a) \\ -0.0014M (34 - t_a) \\ -\dfrac{A_r}{A_D} f_{cl} \Phi_e \\ -f_{cl} h_c (t_{cl} - t_a) \end{array} \right\} \tag{3.118}$$

and t_{cl} changes from (3.65) to

$$\begin{aligned} t_{cl} &= 35.7 \\ &\quad -0.028(M - W) \\ &\quad -I_{cl}\left\{\frac{A_r}{A_D} f_{cl} \Phi_e + f_{cl} h_c (t_{cl} - t_a)\right\} \end{aligned} \tag{3.119}$$

and then we can write

$$t_{cl} = \frac{35.7 \quad -0.028(M - W) \quad -I_{cl} \dfrac{A_r}{A_D} f_{cl} \Phi_e - I_{cl} f_{cl} h_c t_a}{I_{cl} f_{cl} h_c} \tag{3.120}$$

And consequently derived with thermopile voltage U_{TP} we get

$$PMV = \left[0.303e^{-0.036M} + 0.028\right] \times \left\{ \begin{array}{l} \left(M - W\right) \\ -3.05\times10^{-3}\left[5733 - 6.99\left(M - W\right) - p_a\right] \\ -0.42\left[\left(M - W\right) - 58.15\right] \\ -1.7\times10^{-5} M \left(5867 - p_a\right) \\ -0.0014M \left(34 - t_a\right) \\ -4.6938\times10^{4} U_{TP} \\ - f_{cl} h_c \left(t_{cl} - t_a\right) \end{array} \right\} \quad (3.121)$$

and for t_{cl}

$$t_{cl} = \frac{35.7 \quad -0.028\left(M - W\right) \quad - I_{cl}\, 4.6938\times10^{4} U_{TP} - I_{cl}\, f_{cl} h_c t_a}{I_{cl}\, f_{cl} h_c} \quad (3.122)$$

With this modification we can evaluate the PMV indices without the determination of mean radiant temperature, independently on emissivity of surroundings and without iterative computing of t_{cl}.

5 EXPERIMENTAL

Experimental part of this thesis deals with evaluation of thermal comfort according to PMV mathematical model and especially with mean radiant temperature determination.

Chapter 5.1 of this work describes the application for computation of PMV, PPD a DR indices according to (ISO 7730, 2005). The Matlab scripts computing PMV, PPD and DR indices were prepared as a result of this chapter.

The Chapter 5.2 describes the design of real room which is created to validate thermal comfort (PMV index) on real environment. It is also possible to change dimensions of the room, different properties, person position and user can place heating panels on walls to study and verify the influence of mean radiant temperature on PMV index.

Next Chapter 0 introduces the solution allowing the optimization of costs for heating. The basic principle of this optimization is to distribute the total costs between costs on convective heating and costs on radiant heating. The costs on convective heating and costs on radiant heating correspond to the power on heating panels and to the power on radiator respectively. These total costs are optimized with SOMA evolutionary algorithm.

The mean radiant temperature (MRT) is the specific parameter influencing the PMV index and this parameter is the most difficult to determine. The Chapter 5.4 deals with MRT evaluation and with overlapping of scanned areas when using several thermopile sensors. The nonlinear curve fitting of field of fiew of thermopile sensor is done in Chapter 5.4.1. Subsequently, the results of Chapter 5.4.1 are used in Chapters 5.4.2 and 5.4.3 which deal with visualization of total signal of scanned areas and with optimization of field of view.

The important part of experimental section is Chapter 5.5 dealing with design of measurement system. Three measurement systems are prepared: analog version (ambient temperature compensation), digital laboratory version and digital embedded version.

The Chapter 5.6 briefly describes some devices used in this work.

Finally; acquiring experimental data is presented in Chapter 5.7.

5.1 Computing predicted mean vote (PMV) mathematical model

The computation of predicted mean vote (PMV) mathematical model and percentage of dissatisfied (PPD) are done according to (ISO 7730, 2005) see Equations (3.63), (3.64), (3.65) and (3.66). The computer program given by ISO norm is written in BASIC language and therefore it is necessary to rewrite it to Matlab language for further utilization. The computer program has defined set of input variables (see Table 5.1.).

Table 5.1. Input variables of PMV calculation computer program.

Variable	***Unit***	***Symbols in program***
Clothing	clo	CLO
Metabolic rate	met	MET
External work	met	WME
Air temperature	°C	TA
Mean radiant temperature	°C	TR
Relative air velocity	ms^{-1}	VEL
Relative humidity	%	RH
Partial water vapour pressure	Pa	PA

At the beginning, the program converts the values of thermal insulation of the clothing, metabolic rate and external work to SI units. Then it calculates an internal heat production of the human body, clothing area factor, heat transfer coefficient by forced convection and other quantities in order to compute required predicted mean vote. Every quantity can be calculated except the surface temperature of clothing. The equation for calculation of surface temperature of clothing *TCLA* is given implicitly and therefore it may be solved via iteration methods. First; the value of *TCLA* [°C] is guessed according to Equation (4.1):

$$\mathrm{TCLA} = \mathrm{TAA} + \left(35.5 - \mathrm{TA}\right) / \left(3.5 \times \left(6.45 \times \mathrm{ICL} + 0.1\right)\right) \qquad (4.1)$$

Further, the value of *TCLA* is iteratively refined until it is changing more than a 0.0015 °C from previous calculated value. Then the value of predicted mean vote (PMV) index is calculated according to Equations (3.64) and (3.65). Finally the value of predicted percentage of dissatisfied PPD is determined according to the equation (3.66) and both indices (PMV and PPD) are returned as a result.

The validation of script has been also done versus the sample values given by the norm (ISO 7730, 2005). Sample calculated values are given in Table 5.2.

Table 5.2. PMV sample calculated values

Input data	***Value***	***Unit***
Clothing	1.0	clo
Metabolic rate	1.2	met
External work	0.0	met
Air temperature	19.0	°C
Mean radiant temperature	18.0	°C
Relative air velocity	0.1	ms^{-1}
Relative humidity	40.0	%
Output data	***Value***	***Unit***
Predicted Mean Vote	-0.7	-
Predicted percentage of Dissatisfied	15.3	-

5.2 Design and creation model of real room

To practically use the PMV mathematical model and thermal comfort evaluation, the design and creation of model of real room has been done. The application prepared in Matlab environment introduces one room with definable dimensions and wall properties. These are entered by user on the first windows of application (See Fig. 5.1.). The dimensions of the room are taken from text boxes labelled “Room width”, “Room length”

and “Room height” and are related to room diagram on the right bottom of this window. The PMV index is determined at the occupant position which is also defined by user in section “Occupant location” text boxes *X*, *Y* where *X* [m] coordinate represents horizontal position and *Y* [m] represents vertical position with origin in left bottom corner. It is also important to define if occupant is in standing or seated position.

Next, the PMV index depends on mean radiant temperature (MRT) and air temperature. The MRT value is given by interior temperature, surroundings (walls) emissivity and heat transfer from interior to outside through walls and we can modify it with heating panels. It is possible to add (place) and remove these panels in section “Heating panel location and dimension”. The location is given by chosen wall in the list “Wall” and this corresponds to the scheme shown at the bottom of the window and by text boxes *X*, *Y* where *X* [m] coordinate represents horizontal position and *Y* [m] represents vertical position with with origin in the left bottom corner. Finally; the width and height (*W* [m], *H* [m]) of the heating panel must be entered. Button “Add” adds desired panel to the list of heating panels labelled “List of heating panels”.
The section “Wall participating in heat transfer” defines which walls participate in heat transfer. If the room shares walls with other rooms with similar interior air temperature, we can neglect the heat transfer through these walls (or ceiling or floor).

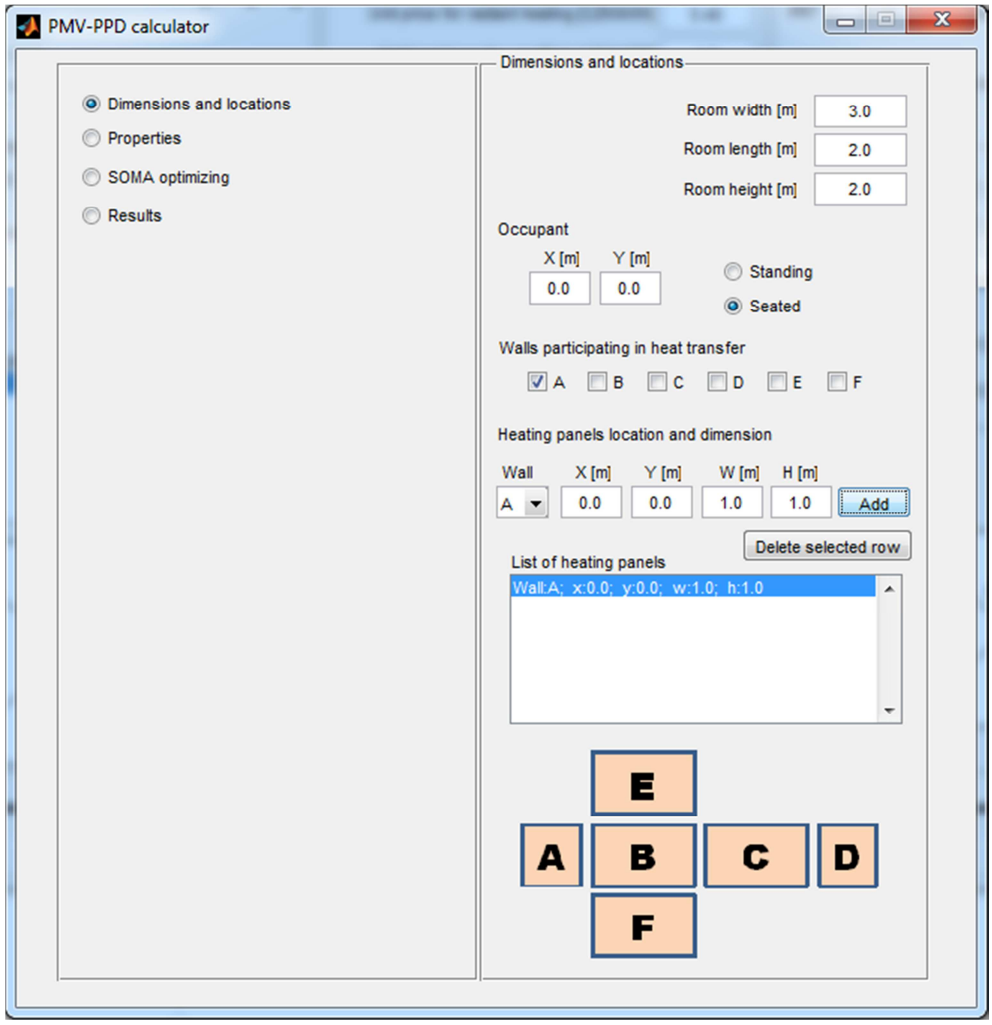

Fig. 5.1. Model of real room – Dimensions and locations

The next window (see Fig. 5.2.) shows all properties related to the room and environmental parameters, heating panels, price for electricity and person activity and clothing. Following is the list of adjustable properties:

- heat panel emissivity [-]
- wall emissivity [-]
- price for electricity [Kč$W^{-1}h^{-1}$]
- wall heat transfer coefficient [Wm^2K]
- efficiency of heat panel [-]
- clothing insulation [CLO]
- metabolic rate [MET]
- external work [WME]
- relative air velocity [ms^{-1}]
- relative air humidity [%]
- water vapour pressure [Pa]

With clicking on the button “Calculate PMV index” we skip “SOMA optimizing” tab discussed later in Chapter 0 and we are redirected to “Results” tab (see Fig. 5.3.).

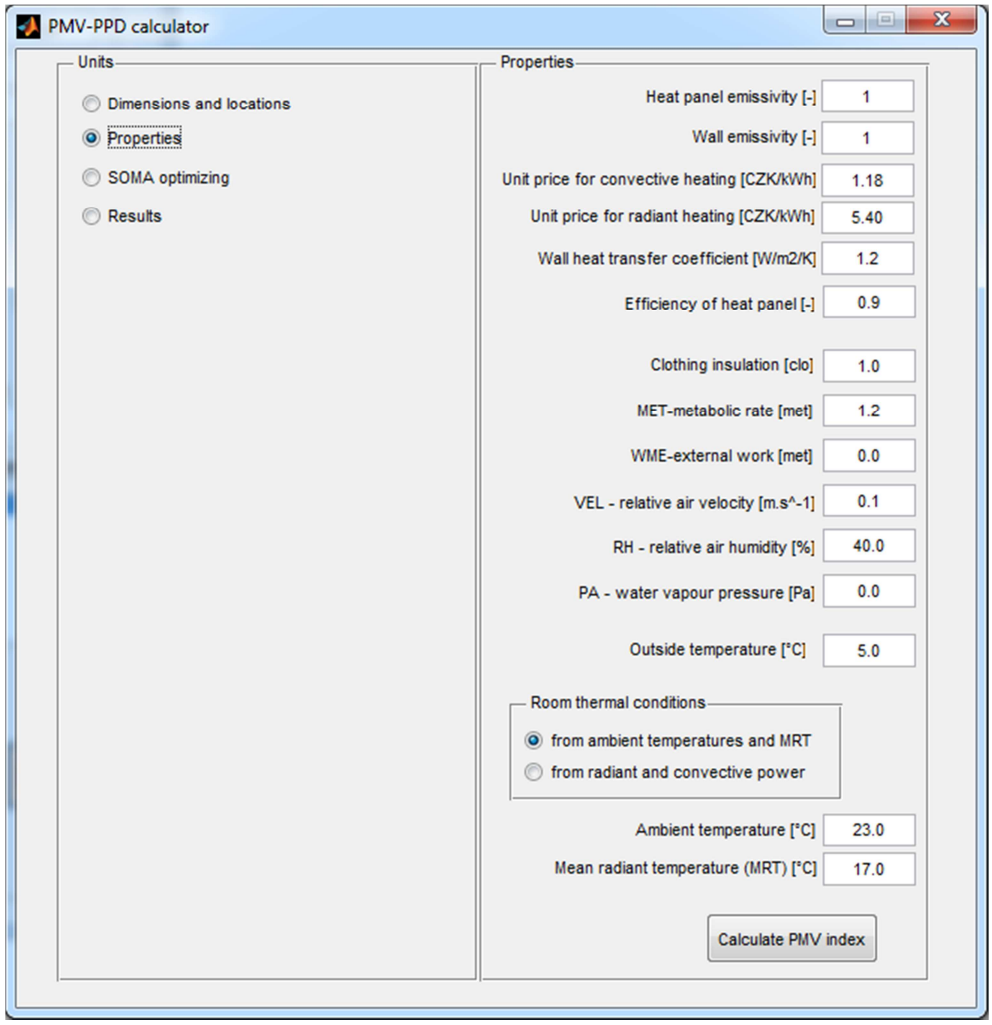

Fig. 5.2. Model of real room – Properties

The last tab (Fig. 5.3.) of this application evaluates the PMV index of person in designed room with properties defined in the previous paragraph and shows the results divided in five categories:

1. calculated properties of room used in PMV evaluation
   a. The total surface of room.
   b. Percent of total surface that participates heat transfer according to "Wall participating heat transfer" input on Fig. 5.1. We can consider the walls shared with the room at ambient temperature same as our examined room that are not participating of heat transfer.
   c. Heating panel angle factor is a function of the shape, the size and the relative positions of the surface in relation to the person and it is needed in mean radiant temperature avaluation. As most building materials have a high emissivity (ε), it is possible to disregard the reflection, i.e. to assume that all the surfaces in the room are black. The equation (4.2) is used to calculate mean radiant temperature:

$$\overline{T}_r^4 = \overline{T}_1^4 F_{p-1} + \overline{T}_2^4 F_{p-2} + \ldots + \overline{T}_N^4 F_{p-N} \tag{4.2}$$

   where T_r [K] is mean radiant temperature, T_N [K] is the surface temperature of surrounding surfaces, F_{p-N} [-] is the angle factor between a person and surface. (ISO 7726, 1998)

   Angle factor may be calculated from the equations (4.3), (4.4) and (4.5):

$$F_{p-N} = F_{\max}\left(1 - e^{-\left(\frac{a}{c}\right)^{\tau}}\right)\left(1 - e^{-\left(\frac{b}{c}\right)^{\gamma}}\right) \tag{4.3}$$

$$\tau = A + B\left(\frac{a}{c}\right) \tag{4.4}$$

$$\gamma = C + D\left(\frac{b}{c}\right) + E\left(\frac{a}{c}\right) \tag{4.5}$$

   where F_{max} [-], A [-], B [-], C [-], D [-], E [-] are coefficients depending on person position (seated, standing) and examined surface (horizontal, vertical), see Table 5.3.

(ISO 7726, 1998)

Table 5.3. Angle factor coefficients (ISO 7726, 1998)

	F_{max} [-]	A [-]	B [-]	C [-]	D [-]	E [-]
Seated person, vertical surfaces	0.118	1.216	0.169	0.717	0.087	0.052
Seated person, horizontal surfaces	0.116	1.396	0.130	0.951	0.080	0.055
Standing person, vertical surfaces	0.120	1.242	0.167	0.616	0.082	0.051
Standing person, horizontal surfaces	0.116	1.595	0.128	1.226	0.046	0.044

2. This section shows
   a. interior air temperature t_a [°C],
   b. temperature of heating panel surface t_{ps} [°C] given by simplified evaluation without convective heat transfer consideration:

$$t_{ps} = \sqrt[4]{\frac{\eta Power_2 \varepsilon}{\sigma S_{PS}} + \left(t_a + 273.15\right)^4} \tag{4.6}$$

   where η [-] is efficiency of heating panel, *Power2* [W] is the input power, ε [-] is emissivity of heating panel surface, σ [$Wm^{-2}K^{-4}$] is the Stefan-Boltzmann constant $\sigma = 5.6693\times10^{-8}$ $Wm^{-2}K^{-4}$, S_{PS} [m^2] is the surface of heating panel, t_a [°C] is interior air temperature.
   c. Mean radiant temperature t_r [°C]

$$t_r = \sqrt[4]{\sum_i F_{HPi}(t_{psi} + 273.15)^4 + (1 - \sum_i F_{HPi})(t_{ip} + 273.15)^4} \tag{4.7}$$

   where F_{HPi} [-] is angle factor between person and i-th heating panel; t_{psi} [°C] is temperature of i-th heating panel surface and t_{ip} [°C] is steady state surface temperature of interior wall given as (Augusta, 1991):

$$t_{ip} = t_i - \frac{t_i - t_e}{R_0} R_i \tag{4.8}$$

   where t_{ip} [°C] is surface temperature of interior wall, t_i [°C] is air temperature of interior, t_e [°C] is external temperature, *Ro* [m^2KW^{-1}] is construction heat

resistance, R_i [m^2KW^{-1}] is heat transfer coefficient, R_i = 0.125 for horizontal constructions (ČSN 73 0542, 1995) .

3. Calculated PMV index.
4. Electric power on radiator heating (Power1) and on heating panels (Power2).
5. Resulting price for electricity per hour, separately the price for heating panels per hour and price for heating by radiator per hour and total price per hour (all in Czech crowns).

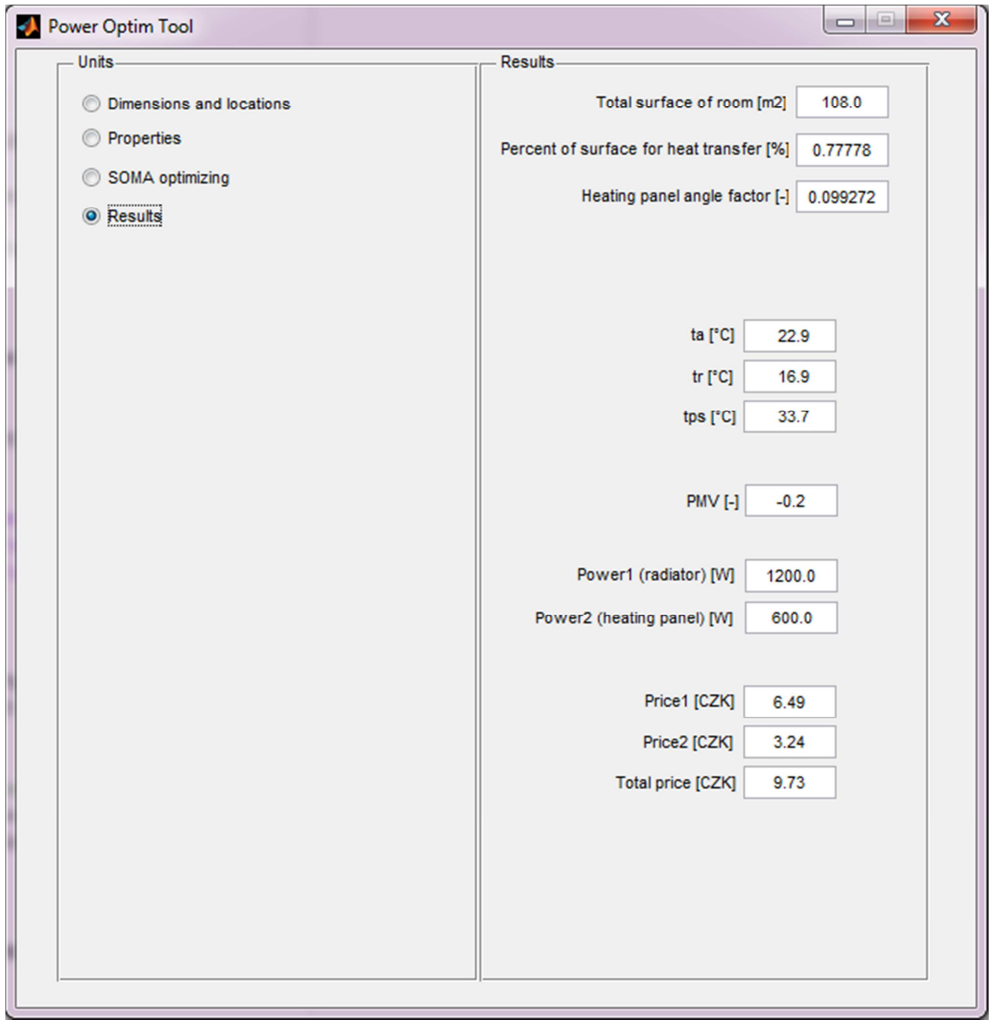

Fig. 5.3. Model of real room - Results

5.3 Optimization of costs for heating proceed by SOMA evolutionary algorithm

The optimization of costs for heating uses for determination of the costs and the PMV value the model of room described in previous chapter. The basic principle is to distribute the electric power between the radiant and the convective heating, which can lead to energy (and also the costs) savings while maintaining thermal comfort. The radiant heating is ensured with radiant heating panels mounted on the wall or ceiling and convective heating is ensured with radiator installed in the room. The optimization changes the electric power on heat panels that changes the mean radiant temperature and the power on radiator that maintains the air temperature.

The Self-Organizing Migrating Algorithm (SOMA) is used to find the optimal electric power on heating panels and the electric power on radiator. During migration cycle, the SOMA generates individuals (set of power on heating panel and power on radiator) in given boundaries. The user sets these boundaries in section “Boundaries of optimized parameters” as the minimal and maximal electric power on radiator and heating panels (See Fig. 5.4.). The SOMA evaluates the cost function which is defined as sum of costs for electric power on heating panels, costs for electric power on the radiator and the absolute value of PMV multiplied by empirically determined constant. The SOMA optimizes the individuals in order to minimalize the result of cost function. To run the optimization the user either changes the SOMA algorithm by setting the parameters or uses default values (values in brackets):

- *step* – the step size of individual during searching (0.21)
- *pathLength* – defines how far the individual stops behind the leaders (best individual) (2.1)
- *prt* - controls the generation of perturbation vector influencing the movement of individual (0.15)
- *minDiv* – terminating parameter, defines the minimal difference between actual and previous cost function value (0.0)
- *migrations* – terminating parameter, number of migrations that must be

performed (16)

- *popSize* – size of population (number of individuals) (10) (Zelinka, 2002)

To start optimization we use the button “Optimize”. During the optimization we can watch the graph of result of cost function on migrations on the bottom of window (see Fig. 5.4.)

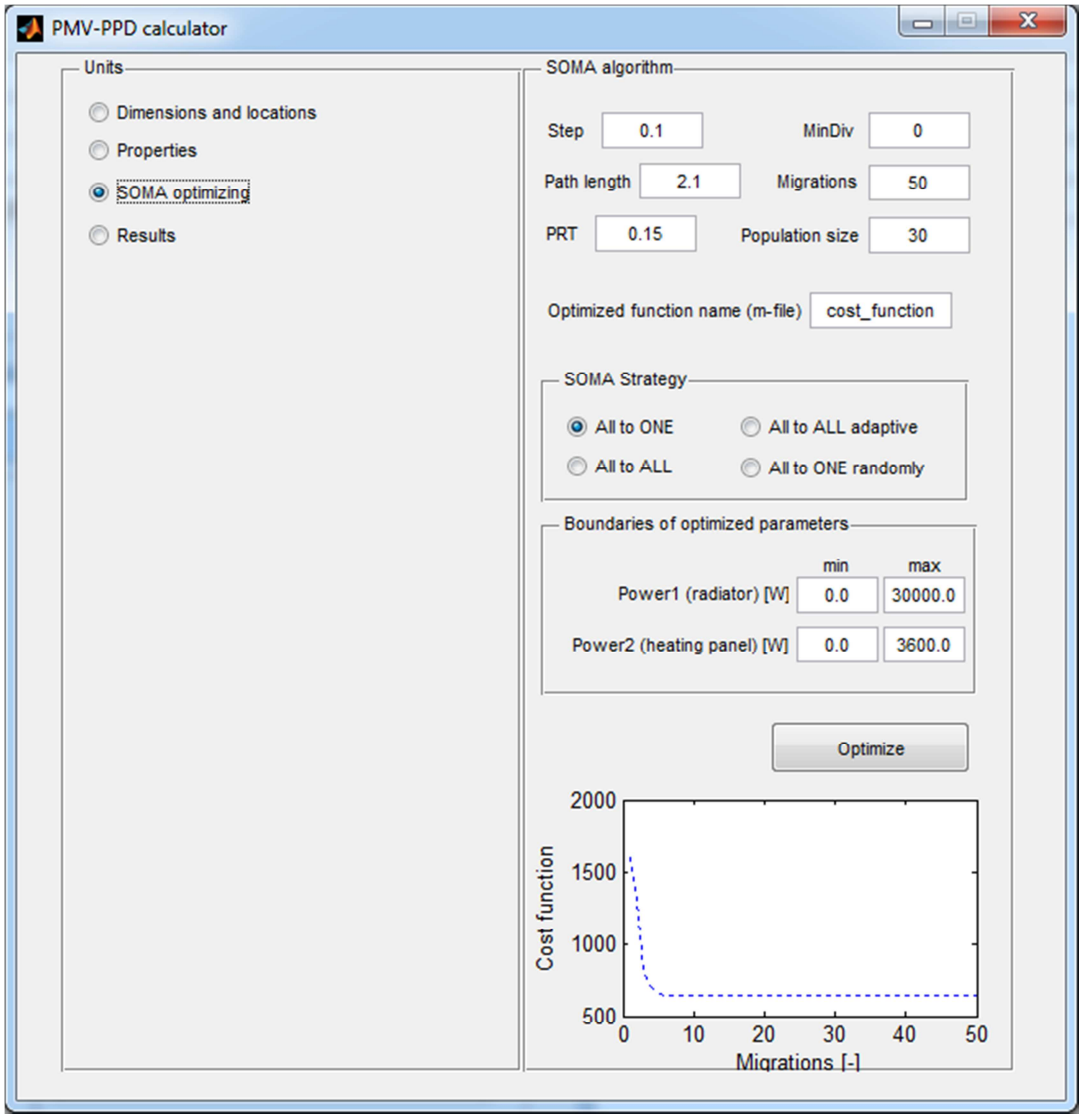

Fig. 5.4. Model of real room – SOMA optimizing

When optimization is finished we are moved to “Result” window, which shows the

quantities described in Chapter 5.2. However the window is the same as is in Chapter 5.2, the results PMV, Power1, Power2 and prices are optimized now.

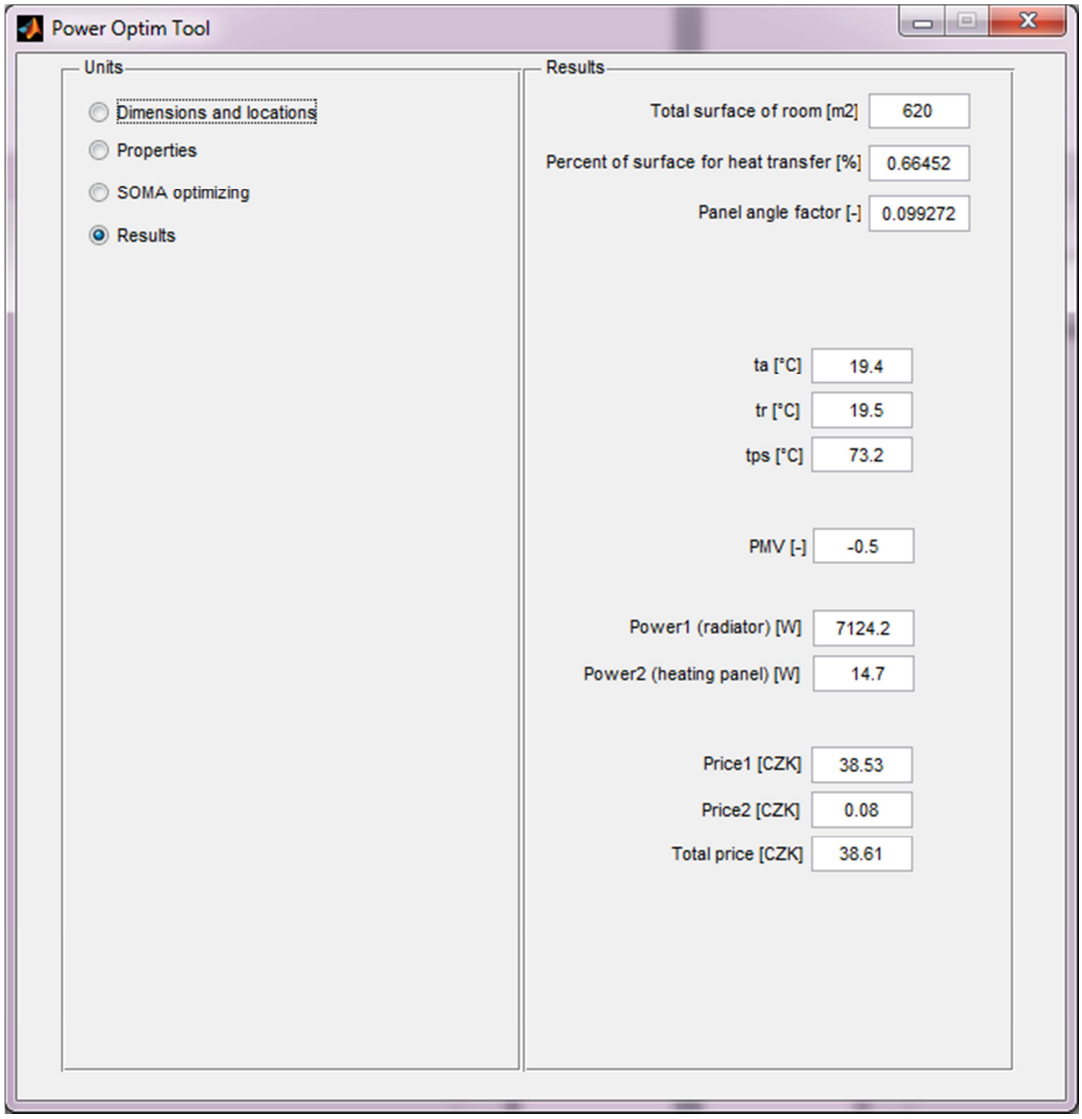

Fig. 5.5. SOMA optimized results

5.4 Mean radiant temperature evaluation and overlapping of scanned areas study

The mean radiant temperature is specific parameter in thermal comfort evaluation. This parameter can be measured with black-globe thermometer, two-sphere radiometer, constant-air-temperature sensor or net radiometer (all described in Chapter 0). In this thesis, the thermopile sensor is taken into account when evaluating mean radiant temperature and following subchapters deal with this particular sensor. Device developed for this purpose consists from sensor's sphere, set of thermopile sensors and evaluation circuits ensuring ambient temperature compensation and signal amplification.

5.4.1 Nonlinear curve fitting of field of view

The output signal of thermopile sensor depends on the amount of incident thermal radiation. This incident radiation is given by temperature of observing object, object surface emissivity and atmospheric absorption spectrum. This statement is true while all incident thermal radiation comes from observing object. With thermopile sensor we can measure only the solid angle given by sensor's field of view. Furthermore, the relative output signal depends on angle of incidence (see Fig. 5.6.). The typical field of view of thermopile sensor up to 100° implies that 50% of normalized response is available at 50° angle of incidence.

Evaluating mean radiant temperature of whole area requires using several sensors to cover whole space (the solid angle of 4π steradians) and we have to know how many sensors are needed and how precisely is the whole space detected and if any blind spaces appear.

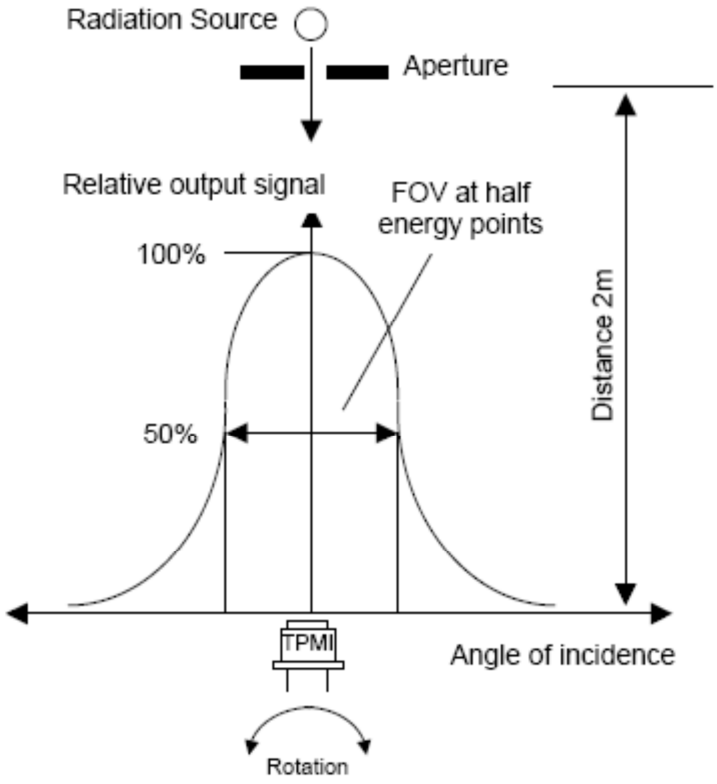

Fig. 5.6. Dependence of relative output signal on angle of incidence (PerkinElmer, 2003)

The FOV of each sensor is defined by producer in datasheet and it is needed to describe the dependency of normalized signal by mathematical formula for further evaluation. Because of different data sources provided from producers it is convenient to rewrite the graphical interpretation (e.g. Fig. 5.7.), which is always available, into set of values (set of pairs) of relative output signal, or normalized signal and angle of incidence, see Table 5.4. It is sufficient to rewrite only one half of the graphic interpretation into the digital form because the normalized signal on angle is an even function and second half of this characteristic is the symmetric one to the first part.

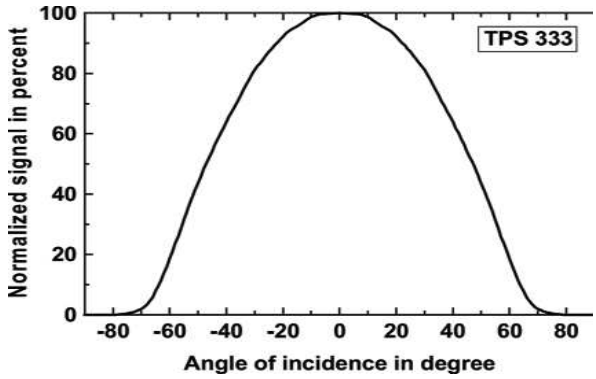

Fig. 5.7. Graphical interpretation of normalized output signal on angle of incidence (PerkinElmer , 2003)

Table 5.4. Obtained data of normalized signal

Angle [°]	***Normalized signal [-]***
-90	0.00
-80	0.02
-70	0.08
-60	0.20
-50	0.42
-40	0.65
-30	0.82
-20	0.93
-10	0.98
0	1.00

We can use this data and create mathematical formula. This procedure is done with the Matlab script (See APPENDIX B). This procedure performs nonlinear curve-fitting with least-squares method with the help of Matlab *lsqcurvefit* function that finds coefficients to the best fitting nonlinear function *f* to the given data.

The *lsqcurvefit* finds coefficients according to following equation:

$$\min_x \left\| F(x, xdata) - ydata \right\|_2^2 = \min \sum_i \left(\left(F(x, xdata_i \right) - ydata_i \right)^2 \qquad (4.9)$$

where *xdata* [vector] is given input data, *ydata* [vector] is observed output data and *F* (*x*, *xdata*) is a vector-valued function. The result of this procedure is nonlinear function fitting the input data (green squares) see Fig. 5.8. It is possible to change the nonlinear function; this is simply done in script myfun.m, where this function is defined (in this work the 6th order polynomial function is used):

$$f = a_6 x^6 + a_5 x^5 + a_4 x^4 + a_3 x^3 + a_2 x^2 + a_1 x + a_0 \qquad (4.10)$$

where *f* is the nonlinear function, a_0, a_1, a_2, a_3, a_4, a_5, a_6 [-] are the best fitting coefficients. The resulting coefficients of thermopile sensor (specifically TPS 333 sensor in our case, detail described in Chapter 5.6) are:

a_6 = -1.7689

a_5 = 7.2354

a_4 = -9.9893

a_3 = -5.6896

a_2 = -2.0559

a_1 = -0.1378

a_0 = 0.9994

and the graph of the best fitting nonlinear function *f* for angle from $-\pi/2$ to 0 radians and its symmetric part for angle from 0 to $+\pi/2$ radians is shown on Fig. 5.8.

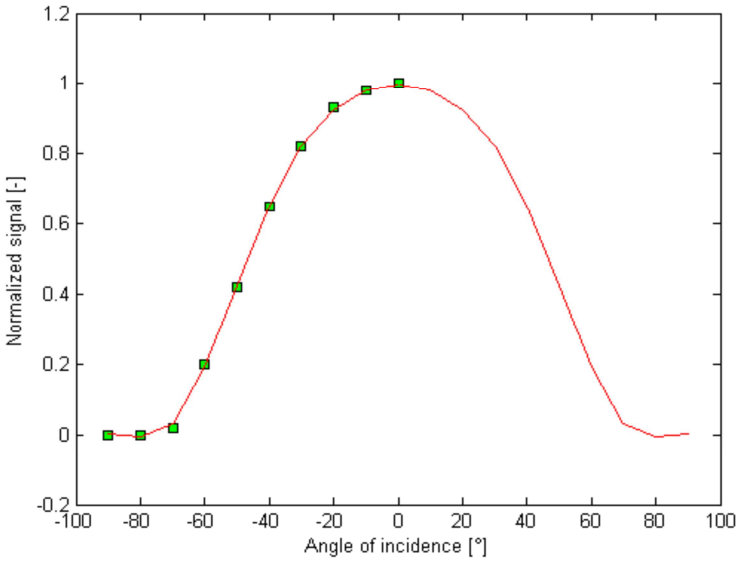

Fig. 5.8. The best fitting nonlinear function

5.4.2 Visualization of total signal of scanned areas

The output of each thermopile sensor represents one part of total radiation received from whole space. To visualize the total radiation received from all sensors placed on sensor head we have to sum up all outputs from individual sensors. This is the three-dimensional summation of sensor's outputs and the result is displayed on unit sphere surface and total sum of normalized signal at any place is presented by colour intensity. The colour bar is also displayed (See Fig. 5.11.). The visualization program has following inputs:

- location of sensors (given as matrix of elevation and azimuth of each sensor)
- quality of resulting image (influence the time needed to compute intensity of every point on sphere surface
- function that describes the output signal on angle of incidence of thermopile sensor (discussed in Chapter 5.4.1)

Visualization script transforms spherical coordinates into Cartesian coordinates and then

we can display normalized signal as 3-D shaded surface of sphere with different colour. Transformation and symbols used in transformation corresponds to diagram on Fig. 5.9.

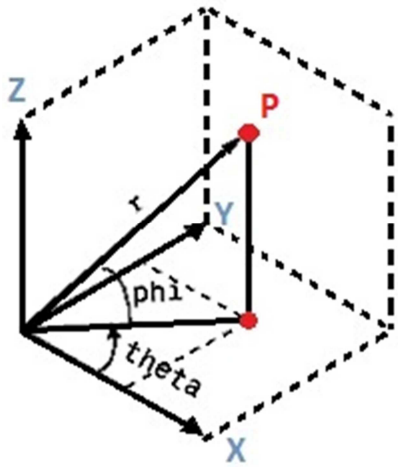

Fig. 5.9. Diagram of transformation between Cartesian and spherical coordinates

Transformation FOV (Field of View) of each sensor into Cartesian coordinate system uses Equations (4.11), (4.12) and (4.13):

$$x = r\sin(\theta)\cos(\varphi) \tag{4.11}$$

$$y = r\sin(\theta)\sin(\varphi) \tag{4.12}$$

$$z = r\cos(\varphi) \tag{4.13}$$

where x [-], y [-], z [-] are Cartesian coordinates; r [-] is radius, φ [-] is azimuth and θ [-] is inclination.

The normalized signal of particular sensor is computed according to the best fitting nonlinear function. To calculate normalized signal in three-dimensional space we have to consider the angle of incidence in non-linear function in Equation (4.10) as a half of an apex angle 2*θ between the sensor's location B and a point on sphere surface A (see Fig. 5.10.). In the diagram the half of an apex angle θ [°] can be determined as follows:

$$\sin\theta = \frac{\frac{distance}{2}}{r} \tag{4.14}$$

$$\theta = \operatorname{asin}\frac{distance}{2} \tag{4.15}$$

where *distance* [-] is Euclidean distance between A and B; *r* is the radius of a unit sphere

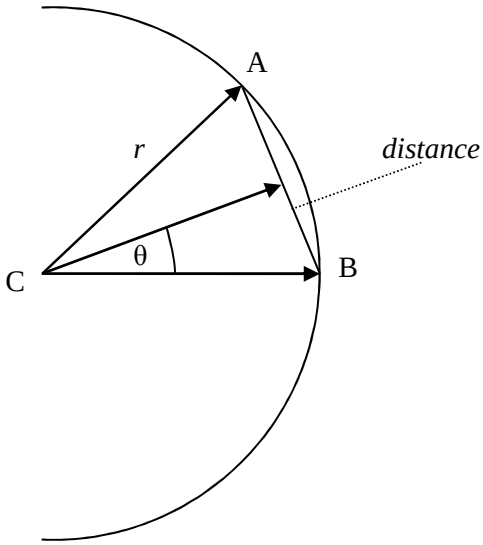

Fig. 5.10. Graphical definition of an apex angle 2*θ

Euclidean distance in three-dimensional space is calculated as

$$distance = \sqrt{\left(x_1 - x_2\right)^2 + \left(y_1 - y_2\right)^2 + \left(z_1 - z_2\right)^2} \tag{4.16}$$

where x_1[-], y_1[-], z_1[-] are coordinates of sensor location; x_2[-], y_2[-] and z_2[-] are coordinates of points on sphere surface.

To evaluate the intensity of any point we can simply use coordinates of the point, calculate the distance and apex angle between point and sensor location and then calculate the normalized intensity with the nonlinear function *f*.

The visualization has been programmed in Matlab environment. These scripts are prepared:

- myFun
- calcIntensity
- calcSphere
- startVisualization

The myFun.m script contains the declaration of **myFun** function that is used to calculate the normalized signal for given angle of incidence. This function takes angle of incidence and coefficients of nonlinear function *f* (4.10) as input parameters.

The **calcIntensity** function computes normalized signal at given point on unit sphere surface. It has following inputs: location of point on sphere surface which is actually processed (given in spherical coordinates as azimuth and inclination), the sensors locations (given as matrix of azimuth and inclination) and number of actually processing sensor. This function transforms actual sensor's location and location of point into Cartesian coordinates according to equations (4.11), (4.12) and (4.13), calculates the distance between points with Equation (4.16) and determines the angle between location of sensor and actually processed point through the Equation (4.15). The calcIntensity calls myFun function with calculated angle of incidence and calculates the normalized signal.

The **calcSphere_optim** function iteratively computes normalized signal of every point on unit sphere surface (iteratively calls calcIntensity function) and this procedure repeats for each sensor. Finally; the normalized signals from each sensor are summed up.

We can use **start_visualization** script to start visualization. This script contains configuration settings such as coefficients of nonlinear function *F* (4.10) and sensors locations and command displaying the sphere surfaces with normalized signals.

The visualization of space with one thermopile sensor located on the top and with dependency of normalized signal on angle of incidence given by (4.10) is shown on the Fig. 5.8. As can be seen the normalized signal is equal to 100 % near the sensors location and from this point the normalized signal is decreasing to 0 %.

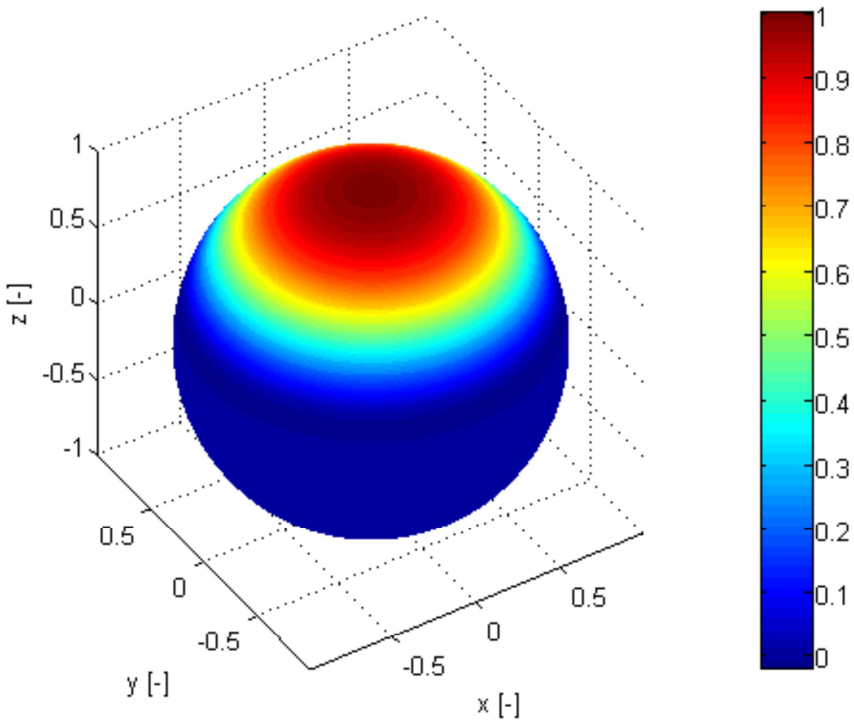

Fig. 5.11. 3-D map of whole space with one thermopile sensor

Fig. 5.12. shows the 3-D map of whole space with six thermopile sensors located on each side, top and bottom.

Statistic results: MIN = 0.9091; MAX = 1.1201; STDEV = 0.0483; MEAN = 1.0000
where MIN is minimal value, MAX is maximal value and STDEV is standard deviation.

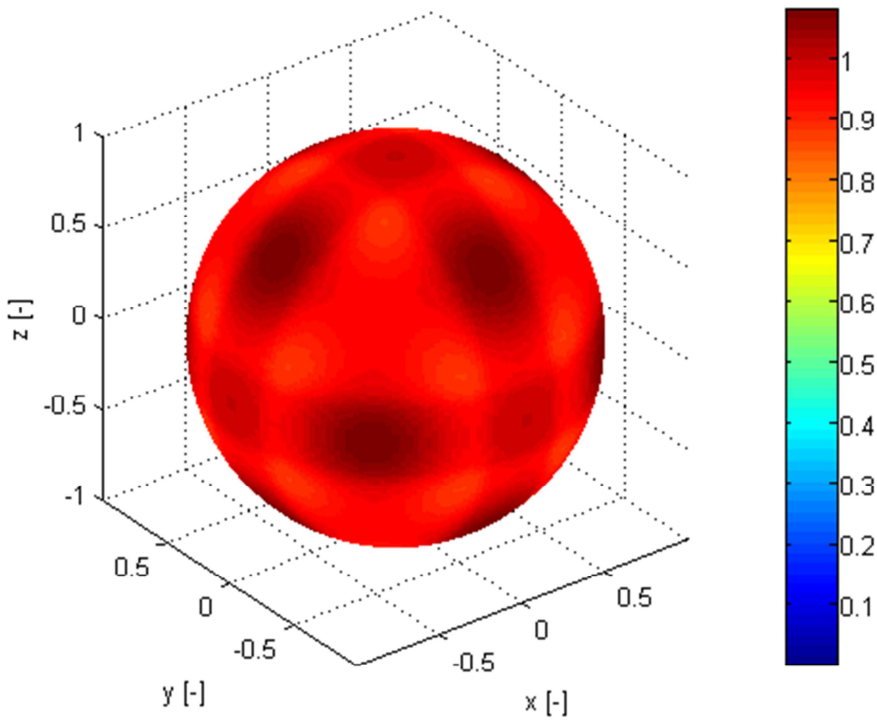

Fig. 5.13. 3-D map of whole space with six thermopile sensors

5.4.3 Field of view optimization

The visualization of six thermopile sensors showed that whole space is not scanned uniformly and places where normalized signal is less than 100% exist. There are two possible ways to resolve this deficiency.

a) change the number of sensors and their locations
b) modify the nonlinear function describing dependency on normalized signal on angle of incidence

The a) optimization has been done experimentally by changing number of sensors and their locations (i.e. changing the matrix of elevation and azimuth of sensors). As a simplification the platonic solids has been tried. Platonic solids are polyhedrons composed from regular

polygon and therefore the vertices are uniformly distributed on sphere surface. We can use Cartesian coordinates defining the vertices of polyhedron, transform them into spherical coordinates and then easily use them as sensor's locations. For example; the Platonic solid dodecahedron has been tried Fig. 5.14. Regular dodecahedron is composed from 12 regular pentagonal faces meeting at each vertex. The Cartesian coordinates of this solid are:

$(\pm 1, \pm 1, \pm 1)$

$(0, \pm 1/\varphi, \pm\varphi)$

$(\pm 1/\varphi, \pm\varphi, 0)$

$(\pm\varphi, 0, \pm 1/\varphi)$

where $\varphi = \frac{1+\sqrt{5}}{2} = 1.618$ is the golden ratio.

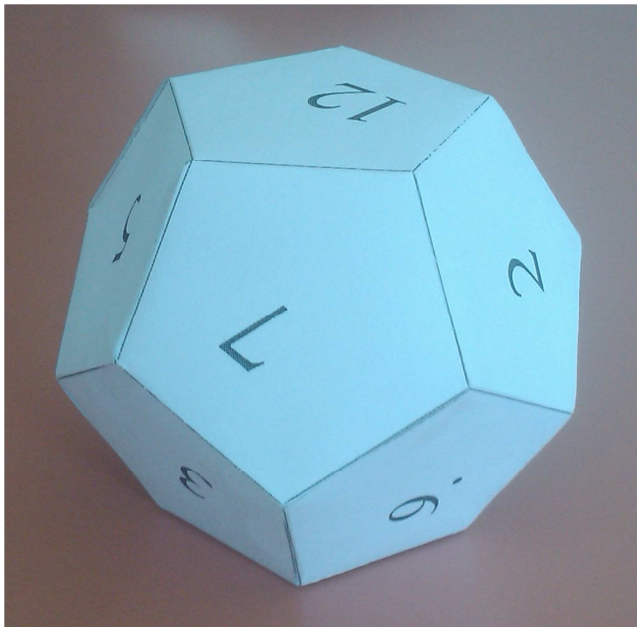

Fig. 5.14. Image of dodecahedron

The visualization of whole space with sensors placed in each vertex of dodecahedron is shown on Fig. 5.15.

Statistic results: MIN = 0.9118; MAX = 1.0805; STDEV = 0.0390; MEAN = 1.0000

where MIN is minimal value, MAX is maximal value and STDEV is standard deviation.

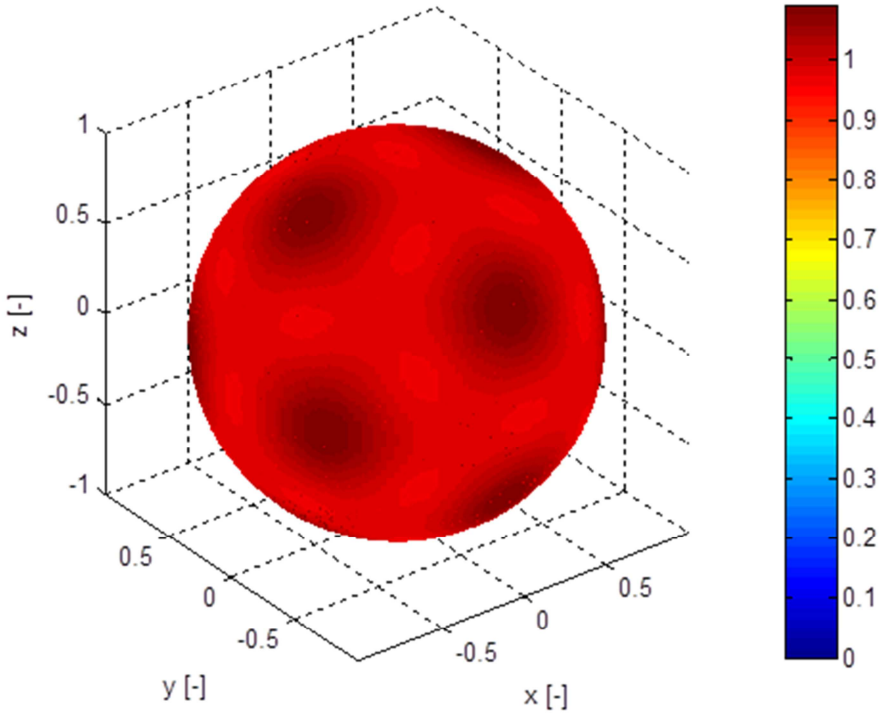

Fig. 5.15. 3-D map of whole space with twelve thermopile sensors

In optimization b) we are modifying nonlinear function *f* defined by (4.10) and its coefficients a_0 to a_6 in order to achieve more uniform distribution of normalized signal. The Field of View (FOV) can be modified with customizing cover hole size and internal aperture (see Fig. 5.16.) of the sensor as described in (Dexter Research Center). The basic idea is to calculate normalized signal of every point of the sphere surface, evaluate the cost function corresponding the the quality of normalized signal distribution, modify coefficients of nonlinear function *f* and repeat this process to achieve the lowest possible value of cost function.

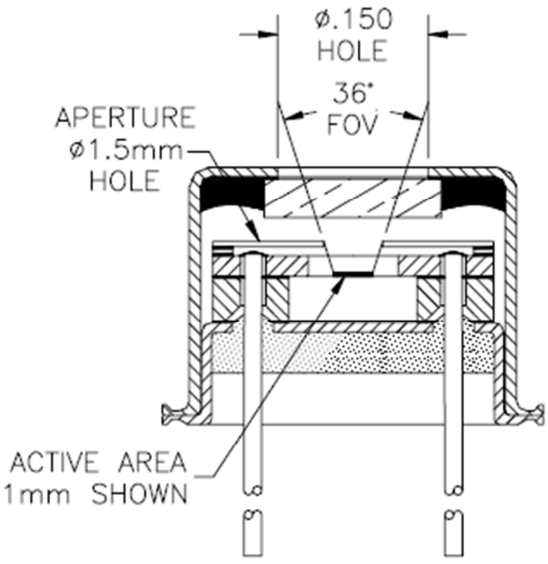

Fig. 5.16. Effects of internal aperture and cover hole on FOV (Dexter Research Center)

We can optimize this numerical problem with some evolutionary algorithm (EA) or genetic algorithm (GA). In this work, the Self-Organizing Migrating Algorithm (SOMA) is used in optimization. The source code of SOMA for Matlab was downloaded from www (Zelinka). There are 5 Matlab functions used in the optimization:

- myFun
- calcIntensity
- calcSphere_optim
- soma_all_to_one
- start_optim_polynomial

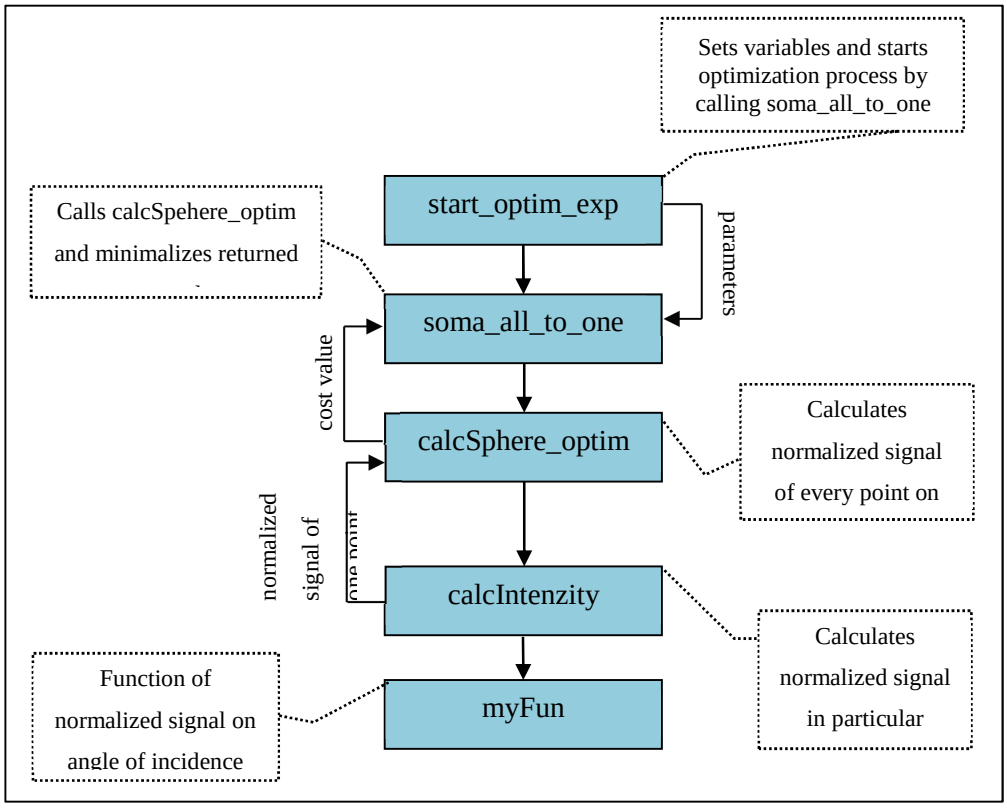

Fig. 5.17. The flowchart representing the optimization process

Functions myFun, calcIntensity and calcSphere_optim are described in Chapter 5.4.2. The calcSphere function is modified because of use in SOMA and this modification returns the cost value given as the sum of standard deviation of normalized signal of all points on sphere surface and the difference between the maximal and the minimal value of normalized signal.

The **start_optim_polynomial** declares and initializes variables

- precision – defines the density of points on surface sphere
- sensors location
- boundaries – limits of acceptable values of coefficients of function *f*
- optimized function as a parameter used in SOMA
- SOMA parameters (*step*, *pathLength*, *prt*, *minDiv*, *migrations*, *popSize*) –

discussed in Chapter 0

and calls the evolutionary algorithm script **soma_all_to_one**. There was used the nonlinear function *f* with six coefficients describing the dependency of normalized signal on angle of incidence in the first concept of this optimalization. Unfortunately, the results were insufficient and evolutionary algorithm could not solve this problem. The six coefficients cause difficulties because small changes in coefficients (especially in term with largest degree, the six degree in our case) causes large change in the shape of function and therefore evolutionary algorithm does not work.

To solve this problem we can replace the polynomial 6^{th} order nonlinear function with more appropriate one and as suitable function can be used

$$f_{\exp} = \frac{1}{1 + ae^{-b(angle+c)}} \tag{4.17}$$

where *a*, *b*, *c* [-] are coefficients.

The optimization with SOMA found the optimal solution where the sum of standard deviation of normalized signal of all points on sphere surface and the difference between the maximal and the minimal value of normalized signal is minimal. The optimization set the coefficients of f_{exp} to

a = 37.1960

b = 5.9368

c = 1.4108

and optimized FOV is shown on Fig. 5.18. This result is after 16 migration cycles (Fig. 5.19.) and optimized 3-D map of whole space is presented on Fig. 5.20.

Statistic results: MIN = 0.8809; MAX = 1.0439; STDEV = 0.0334; MEAN = 1.0000

where MIN is minimal value, MAX is maximal value and STDEV is standard deviation.

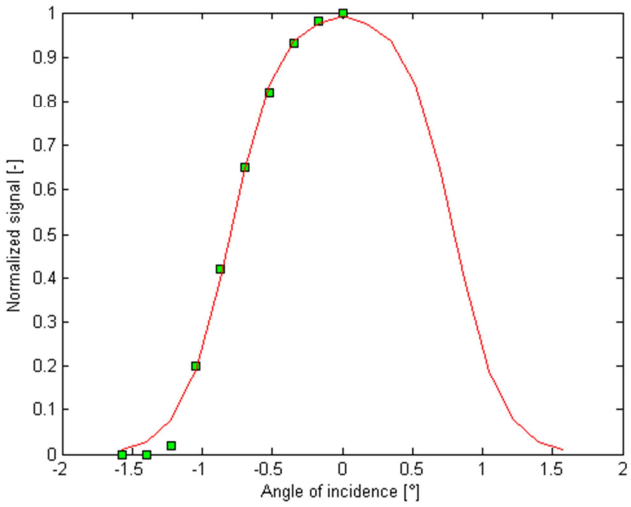

Fig. 5.18. The best fitting f_{exp} function

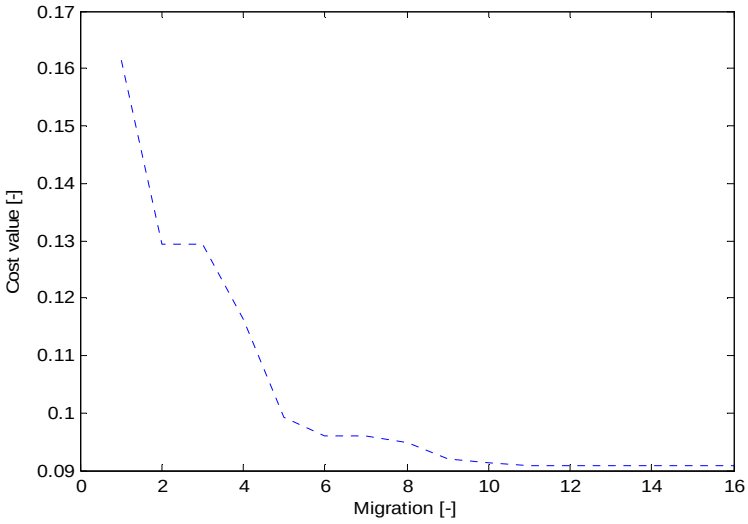

Fig. 5.19. Course of cost function on migration cycles

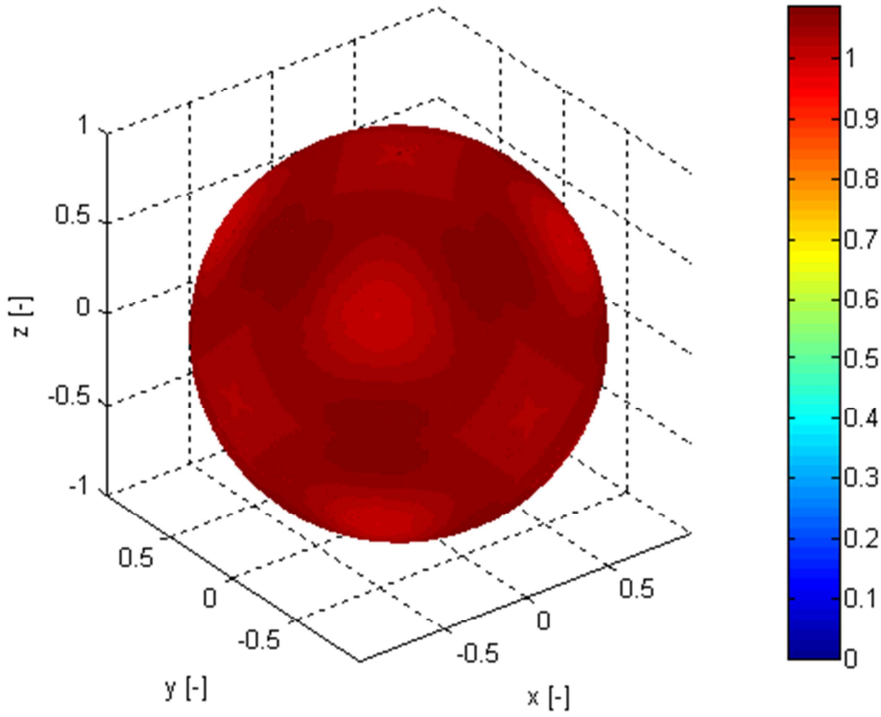

Fig. 5.20. Optimized 3-D map of whole space with six thermopile sensors

5.4.4 Evaluation of mean radiant temperature asymmetry

This chapter deals with radiant asymmetry that is not possible to measure with standard globe thermometer which is recommended by ISO 7726 standard. Globe thermometer provides only one temperature – the temperature of the black globe, which is use for mean radiant temperature determination. With this principle we are unable to measure radiant asymmetry that can alslo cause discomfort. As stated in Chapter 4.3.14, most people are sensitive to radiant asymmetry caused by warm ceilings or cool walls, and therefore ISO 7730 provides Equations (3.70) to (3.73) used for determination of percentage dissatisfied (PD) from radiant asymmetry. To evaluate these equations we have to know the temperature of ceiling, floor and walls. With the concept of MRT measurement with several thermopiles (at least six) presented in this thesis we can determine the temperature of ceiling, floor and walls independently, calculate radiant asymmetry Δt_{pr} and determine

the percentage of dissatisfied with Equations (3.70), (3.71), (3.72) and (3.73) for warm ceiling, cool wall, cool ceiling and warm wall respectively.

Non-contact two-dimensional area temperature measurement

The study of influence of local temperature differences on thermal comfort (discomfort) has been done within the scope of this work and presented as (Non-contact two-dimensional area temperature measurement, 2009) at the 20th International DAAAM Symposium. In this work the series of measurements in different parts of building (especially in places with cooling, heating, window surroundings and others) has been done (See Fig. 5.21.). The measurement was performed with Horiba ii-1064 infrared thermometer containing 64-element thermopile array (8x8 elements) combined with CCD camera. The main purpose of this work was to qualitatively and quantitatively describe these influences on thermal comfort.

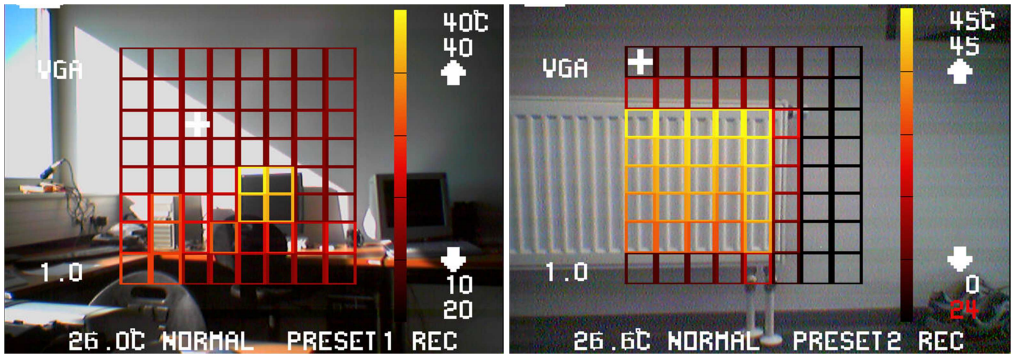

Fig. 5.21. Sample images of measurement

5.5 Measurement system design

This chapter describes measurement system used for verification of validity of standard PMV model. There were designed three measurement systems:

Analog version - ambient temperature compensation

This measurement system provides device capable of analog mean radiant temperature

measurement of half space with five thermopile measurement. The emissivity and ambient temperature compensation are taken in account. This version has been alredy verified by (Skocik, 2004).

Digital laboratory version (solution)

This verification system is used for laboratory measurement and it is designed with high modularity and easy to operate. It utilizes Datalab IO (input/output devices) communicating with personal computer with Control Web software. This device enables to connect different sensors and signal processing. With this capability it is easy to set up and reconfigure the system.

Digital embedded version (solution)

This solution presents design of embedded version that is able to measure and evaluate thermal comfort. This system uses microcontroller (ADuC845 device) from Analog Devices that incorporates many features such as analog/digital interface, microprocessor, and flash memory on single chip, communication ports, watchdog and others). This system is prepared on the evaluation board, sensors and LCD were connected and application is programmed.

5.5.1 Analog version - ambient temperature compensation

As a result of thermopile principle (described in Chapter 0) the measurement with this sensor is influenced by ambient temperature and therefore the ambient temperature compensation must be done. According the Stefan-Boltzmann law the total radiation power P_o emitted by measured area of temperature T_o and emissivity ε_o is

$$P_o = \varepsilon_o \sigma T_o^4 \tag{4.18}$$

where ε_o [-] is emissivity of detected area and σ [$Wm^{-2}K^{-4}$] is the Stefan-Boltzmann constant $\sigma = 5{,}6693\times10^{-8}$ $Wm^{-2}K^{-4}$.

Analogically to measured area the thermopile detector emits radiation of power P_s [Wm-*2*]

$$P_s = \varepsilon_s \sigma T_s^4 \tag{4.19}$$

where ε_s [-] is sensor emissivity and T_s [K] is sensor temperature (we can consider it equal to the ambient temperature.

Then the incident radiant flux on the thermopile is

$$\Phi_e = \varphi_{12} \sigma \left[\varepsilon_o T_o^4 - \varepsilon_s T_s^4 \right] \tag{4.20}$$

where φ_{12} is field of view (-)

Incident radiation generates on thermopile the voltage U_{TP} [V]

$$U_{TP} = G \varphi_{12} \sigma \left[\varepsilon_o T_o^4 - \varepsilon_s T_s^4 \right] = K S_s \varphi_{12} \sigma \left[\varepsilon_o T_o^4 - \varepsilon_s T_s^4 \right] \tag{4.21}$$

where G [Vm^2W^{-1}] is sensor constant; K [VW^{-1}] instrument sensitivity and S_s [m^2] is sensitive area of sensor.

The output voltage of detector is in the range of millivolts and therefore it is needed to amplify it with low noise and low offset operational amplifier. We obtain the resulting voltage

$$U_{TP}^* \left(T_o, T_s \right) = A_{TP} G \varphi_{12} \sigma \left[\varepsilon_o T_o^4 - \varepsilon_s T_s^4 \right] \quad [V] \tag{4.22}$$

where A_{TP} [-] is gain of operational amplifier.

The thermopile detects whole area with $\varphi_{12} = 1$ at mean radiant temperature $\overline{T}_o$. This lead to the equation

$$U_{TP}^* \left(T_o, T_s \right) = A_{TP} G \sigma \left[\varepsilon_o \overline{T}_o^4 - \varepsilon_s T_s^4 \right] \tag{4.23}$$

From (4.23) can be seen that amplified voltage at thermopile depends on temperature of detected area and also on ambient temperature. To compensate this dependency we have to add to the thermopile signal $U_{TP}^*(\overline{T}_o, T_s)$ a voltage of value

$$U_s \left(T_s \right) = A_{TP} G \sigma_0 \varepsilon_s T_s^4 \tag{4.24}$$

To obtain this voltage and compensate output signal to ambient temperature we can use thermistor incorporated in thermopile housing that is recording sensor's temperature. In this research we have designed electronic circuit using non-linear thermistor characteristics, operational amplifier, serial-parallel combination of R_1, R_2 thermistors

and adjustable voltage input U_{in} [V] (see Fig. 5.22)

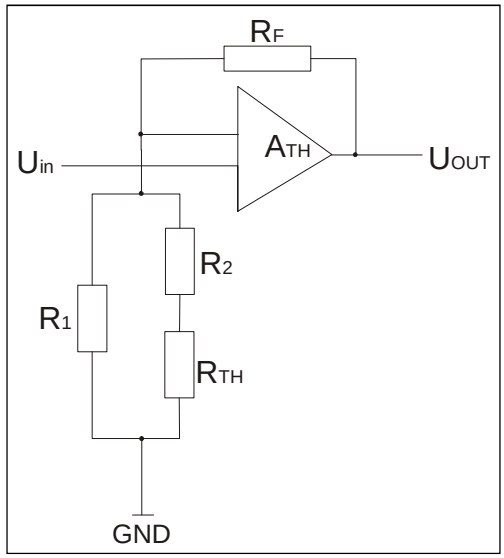

Fig. 5.22. Circuit diagram of compensation (Pálka, 2004)

This compensating signal is then added to thermopile signal and the resulting voltage is then

$$U_{TP}^{*}\left(\overline{T}_o, T_s\right) = A_{TP} G\sigma\left[\varepsilon_o \overline{T}_o^4 - \varepsilon_s T_s^4\right] = A_{TP} G\sigma\varepsilon_o \overline{T}_o^4 - A_{TP} G\sigma\varepsilon_s T_s^4 \qquad (4.25)$$

$$U_{TP}^{*}\left(\overline{T}_o, T_s\right) + U_s(T_s) = A_{TP} G\sigma\varepsilon_o \overline{T}_o^4 - A_{TP} G\sigma\varepsilon_s T_s^4 + A_{TP} G\sigma\varepsilon_s T_s^4 \qquad (4.26)$$

$$U_{TP}^{*}\left(\overline{T}_o, T_s\right) + U_s(T_s) = U_o(\overline{T}_o) = A_{TP} G\sigma\varepsilon_o \overline{T}_o^4 \qquad (4.27)$$

Finally, from equation (4.27) (which is independent of the ambient temperature) is derived the temperature T_o [K] of measured area

$$\overline{T}_o = \sqrt[4]{\frac{U_o(\overline{T}_o)}{A_{TP} G\sigma\varepsilon_0}} = \sqrt[4]{\frac{U_{TP}^{*}\left(\overline{T}_o, T_s\right) + U_s(T_s)}{A_{TP} G\sigma\varepsilon_0}} \qquad (4.28)$$

For calculation we have to know the emissivity of detected area. For most substances the emissivity is 0.93 ± 0.05 [-]. If precisely measurement is needed, the emissivity has to be find out (the Table 4.1 shows the list of materials with emissivity). The final electronic

circuit that ensures low level thermopile voltage amplification and compensation on ambient temperature is shown in Fig. 5.23. (Pálka, 2004).

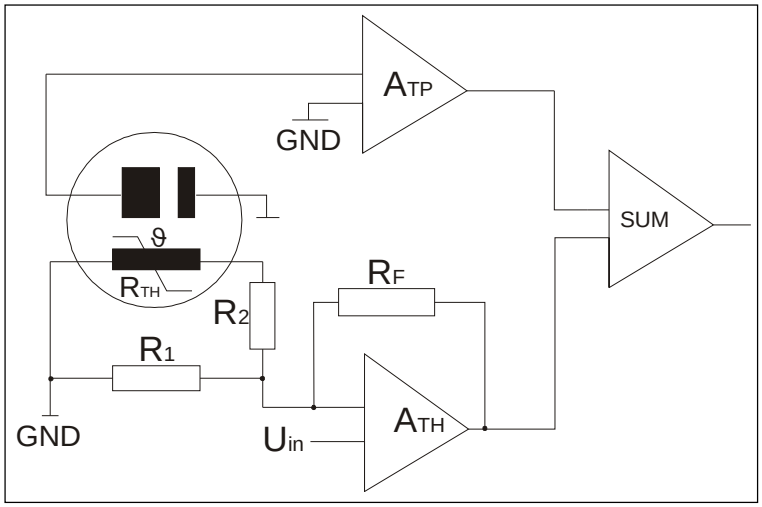

Fig. 5.23. Ambient temperature compensation electronic circuit (Pálka, 2004)

Described solution has been also experimentally verified in testing chamber constructed for these purposes. This work has been done in (Skocik, 2004). The walls of chamber were made from known emissivity and MRT was adjusted to different values. Adjustment has been done by inserting a hotplate with regulated temperature and known surface emissivity. Different ways of measurement and obtained results are described in (Skocik, 2004).

5.5.2 Sensor's sphere construction

Measurement of mean radiant temperature with several thermopile sensors requires object that will hold sensors. The object should hold variable number of sensors and different sensor's location. As a result of this requirement, the object should have a shape of sphere. The sphere has six holes with 4.7 mm in diameter in case of our measurement with six thermopiles TPS 333. The thermopile output is low level voltage signal (tens and hundreds of microvolts) therefore the length of wires linkink the thermopiles and DataLab unit must be as short as possible. To achieve this, the DataLab IO[1] is placed inside of sphere. The maximal power consumption of DataLab IO1 is 190 mA at 5 V, i.e. 0.95 W and therefore

the heating can be neglected. Nevertheless, if any heating (and temperature of sensor's sphere change) arise; the radiant temperature is compensated according to temperature of sensor's sphere.

The diameter of sphere is chosen with the respect of

a) diameter of black globe thermometer recommended by (ISO 7726, 1998) that is 0.15 m
b) the dimensions of DataLab IO[1] included inside of senso

Sensor's sphere surface is painted with shiny silver colour in order to reflect radiation and to have the temperature of sensor's sphere the same as ambient temperature.

Fig. 5.24. Sensor's sphere

5.5.3 Digital laboratory solution

This solution is intended for laboratory testing to experimentally verify assumptions declared in previous chapters. This system is based on DataLab unit produced by Moravian Instruments. DataLab is modular device with one, two or four slots for I/O modules and we can choose how many modules and which modules we will use. In this solution we use module DataLab IO[1] (Fig. 5.25.) equipped with module AI3 having 8 analog inputs with 16-bit resolution. DataLab IO[1] is connected to personal computer via USB and read data is processed in Control Web software, which is intended for the usage with DataLab units.

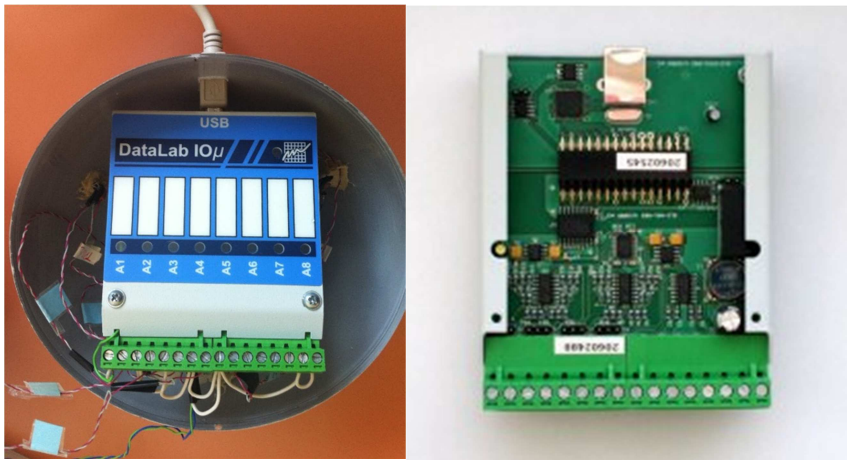

Fig. 5.25. Datalab IO[1] device placed in sensor sphere (left) and AI3 module inside (right) (Moravian Instruments, 2009)

The variability of this digital laboratory solution is given by analog inputs which can be used for different purposes (for measurement different sensors with voltage or current output). Easy to operate mentioned above means that connecting sensor to DataLab is the only hardware operation needed because signal evaluating and processing is accomplished with the DataLab unit configuration and application programmed in ControlWeb. The block diagram of digital laboratory solution is presented on Fig. 5.26. The environment and physical parameter are represented by "Monitored area" block. The device that measures the physical quantity and converts it into signal is represented by "Sensor" block. Outputs from sensors are read by DataLab IO[1] unit with AI3 module. This uses a 16-bit resolution analog to digital converter and programmable gain amplifier in order to be able measure low level signals. The result of DataLab unit – digitized data – is send via universal serial bus (USB) to personal computer with ControlWeb software installed. An application programmed in ControlWeb provides data processing, computations, presents results, archives data and communicates with user via LCD, keyboard and mouse.

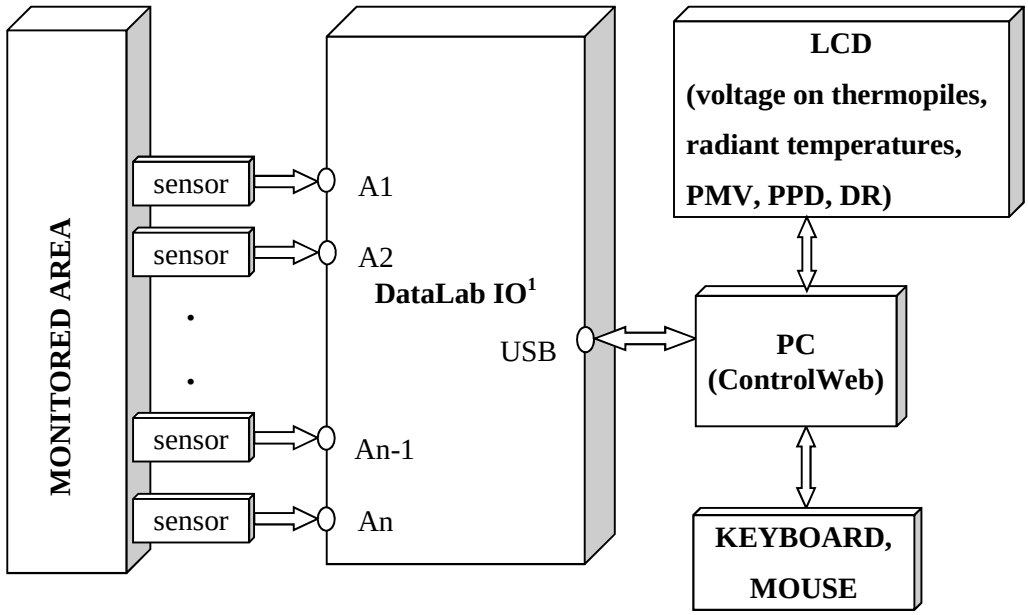

Fig. 5.26. Block diagram of digital laboratory solution

The application “PMV-PPD meter” displayed on Fig. 5.27. is programmed in ControlWeb environment and the basic function of this application is to present measured and processed data in graphical form. Secondary, this application archives all measured data in MS Excel.

The “PMV-PPD meter” application provides processing of measured signals from thermopile sensors, thermistor incorporated in thermopile housing (described in Chapter 5.5.1) and humidity sensor. The application displays measured thermopile outputs u_{TP} [μV] on all channels (thermopile sensors). The need of DataLab ADC offset value measurement resulted from measurement discussed later in Chapter 5.7.2. The offset value is displayd informatively; its value is applied automatically on each channel. Application provides real-time calculation of radiant temperatures t_r [°C] from corresponding thermopile outputs and compensated according to ambient temperature t_a [°C] obtained from thermistor. The emissivity constant in application is set to the value of 0.95.

Beside measured values, the user can input the values in editable, white text boxes which are related to human activity (metabolic rate, external work) and clothing insulation. The value of relative air velocity is also editable; in this thesis, the relative air velocity was measured externally with Testo 435-4 described in Chapter 5.6.1.

Results:

MRT [°C] – resulting mean radiant temperature computed from individual radiant temperatures

Thermal comfort indices – predicted mean vote (PMV [-]), predicted percentage dissatisfied (PPD [%]), draught rating (DR [%])

Graph with course of 1st thermopile output in time.

Fig. 5.27. PMV-PPD meter

5.5.4 Digital embedded solution

For digital embedded solution we need a system providing high-resolution analog to digital converter (ADC) for data acquisition, microprocessor used for calculations, programmable gain amplifier (PGA) for low-level signal measurement, user and data memory, communication peripherals.

There are several international corporations producing these systems: Texas Instruments, Analog Devices, National Semiconductor, Atmel, Freescale Semiconductor and others. The comparison of available products according to many parameters such as number of analog inputs, A/D resolution, common-mode rejection ratio (CMMR), the way of code development, evaluation board, price and others was done. As a result of comparison, the ADuC845 microcontroller from Analog Devices was chosen. This microcontroller (also called microconverter) includes:

- 24-bit Σ-Δ ADC, up to 10-channel, input multiplexing
- 8-bit microcontroller based on Intel 8051
- programmable gain amplifier from 1 to 128
- 62 kbyte Flash program memory
- 4 kbyte Flash data memory
- 12-bit voltage output DAC
- 16-bit Σ-Δ DAC
- on-chip temperature sensor
- serial input/output – UART (Universal Aasynchronous Receiver/Transmitter), I^2C (Inter-Integrated Circuit) and SPI (Serial Peripherial Interface)

With this device we can measure up to 10 different quantities with 24-bit ADC resolution which is sufficient for thermopile low level voltage measurements, evaluate thermal comfort indices, and display results on LCD, archive data and eventually control climate systems. Block diagram of system using all possible features is shown on Fig. 5.28.

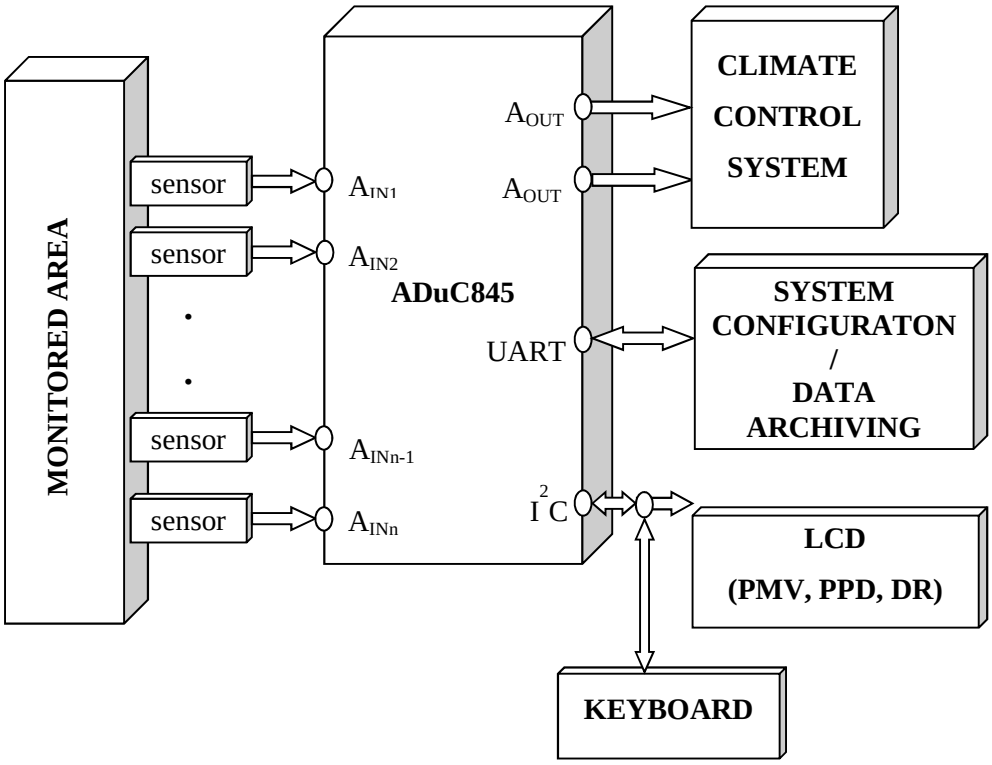

Fig. 5.28. Block diagram of digital embedded solution

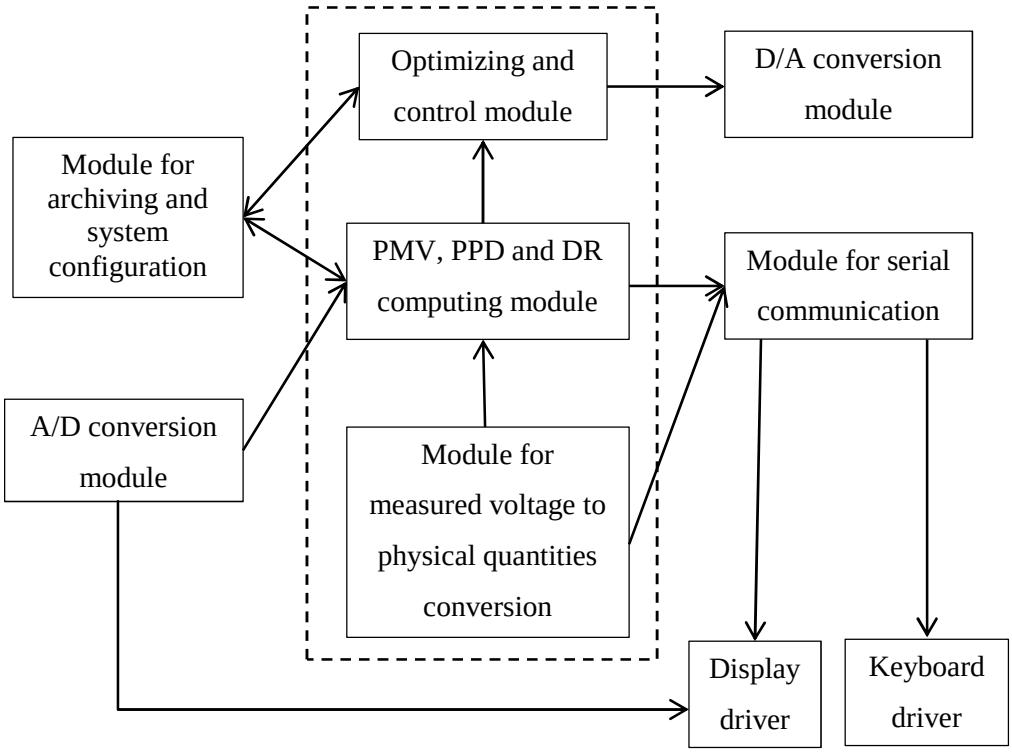

Fig. 5.29. Block diagram of software on ADuC845 microcontroller

Sofware is programmed in C language in KEIL embedded development tool.

5.5.5 Microconverter programming

Program created on ADuC845 uses modular programming principles, which brings advantages such as simpler and clearer program building, easier debugging, program modification and multiple usage of single module. With appropriate definition of inputs and outputs, which is one of the basic condition we can debug modules independently and finally link verified modules into final program. Creation of modules can be described with following procedure (presented on Fig. 5.30.):

- description of programming task

- appropriate algorithms design
- tasks splitting into smaller parts, represented by subprograms
- choosing suitable programming language (assembly language or high-level programming language i.e.C language, Basic or other)
- translation of source codes with compiler into assembly language
- translation with assembler into object code (module)
- linking modules and libraries into absolute program
- conversion of absolute program into machine code file
- follows debugging, function testing and uploading into EPROM memory of controller

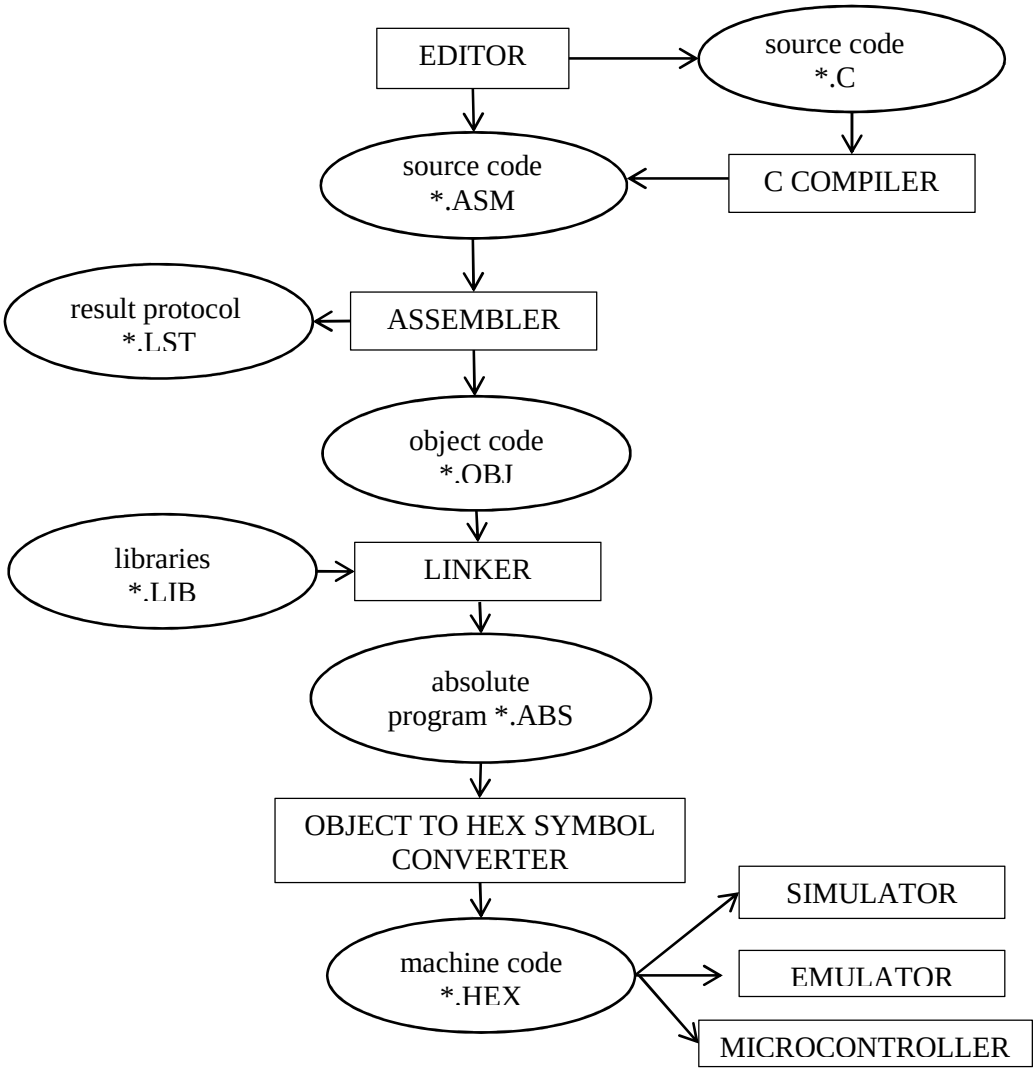

Fig. 5.30. Procedure of creating program

The complete program consists of six modules performing required functions. A brief description of each module is given in following paragraphs.

A/D conversion subprogram

At first, the subprogram configures the ADC:

- Input voltage range choosing with setting the programmable gain amplifier (PGA)
- Bipolar / unipolar configuration of ADC. Analog input can accept either unipolar or bipolar input voltage ranges. Bipolar input ranges do not imply that the part can handle negative voltages with respect to system ground, but rather with respect to the negative reference input. Unipolar and bipolar signals on the positive analog input on the ADC are referenced to the voltage on the respective negative analog input input.
- Data output coding. When the primary ADC is configured for unipolar operation, the output coding is natural (straight) binary with a zero differential input voltage resulting in a code of 000...000, a midscale voltage resulting in a code of 100...000, and a full-scale voltage resulting in a code of 111...111. The output code for any analog input voltage on the main ADC can be represented as follows (ADuC845, 2005) :

$$Code = (AIN \times GAIN \times 2^N) / 1.024 \times V_{REF} \quad (4.29)$$

where AIN is the analog input voltage; GAIN is the PGA gain (from 1 to 128); N = 24 (for ADuC845).

When the primary ADC is conf ured for bipolar operation, the coding is offset binary with negative full-scale voltage resulting in a code of 000...000, a zero differential voltage resulting in a code of 800…000, and a positive full-scale voltage resulting in a code of 111...111. The output from the primary ADC for any analog input voltage can be represented as follows (ADuC845, 2005):

$$Code = 2^{N-1} \left[\left(AIN \times GAIN \right) / \left(1.024 \times V_{REF} \right) + 1 \right] \quad (4.30)$$

where AIN is the analog input voltage; GAIN is the PGA gain (from 1 to 128); N = 24 (for ADuC845).

- Buffering enabled or disabled.
- Digital filtering to remove the quantization noise with low-pass $Sinc^3$ filter.

Then the program runs conversion function which reads the value from the analog input,

waits until the read is finished and read from next analog input. This reading repeats periodically in a loop.

Subprogram for measured voltages to physical quantities conversion

This subprogram contains algorithms for calculation physical quaintities needed for thermal comfort indices evaluation (voltage values in most cases).

Thermal comfort indices calculation subprogram

This subprogram calculates thermal comfort indices (Predicted Mean Vote, Predicted Percentage of Dissatisfied, Drought Rate) from physical activity and clothing and measured environmental parameters. These models are programmed according (ISO 7730, 2005) and the code given by norm had to be modified to be compilable and runnable on ADuC845 device.

Display driver

This part of program is created for communication with display SIC2004AGPDEB20c from Snail Instruments. The communication is ensured via I^2C bus of ADuC845 device and the driver is programmed according to (PCF2116, 1997).

D/A conversion subprogram

This subprogram provides method that sets the analog voltage output to required voltage. The process is analogous to A/D conversion, ie. DAC must be configured; voltage value must be coded into the binary number.

5.6 Used instruments

This section presents pictures and short description of devices used in experimental part of this work.

5.6.1 Testo 435-4 (Testo)

Testo 435-4 AC System Analyzer is a measuring instrument for ambient air conditions

such as air temperature, humidity, velocity and others (see Fig. 5.31. on the left). The air parameters are measured with specific probes. There was used the thermal velocity probe with built-in temperature and humidity measurement (Fig. 5.31. on the right) in this work. This probe has telescopic handle (max. 745 mm) and measurement ranges are -20 to +70 °C for temperature, 0 to +100 %RH for humidity and 0 to +20 ms^{-1} for velocity.

Fig. 5.31. Testo 435-4 (left) and velocity probe (www.testo.com)

5.6.2 TPS 333 thermopile detector (PerkinElmer – Excelitas Technologies)

TPS 333 is a thermopile detector encased in miniature sensor housing TO 18 (Fig. 5.32.). This device contains thermistor as a temperature reference for ambient temperature compensation. The detector is characterized with constant sensitivity characteristics over the wavelength. (PerkinElmer , 2003). Its major usage is in ear thermometers and miniature pyrometers. The datasheet of this device is in APPENDIX H.

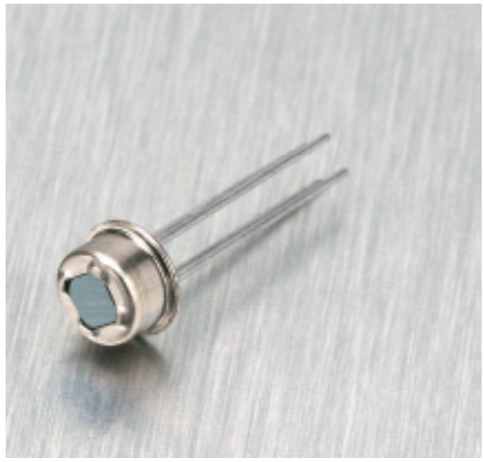

Fig. 5.32. Thermopile sensor (PerkinElmer , 2003)

5.6.3 I-square two-dimensional infrared thermometer ii-1064 (Horiba)

This infrared thermometer (Fig. 5.33.) displays photo of object and the two-dimensional image of temperature distribution on LCD. This thermometer is based on 64-element (8 by 8 matrix) thermopile array. Temperature of each area on frame (each element) is represented with color and it can be also displayed in digital form by selecting the particular are with cursor.

Fig. 5.33. I-square two-dimensional infrared thermometer ii-1064 (www.horiba.com, 2003)

5.6.4 34420A Micro-Ohm Meter (Agilent Technologies)

The Agilent 34420A (on Fig. 5.34.) is nanovolt and microohm meter. This device is a high-sensitivity multimeter optimized for low-level measurements with up to 7½ digit resolution.

Fig. 5.34. Agilent 34420A (www.agilent.com)

5.6.5 ADuC845 24-bit analog to digital converter (Analog Devices)

ADuC845 is a complete smart transducer front end, integrating multichannel 24-bit Σ-Δ analog to digital converter, microcontroller unit, memory on single chip (Fig. 5.35.). The digital embedded solution described in Chapter 5.5.4. uses this chip as the core. The development of digital embedded solution is processed on evaluation board which carries ADuC845 chip with all usable terminals connected to printed circuit board (PCB). The PCB contains pads and terminals for simple connection of external pheripherals (e.g. sensors).

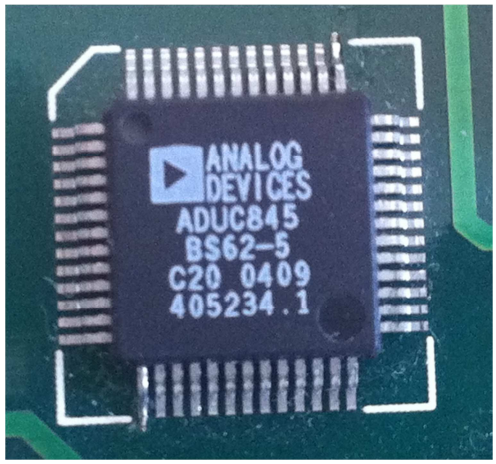

Fig. 5.35. ADuC845 ADC converter

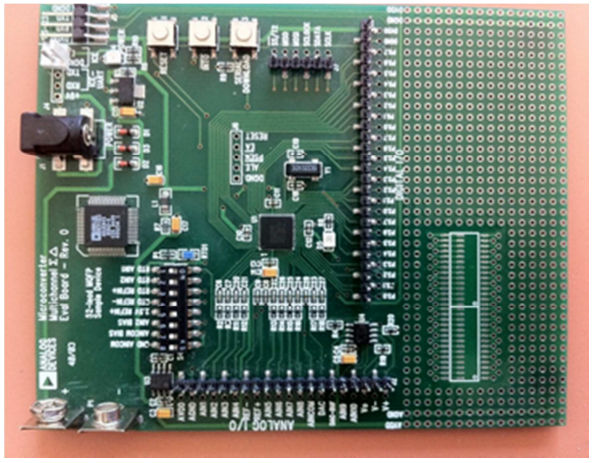

Fig. 5.36. ADuC845 evaluation board

The evaluation board with ADuC845 chip was connected to PC via debug hook from Accutron. This hook provides enhanced debugging and emulation used for microprocessor system development.

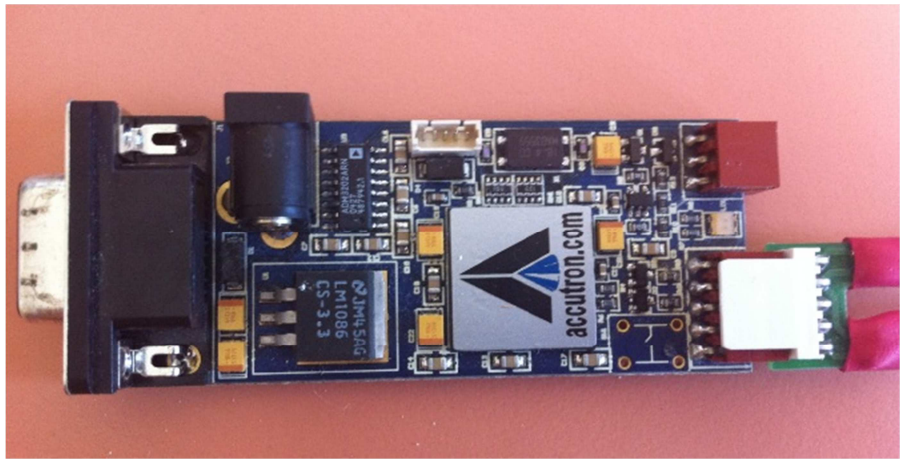

Fig. 5.37. Debug hook for microprocessor systems

5.7 Acquiring experimental data

This chapter presents measurement of thermopile noise with DataLab unit and comparative measurement with accurate nanovolt meter Agilent 34420. Second part of acquiring data deals with FOV measurement.

5.7.1 Thermopile noise measurement

Measurement of thermopile output (voltage) in during unchanging conditions. The measurement of very low voltage signal from thermopile is performed with accurate nanovolt meter Agilent 34420A.

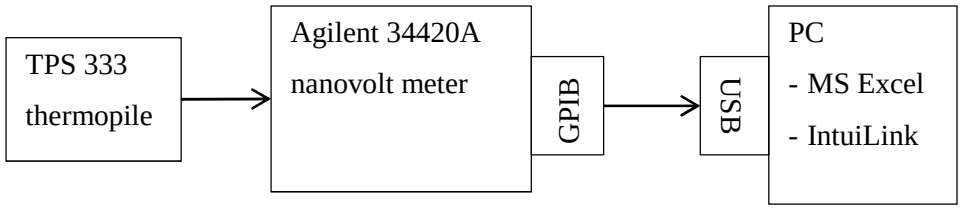

Fig. 5.38. Measurement chain I

In first measurement we use measurement chain displayed on Fig. 5.38. It consists of thermopile sensor TPS 333 exposed to stable environmental conditions (sensor is placed in testing chamber to not be influenced by unstable thermal sources such as sun radiation or operator). Thermopile is connected to a nanovolt meter Agilent 34420A by cable conductor. Measured data is sent to a PC via GPIB/USB (General Purpose Interface Bus to Universal Serial Bus) interface and stored in MS Excel with the help of IntuiLink Connectivity software from Agilent. Agilent 34420A is configured for highest accuracy measuremens (according to Agilent 34420A User's Guide) to work with 7½ digit resolution, channel 1 input, and digital filter on. There were taken 100 values during measurement and stored in MS Excel. The graph of measured data is shown on Fig. 5.39. and sample data of measurement is presented in APPENDIX F and the statistics are presented in Table 5.5.

Table 5.5. Statistics of thermopile noise measurement with Agilent 34420A

Min [µV]	Max [µV]	Average [µV]	Standard deviation [µV]	Relative error [%]
-50.6	-56.7	-53.7	1.5	2.9

After this analysis and according to accuracy specifications of Agilent 34420A (Agilent Technologies, 2003) we can claim, that nanovolt meter uncertainities can be neglected. Agilent 34420 has an error of ±0.0050 % of reading and ±0.0020 % of range gives at 1 mV range an error of 0.005 % x 1.2 mV + 0.002 % x 1 mV = ±80 nV.

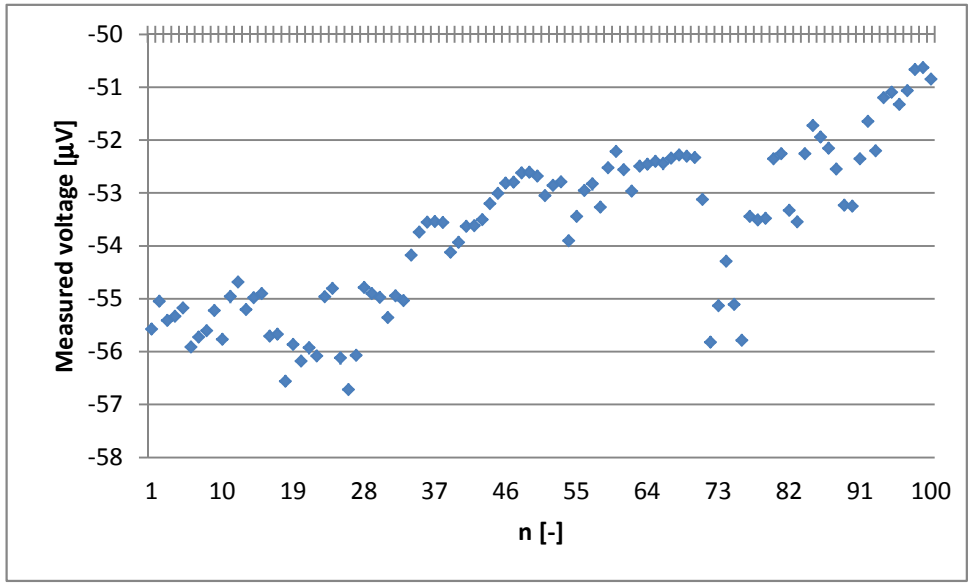

Fig. 5.39. Thermopile noise measurement with Agilent 34420A

Second measurement is focused on thermopile noise measurement with DataLab IO[1]. The assumption is that DataLab unit is able to measure thermopile low level signals but accuracy specification in DataLab documentation is weak and only temperature drift is mentioned. This measurement will show the uncertainities arisen from measurement with DataLab IO[1] in comparison to professional nanovolt meter Agilent 34420A. The measurement chain with DataLab unit is shown on Fig. 5.40.

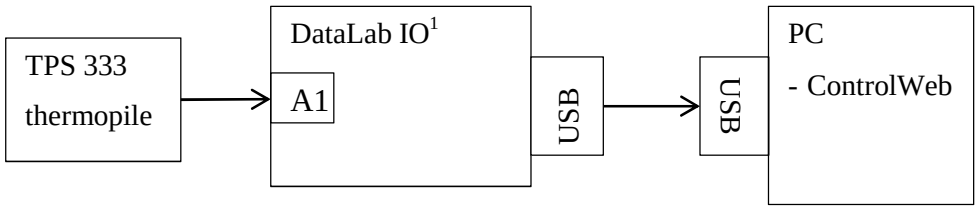

Fig. 5.40. Measurement chain II

Thermopile is exposed to the same environmental conditions as it was at measurement with Agilent 34420A and is connected to DataLab IO[1] on A1 input. DataLab unit is configured - analog inputs are set to voltage mode and bipolar 100 mV voltage range and application in ControlWeb saves values into the MS Excel file. The results are shown on Fig. 5.41. and statistics are presented in Table 5.6.

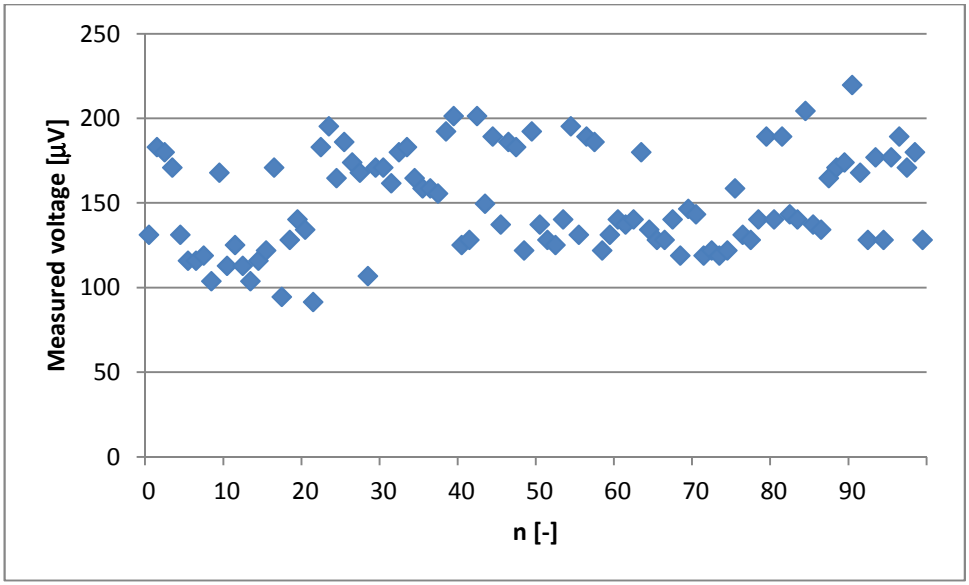

Fig. 5.41. Thermopile noise measurement with DataLab IO[1]

Table 5.6. Statistics of thermopile noise measurement with DataLab IO[1]

Min [μV]	Max [μV]	Average [μV]	Standard deviation [μV]	Relative error [%]
91.6	219.7	150.8	29.2	19.3

Statistics show that DataLab unit can measure the thermopile output with 29.2 μV standard deviation, it means about 0.27 °C temperature deviation (or 1.74 Wm^2 radiant heat flux)

5.7.2 Datalab Offset measurement

The measurement with DataLab has shown very different statistical average in comparison with Agilent 344420A measurement. DataLab unit does not provide automatic input offset voltage cancelling (even the analog to digital converter ADS1216 used in DataLab unit provides an offset correction according to technical documentation (Texas Instruments ADS1216, 2006)), therefore it is needed to compensate it by ourself. We can use one unconnected differential input on DataLab AI3 and short-circuit it to ground. With this design, we can read offset value of analog to digital converter (the offset is identical for all inputs because multiplexing of input signals is used). Read offset is in digital form and we can simply numerically substract the offset from digital values on all measured channels.

5.7.3 Field of View (FOV) measurement

The Chapter 5.4 has dealt with field of view (FOV) of thermopile sensor and taken the FOV characteristics from datasheet. This subchapter describes field of view measurement of real thermopile TPS 333 sensor. The measurement is done in accordance with GE Thermometrics Technologies Application Note. The block diagram on Fig. 5.42. describes the principle of measurement. Data acquisition system measures thermopile output depending on angle of incidence φ. The angle of incidence changes with moving IR point source (representing heat source). The dependency is measured with step of 10 degrees of arc from 0° to 90° and graphical interpretation of normalized thermopile output on angle of incidence is shown on Fig. 5.43. Figure shows the measured FOV (blue stars) and for comparison, the origin FOV taken from TPS 333 datasheet (red squares) is also added.

Sample data of measurement is presented in APPENDIX G.

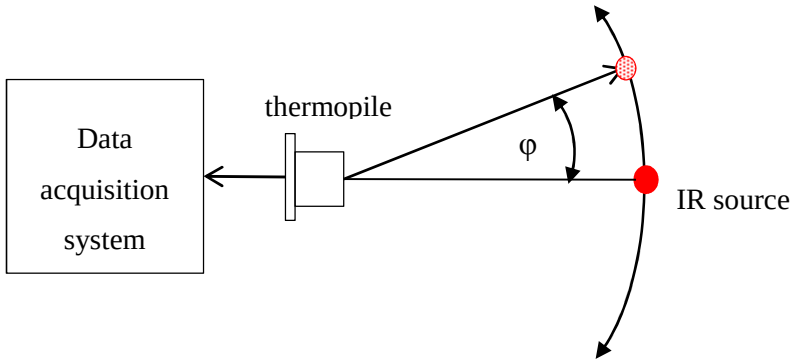

Fig. 5.42. Block diagram of FOV measurement

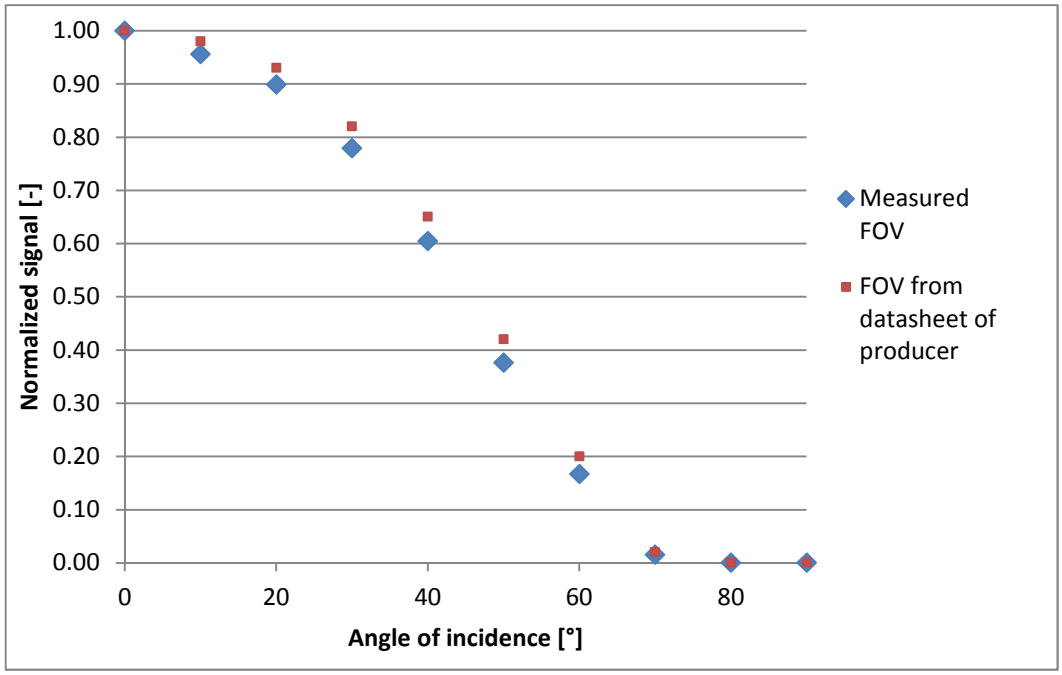

Fig. 5.43. Results of FOV measurement

6 DISCUSSION OF THE RESULTS

The main subject of this thesis deals with evaluation of thermal comfort of a man. In past hundred years people developed many thermal models based on different principles, some of them are standardized, however their practical application is still rare. This work is focused on elimination of limitations and problems in thermal comfort determination. Theoretical part solved some of shortcomings with modification of most widely used PMV-PPD model, which then enables its convenient utilization and more accurate results. The modification is based on computing PMV index from radiant heat flux instead of mean radiant temperature, which is the most problematic determinable parameter.

The software tool computing thermal comfort indices according to PMV mathematical model in Matlab environment was prepared within the experimental part. This tool is then used in evaluation of thermal comfort in “PMV-PPD calculator”. The “PMV-PPD calculator” is the Matlab application created within the experimental part and it represents simplified real room with definable dimensions, position of occupant in room, his/her position and properties influencing thermal comfort. Furthermore, it is possible to place heating panels on the walls in order to adjust the mean radiant temperature and thus modifiy the thermal comfort of the occupant. The fisrts function of “PMV-PPD calculator” is the determination of thermal indices. The second function is the optimization of costs for heating while maintaining thermal comfort. This is optimized with self-organizing migrating algorithm (SOMA).

The important part of this work is intended to determination of mean radiant temperature - the input parameter, which is the most difficult to determinable of all input parameters of PMV model. In this thesis, the specific solution using several thermopile sensors was developed. The overlapping of scanned areas problem was solved with numerical solution and also the visualization of total signal measured on thermopile sensors is done. The determination and visualization of mean radiant temperature helps to quaintitatively and qualitatively describe how precisely the whole space is detected.

Based on this research, the improvements in mean radiant temperature measurement are performed (with changing number of sensors and modification of thermopile FOV). This improvement is based on minimization of standard deviation and is done with SOMA. The results of optimization are statistically evaluated and graphically presented at each method. Furthermore, the proposed solution with thermopiles enables to evaluate mean radiant temperature asymmetry, which is impossible to measure with the standard globe thermometer recommended by ISO 7730.

In conclusion of this work, the thermal comfort evaluation systems were designed and created. There were prepared two versions: laboratory and embedded. The former uses DataLab unit from Moravian Instruments providing high flexibility, easy configuration and programming. The latter solution is based on ADuC845 converter from Analog Devices incorporating high resolution analog to digital converter, programmable gain amplifier, microprocessor and memory. Necessary subprograms (modules) ensuring A/D conversion, conversion of measured signals into physical quantities, thermal comfort indices calculation, display support and D/A conversion were programmed. The source code of created software is presented in appendices B, C, D and E.

Various measurements were taken during this work, but only some of them are presented in appendices. Moreover, the sets of values were trimmed to 20 values in order to keep the volume of this book in reasonable size.

Suggestions for further research in this field:

- to utilize an IR thermometer that consists both the thermopile detector and the signal conditioning chip in the same package and with the communication via SMBus. This device provides higher accuracy up to 0.1 °C in the range from 20 °C to 30 °C, and example of this is Melexis MLX90615
- to finalize the prototype on evaluation board and design and create own printed circuit board

- to use developed sensor’s sphere capable of directional radiant heat flux measurement for thermal comfort control in specific places such as trains or cars. In this area the smart windows (switchable windows) with electrically controlled transmissivity glass would be efficient.

7 OUTPUTS FOR MANUFACTURING PRACTICE

One of the most important results was the proposed solution that uses thermopile sensors as a basis in mean radiant temperature (MRT) determination, which solves the limits given by standard globe thermometer and enables evaluation of mean radiant temperature.

Second practical usage can be seen in predicted mean vote modification which deals with evaluation of PMV index independently on MRT calculation which is very problematic. Instead of MRT, the radiant heat flux measured by thermopile sensors is used in PMV-PPD determination.

Last, but not least significant output was the design and creation of measurement systems. Created digital laboratory solution is modular, versatile, easy to operate and able to evaluate thermal comfort of a man according to PMV mathematical model. Designed digital embedded solution was programmed on ADuC845 microconverter with modular programming principles. This embedded solution is prepared on evaluation board.

REFERENCES

Dexter Research Center. Package Hole Size and Aperture Options. *Dexter Research.* [Online] [Cited: 20 4 2009.] www.dexterresearch.com.

ADuC845. 2005. *ADuC845 Data Sheet.* s.l. : Analog Devices, 2005.

Agilent Technologies. 2003. Agilent 34420A User's Guide. *Agilent 34420A User's Guide.* s.l. : Agilent Technologies, 2003.

Alfano, Francesca Romana d'Ambrosio. 2011. The role of measurement accuracy on the thermal environment assessment by means of PMV index. *Building and Environment.* 2011, Vol. 7, 46.

ASHRAE 55, Standard. 2004. ANSI/ASHRAE Standard 55-2004. 2004. ISSN 1041-2336.

Augusta, Ivo. 1991. *Stavební tepelná technika pro každého.* 1991. ISBN 80-85380-01-3.

Auliciems, Andris and Szokolay, Steven V. 2007. *Thermal Comfort.* 2007. ISBN 0 86776 729 4.

Awbi. 1991. *Ventilation of Buildings.* New York : Spon Press, 1991. 9780419156901.

Centnerová, Lada. 2001. *Tradiční a adaptivní model tepelné pohody. Disertační práce.* Praha : České vysoké učení technické v Praze. Fakulta stavební, 2001.

ČSN 73 0542. 1995. *Method of estimation of energy balance of glazed area in external building structures.* 1995.

DataLab IO Manual. 2007. *DataLab IO Manual.* s.l. : Moravian Instruments, 2007.

Dereniak, E.L. 1984. *Optical Radiation Detectors.* s.l. : John Willey and Sons, 1984.

Epstein, Yoram and Moran, Daniel S. 2006. Thermal Comfort and the Heat Stress Indices. *Industrial Health.* 44, 2006.

Fanger, P. O. 1967. Calculation of thermal comfort: Introduction of a basis comfort equation. s.l. : ASHRAE Transactions, 1967. Vol. III, 73.

Fanger, P. O. 1970. Thermal Comfort. Copenhagen : Danish Technical Press, 1970.

Fukátko, Tomáš. 2007. *Detekce a měření různých druhů záření.* Praha : Nakladatelství BEN - technická literatura, 2007. ISBN 978-80-7300-193-3.

Gagge, A. P., Fobelets, A. P. and Berglund, L. 1986. A standard predictive index of human response to the thermal environment. *ASHRAE Transactions.* 1986, Vol. 92, pp. 709-731.

Guggenheim, E. A. 1957. *Thermodynamics.* Amsterdam, North-Holland : s.n., 1957.

Hansman, John R. *Infrared Temperature Measurement, MIT Video Series.* s.l. : Massachusetts Instituce of Technology.

Health and Safety Executive. 2005. Thermal Comfort - Six basic factors. *http://www.hse.gov.uk.* [Online] 29 09 2005. [Cited: 1 2 2011.] http://www.hse.gov.uk/temperature/thermal/factors.htm.

Holman, J. P. 2009. *Heat Transfer.* 10th ed. New York : McGraw-Hill, 2009. Vol. II.

Hruška, František. 2003. *Měření střední radiační teploty pro stanovení indexů tepelné pohody:habilitation thesis.* Zlín : Tomas Bata University in Zlín, 2003. p. 87.

ISO 7243. 1989. *Hot environments - Estimation of the heat stress on working man, based on the WBGT-index (wet bulb globe temperature).* 1989.

ISO 7726. 1998. *Ergonomics of the thermal environment - Instruments for measuring physical quantities.* 1998.

ISO 7730. 2005. *Ergonomics of the thermal environment.* 2005.

ISO 7933. 2004. *Ergonomics of the thermal environment - Analytical determination and interpretation of heat stress using calculation of the predicted heat strain.* 2004.

Jaumont, F. E. 1960. Direct conversion of heat to Electricity: Review of thermoelectric effects. 1960. Vol. Chapter 4.

Keithley Instruments, Inc. 2004. *Low Level Measurements Handbook.* s.l. : Keithley Instruments, Inc., 2004.

Korn, G. A. and Korn, T. M. 1968. *Mathematical Handbook for Scientists and Engineers.* New York : McGraw-Hill, 1968.

Kreidl, Marcel. 2005. *Měření teploty.* Praha : Nakladatelství BEN - technická literatura, 2005. ISBN 80-7300-145-4.

Lysenko, Vladimír. 2005. *Detektory pro bezdotykové měření teplot.* Praha : Nakladatelství BEN - technická literatura, 2005. ISBN 80-7300-180-2.

Magison, E. C. 1990. Temperature measurement in industry. s.l. : Instrument Society of

America, 1990.

McAdams, W. H. 1954. *Heat Transmission.* 3rd ed. New York : McGraw-Hill, 1954.

McNall, P. E. Jr., et al. 1967. *Thermal comfort (and thermally neutral) conditions for three levels of activity.* s.l. : ASHRAE Transaction, 1967. 73.

Moravian Instruments. 2009. DataLab IO — modular system of industrial I/O devices. *Moravian Instruments.* [Online] 1 6 2009. [Cited: 1 5 2010.] http://www.mii.cz/art?id=134&cat=77&lang=409.

Nevins, R.G., Springer, F.H. and Feyerherm, A.M. 1966. *A temperature-humidity chart for thermal comfort of seated persons.* s.l. : ASHRAE Transactions, 1966. Vol. 72.

Non-contact two-dimensional area temperature measurement. **Pálka, Jiří. 2009.** Vienna : The 20th International DAAAM symposium, 2009. pp. 1567-1568. ISBN 978-3-901509-70-4.

Norkus, V., Hofman, G. and Schiewe, Ch. 1966. *Uncooled Multispectral Detectors and their Applications.* 1966.

Omega. 2008. Transactions in Measurement and Control. *www.omega.com.* [Online] 2008. [Cited: 1 1 2010.] www.omega.com/literature/transactions/Transactions_Vol_I.pdf.

P P L Regtien. 2004. *Measurement Science for Engineers.* London : P P L Regtien, 2004. ISBN 1 9039 9658 9.

Pálka, Jiří. 2004. *Noncontact temperature measuring with thermopile sensor.* s.l. : Fine Mechanics and Optics. Scientific-Technical Journal, 2004.

PCF2116. 1997. *PCF2116 family LCD controller/drivers.* s.l. : Philips Semiconductor, 1997.

PerkinElmer. 2003. A2TPMI Datasheet. *Thermopile with integrated signal processing circuit.* . s.l. : PerkinElmer, 2003.

PerkinElmer . 2003. TPS 333 Thermopile Detector. *www.perkinelmer.com.* [Online] 2003. [Cited: 01 06 2007.] www.perkinelmer.com/optoelectronics.

Petela, Richard. 2010. *Engineering Thermodynamics of Thermal Radiation: for Solar Power Utilization.* s.l. : McGraw-Hill Professional Publishing, 2010. ISBN-13: 9780071639620.

—. 1983. *Heat Transfer.* Warsawa : PWN, 1983.

Pollock, D.D. 1971. *The Theory and Properties of Thermocouple Elements.* s.l. : American Society for Testing and Materials, 1971.

Progress on the Development of Multi-wavelength Imaging Pyrometer. **Kaplinsky, M. B., Li, J.. and McCaffrey, N.J. 1996.** 1996. SPIE Proceedings.

Schmidt, E. 1963. *Einführung in die technische Thermodynamik.* Berlin : Springer-Verlag, 1963.

Skocik, Petr. 2004. *Spatial measurement of mean radiant temperature. Master's thesis.* Zlin : Tomas Bata University in Zlin, 2004.

Texas Instruments ADS1216. 2006. ADS1216 documentation. *Texas Instruments WWW.* [Online] 2006. [Cited: 1 11 2010.] http://www.ti.com/product/ads1216.

Tinsley, Bear F. G. and Adams, Bruce. 1991. Evolution in the Application of Optical Fiber Thermometry. s.l. : Proceedings of the International Conference and Exhibitions, Instrument Society of America, 1991.

Weckmann, Stephanie. 1997. *Dynamic Electrothermal Model of a Sputtered Thermopile Thermal Radiation Detector for Earth Radiation Budget Applications. Master's Thesis.* s.l. : faculty of the Virginia Polytechnic Institute and State University, 1997.

www.horiba.com. 2003. I-square two-dimensional infrared thermometer ii-1064 isquare. *www.horiba.com.* [Online] 2003. [Cited: 7 3 2009.] www.horiba.com.

www.melexis.com. 2007. MEMs-Based IR Thermopile Resolves to 0.01°C - EDN Magazine. *http://melexis-hall-effect.com.* [Online] Melexis, 30 10 2007. [Cited: 15 04 2008.] http://melexis-hall-effect.com/News/MEMs-Based-IR-Thermopile-Resolves-to-001%C2%B0C---EDN-Magazine-217.aspx.

Zaplatílek, Karel and Doňar, Bohuslav. 2004. *Matlab tvorba uživatelskýcj aplikací.* Praha : Nakladatelství BEN - technická literatura, 2004. ISBN 80-7300-133-0.

Zelinka, Ivan. 2002. *Umělá inteligence v problémech globální optimalizace.* Praha : Nakladatelství BEN - technická literatura, 2002. 80-7300-069-5.

Zelinka, Ivan. SOMA Homepage. *SOMA Homepage.* [Online] [Cited: 1 11 2010.] http://www.fai.utb.cz/people/zelinka/soma/.

PUBLICATIONS

Conference papers

1. Pálka, J., Hruška, F.: Spotřeba tepla pro vytápění a aspekty tepelné pohody. 7. Mezinárodní conference CP&HS 2006
2. PÁLKA, J. – HRUŠKA, F.: Ambient temperature compensation in thermopile signal conditioning. Proceedings of the 15th International DAAAM Symposium, pp. 327-328. ISBN 3-901509-42-9. Vienna, Austria, 3-6.11.2004
3. PÁLKA, J. – HRUŠKA, F.: Embedded systém pro vyhodnocování tepelné pohody. SEKEL – Mezinárodní odborný seminář, ISBN 80-7318-346-3, Rusava, ČR, 17-16.9.2005
4. PÁLKA, J – HRUŠKA, F.: Embedded system for evaluation of thermal comfort of a man. Efektywność wdrażania technologii informatycznych, VII Ogólnopolska Konferencja Naukowo-Techniczna Komputer w Ochronie Środowiska – KOŚ, Polska, Poznań-Gniezno 14-16.9. 2005, str. 183-190, ISBN 83-60055-07-6, ISBN 83-89696-75-4
5. PÁLKA, J – HRUŠKA, F.: Non-contact two-dimensional area temperature
6. ICCC 2006, 7th International Carpathian Control Conference, Rožnov pod Radhoštěm, ČR, 29-31.5.2006, str. 405-408, ISBN 80-248-1066-2
7. PÁLKA, J – HRUŠKA, F.: Tepelná pohoda člověka řešená pomocí mikrokontroleru ADuC845. ŘÍP 06, 7. vědecko-technická konference, Kouty nad Desnou, ČR 13-16.6.2006, str. 228, ISBN 80-7194-860-8
8. PÁLKA, J. – HRUŠKA, F.: Visualization of overlapping of scanned areas in mean radiant temperature measurement. Proceedings of the 22th International DAAAM Symposium, ISBN 978-3-901509-93-4. Vienna, Austria, 2011-11-23/26 (approved)

Contributions to the technical journals

1. PÁLKA, J.: Bezdotykové měření teploty pomocí termočlánkové baterie. Jemná mechanika a optika, pp. 81-82. ISSN 0447-6441 Index 46 723. 3/2004
2. PÁLKA, J. – HRUŠKA, F.: Technické prostředky pro měření a řízení parametrů tepelné pohody. In: Jemná mechanika a optika, 3/2006, str. 67-70, ISSN 0447-

CURRICULUM VITAE

Osobní údaje:

Jméno:	Jiří Pálka
Datum narození:	15. květen, 1980
Adresa:	Kúty 1941, Zlín 760 01, Česká republika
Telefonní číslo:	+420 777 798 509
E-mail:	jiri.palka@gmail.com
Stav:	ženatý

Ukončené vzdělání:

2003 - dosud	Doktorské studium na Univerzitě Tomáše Bati ve Zlíně
1998-2003	Univerzita Tomáše Bati ve Zlíně Fakulta technologická
1994-1998	Gymnázium Zlín Lesní Čtvrť

Studijní pobyty:

4/2005-7/2005	Ruhr-Universität Bochum

Praxe:

2006 – dosud	Odborný asistent. Ústav elektroniky a měření. Fakulta aplikované informatiky, Univerzita Tomáše Bati ve Zlíně
2003 – 2006	Výuka předmětů Základy výpočetní techniky, Technické prostředky automatizace II, III a IV na Univerzitě Tomáše Bati ve Zlíně v rámci doktorského studia
6/2002-9/2002	USA – South Carolina – práce v hotelu, práce v restauraci

Zájmy:

programování, fitness, fotbal, cyklistika, šachy

Znalosti:

řidičský průkaz sk. A, B

jazyky: angličtina - pokročilý, němčina – mírně pokročilý

programovací jazyky: MS SQL, C#

software: MS Office, MS Windows, AutoCAD

APPENDIX A

Table of proposed systems for rating heat stress and strain (heat stress indices) (Epstein, et al., 2006)

Year	Index	Authors
1905	Wet-bulb temperature (T_w)	Haldane
1916	Katathermometer	Hill et al.
1923	Effective temperature (ET)	Houghton & Yaglou
1929	Equivalent temperature (T_{eq})	Dufton
1932	Corrected effective temperature (CET)	Vernon & Warner
1937	Operative temperature (OpT)	*Winslow et al.*
1945	Thermal acceptance ratio (TAR)	Ionides et al.
1945	Index of physiological effect (E_p)	*Robinson et al.*
1946	Corrected effective temperature (CET)	Bedford
1947	Predicted 4-h sweat rate (P4SR)	*McArdel et al.*
1948	Resultant temperature (RT)	*Missenard et al.*
1950	Craig index (I)	Craig
1955	Heat stress index (HIS)	Belding & Hatch
1957	Wet-bulb globe temperature (WBGT)	Yaglou & Minard
1957	Oxford index (WD)	Lind & Hellon
1957	Discomfort index (DI)	Thom
1958	Thermal strain index (TSI)	Lee & Henschel
1959	Discomfort index (DI)	Tennenbaum et al.
1960	Cumulative discomfort index (CumDI)	Tennenbaum et al.
1960	Index of physiological strain (I_s)	Hall & Polte
1962	Index of thermal stress (ITS)	Givoni
1966	Heat strain index (corrected) (HSI)	McKarns & Brief
1966	Prediction of heart rate (HR)	Fuller & Brouha
1967	Effective radiant field (ERF)	Gagge et al.
1970	Predicted mean vote (PMV)	Fanger

	Threshold limit value (TLV)	
1970	Prescriptive zone	Lind
1971	New effective temperature (ET^*)	Gagge et al.
1971	Wet globe temperature (WGT)	Botsford
1971	Humid operative temperature	Nishi & Gagge
1972	Predicted body care temperature	Givani & Goldman
1972	Skin wettedness	Kerslake
1973	Standard effective temperature (SET)	Gagge et al.
1973	Predicted heart rate	Givoni & Goldman
1978	Skin wettedness	Gonzales et al.
1979	Fighter index of thermal stress (FITS)	Nunneley & Stribley
1981	Effective heat strain index (EHSI)	Kamon & Ryan
1982	Predicted sweat loss (m_{sw})	Shapiro et al.
1985	Required sweating (SW_{req})	ISO 7933
1986	Predicted mean vote (modified) (PMV*)	Gagge et al.
1996	Cumulative heat strain index (CHSI)	Frank et al.
1998	Physiological strain index (PSI)	Moran et al.
1999	Modified discomfort index (MDI)	Moran et al.
2001	Environmental stress index (ESI)	Moran et al.
2005	Wet-bulb dry temperature t WBDT)	Wallace et al.
2005	Relative humidity dry temperature (RHDT)	Wallace et al.

APPENDIX B

```
% Finds coefficients to best fit the nonlinear function myfun
% to input data saved in data.txt
%
% Myfun declaration is included in myfun.m file.
% function f = myfun(x,angle)
% a = x(1);
% b = x(2);
% c = x(3);

% f = 1./(1 + a*exp(-b*(angle+c)));

% load input data from data.txt file
[data] = load('data.txt','-ascii');
angle = data(:,1);
f = data(:,2);

% initial essessment
x0 = [4e-7, 0.1, -90];

% solve nonlinear curve-fitting
[x,resnorm] = lsqcurvefit(@myfun,x0,angle,f);

% found coefficients
a = x(1)
b = x(2)
c = x(3)

% print the result (source data and function)
plot(angle,f,'b.');
hold on;
angle = -90:0.1:0;
plot(angle,myfun(x,angle),'r');

angle = 0:0.1:90;
plot(angle,myfun(x,-angle),'r');

% describe axis
xlabel('Angle of incidence [°]');
ylabel('Normalized signal [-]');
```

APPENDIX C

```
% Function calculating Predicted Mean Vote (MPV) index and
% Predicted Percentage of Dissatisfied (PPD) index
% Author:   Jiri Palka
% Date:     7.8.2006

function [PMV,PPD,HL]=PMV(CLO, MET, WME, TA, TR, VEL, RH, PA)
% inputs:
% CLO(clothing),
% MET(energy expenditure of human body)
% WME(external work)
% TA(air temperature)
% TR(mean radiant temperature)
% VEL(relative air velocity)
% RH(relative humidity)
% PA(water vapour pressure)

HL = 0;
if nargin == 0
    %CLO - clothing. 1CLO= 0.155m^2.°C.W^-1 [clo]
    CLO = input('Input thermal resistance of clothes. 1CLO=
0.155m^2.°C.W^-1 [clo]>\n');
    if isempty(CLO)
        CLO=1.0;
    end

    %MET - metabolic rate. 1MET=58.2W.m^-2 [met]
    MET=1.2;
    %WME - external work. In most cases equal to 0. [met]
    WME=0;
    %TA - air temperature [°C]
    TA=19;
    %TR - mean radiant temperature [°C]
    TR=18;
    %VEL - relative air velocity [m.s^-1]
    VEL=0.1;
    %RH - relative humidity [%]
    RH=40;
    %PA - water vapour presure [Pa]
    PA=0;
end

% water vapour pressure [Pa]
if PA==0
    PA=RH*10*exp(16.6536-4030.183/(TA+235));
end
```

```
% clothing [m^2K.W^-1]
ICL=0.155*CLO;
% MET - metabolic rate [W.m^-2]
M=MET*58.15;
% W - external work [W.m^-2]
W=WME*58.15;
% MW - internal heat production in the human body [W.m^-2]
MW=M-W;

% FCL - clothing area factor [-]
if (ICL<0.078)
    FCL=1.00+1.290*ICL;
else
    FCL=1.05+0.645*ICL;
end

% HCF - heat transfer coeff. by forced convection
HCF=12.1*sqrt(VEL);
% TAA - air temperature [K]
TAA=TA+273;
% TRA - mean radiant temperature [K]
TRA=TR+273;

% ITERATIVE CALCULATION OF surface temperature of clothing
TCLA=TAA+(35.5-TA)/(3.5*(6.45*ICL+0.1));
% first guess for surface temperature of clothing
P1=ICL*FCL;
P2=P1*3.96;
P3=P1*100;
P4=P1*TAA;
P5=308.7-0.028*MW+P2*(TRA/100)^4;
XN=TCLA/100;
XF=XN;
N=0;
EPS=0.00015;

% HCN - heat transfer coefficient by natural convection
HC=0;
for N=0:150,
    XF=(XF+XN)/2;
    HCN=2.38*abs(100*XF-TAA)^0.25;
    if HCF>HCN
        HC=HCF;
    else
        HC=HCN;
    end
    XN=(P5+P4*HC-P2*XF^4)/(100+P3*HC);
    if abs(XN-XF)<EPS
        break;
    end
```

```
end

% surface temperature of clothing
TCL=100*XN-273;

% HL1 - heat loss diff through skin
HL1=3.05*0.001*(5733-6.99*MW-PA);
% HL2 - heat loss  by sweating(comfort)
if MW>58.15
    HL2=0.42*(MW-58.15);
else
    HL2=0;
end

% HL3 - latent respiration heat loss
HL3=1.7*0.00001*M*(5867-PA);
% HL4 - dry respiration heat loss
HL4=0.0014*M*(34-TA);
% HL5 - heat loss by radiation
HL5=3.96*FCL*(XN^4-(TRA/100)^4);
% HL6 - heat loss by convection
HL6=FCL*HC*(TCL-TA);
% TS - thermal sensation tran coeff.
TS=0.303*exp(-0.036*M)+0.028;
% PMV - predicted mean vote
PMV=TS*(MW-HL1-HL2-HL3-HL4-HL5-HL6);
% PPD - predicted percentage of dissatisfied
PPD=100-95*exp(-0.03353*PMV^4-0.2179*PMV^2);
```

APPENDIX D

```
//zapise byte pres I2C

void SENDBYTE(unsigned char OUTPUT)
{
    // nastav SDATA pin jako vystup
    MDE = 0x01;
        LEDBLINK();

    for (i=0; i < 8; i++)
    {
        // nastav hodiny na low
        MCO = 0x00;

        // nastav pozadovany bit
        if ((OUTPUT & 0x80) == 0x80)
            MDO = 1;
        else
            MDO = 0;
        LEDBLINK();

        // nastav hodiny k poslani bitu
        MCO = 0x01;
                LEDBLINK();

        // vynuluj hodiny
        MCO = 0x00;
        LEDBLINK();

        // prejdi na dalsi bit
        OUTPUT = OUTPUT << 1;
    }
    // uvolni datovou sbernici pro acknowledge  (pro vstup)
    MDE = 0x00;
        LEDBLINK();

    // nastavi SCLOCK pro acknowledge
    MCO = 0x01;
        LEDBLINK();
```

APPENDIX E

```
    TCL=100*XN-273;

    HL1=3.05*0.001*(5733-6.99*MW-nPA);

    if (MW > 58.15) then
        HL2=0.42*(MW-58.15);
    else
        HL2=0;
    end;

    HL3=1.7*0.00001*M*(5867-nPA);

    HL4=0.0014*M*(34-TA);

    HL5=3.96*FCL*(pow(XN,4)-(pow((TRA/100),4)));

    HL6=FCL*HC*(TCL-TA);

    TS=0.303*exp(-0.036*M)+0.028;

    PMV=TS*(MW-HL1-HL2-HL3-HL4-HL5-HL6);

    PPD=100-95*exp(-0.03353*pow(PMV,4)-0.2179*pow(PMV,2));
    end_procedure;

  end_sequencer;

end_timer;

instrument

  panel backpane;
    rem = 'hlavní panel aplikace';
    owner = background;
    position = 27, 48, 623, 480;
    window = normal;
    win_title = 'PMV_evaluation';
    win_disable = zoom;

    procedure OnStartup();
    begin
      MoveTo( WorkX + WorkW / 2 - ( 640 + NoZoomWinReduceW ) / 2,
              WorkY + WorkD / 2 - ( 480 + NoZoomWinReduceD ) / 2 );
      Select();
    end_procedure;

  end_panel;

  label label_3;
    owner = backpane;
    position = 153, 292;
    win_disable = zoom, maximize;
    text_list
      text = 't6 [°C]';
    end_text_list;
  end_label;

  label label_3;
    owner = backpane;
    position = 153, 267;
    win_disable = zoom, maximize;
```

APPENDIX F

Table: Thermopile noise measurement

Measurement with Agilent 34420A			Measurement with DataLab AI3	
n [-]	**Measured voltage [µV]**		**n [-]**	**Measured voltage [µV]**
1	-55.57471		1	131.23
2	-55.04785		2	183.11
3	-55.40914		3	180.05
4	-55.33314		4	170.90
5	-55.17119		5	131.23
6	-55.90958		6	115.97
7	-55.72467		7	115.97
8	-55.60298		8	119.02
9	-55.21973		9	103.76
10	-55.76477		10	167.85
11	-54.95822		11	112.92
12	-54.68301		12	125.12
13	-55.20395		13	112.92
14	-54.98161		14	103.76
15	-54.90206		15	115.97
16	-55.70549		16	122.07
17	-55.67108		17	170.90
18	-56.56042		18	94.60
19	-55.86394		19	128.17
20	-56.17575		20	140.38

Appendix shows sample data only. All data is save in electronic form and is available on my computer.

APPENDIX G

Table: Thermopile FOV measurement

	Angle of incidence [°]									
	0	10	20	30	40	50	60	70	80	90
	Normalized thermopile output [µV]									
1	1146.6	1084.9	1008.7	884.8	681.5	415.1	190.8	10.3	2.1	0.7
2	1144.3	1087.2	1009.9	883.7	680.4	415.1	189.7	11.4	2.1	4.3
3	1142.0	1086.0	1007.6	884.8	680.4	414.0	188.7	11.4	2.1	4.5
4	1139.7	1086.0	1006.5	883.7	679.3	414.0	189.7	10.3	2.1	1.7
5	1138.6	1087.2	1007.6	882.5	680.4	415.1	190.8	12.4	0.0	-2.0
6	1138.6	1086.0	1008.7	883.7	679.3	416.2	189.7	13.4	0.0	2.2
7	1137.4	1086.0	1011.0	884.8	679.3	417.2	189.7	13.4	-2.1	-4.1
8	1136.3	1086.0	1011.0	883.7	678.2	416.2	188.7	14.5	-1.0	-0.5
9	1135.1	1087.2	1013.3	883.7	677.1	417.2	187.6	14.5	0.0	2.1
10	1132.9	1087.2	1015.5	883.7	676.0	417.2	187.6	15.5	-2.1	-0.2
11	1131.7	1088.3	1017.8	883.7	674.9	417.2	188.7	15.5	-2.1	-2.4
12	1131.7	1086.0	1017.8	884.8	673.8	417.2	188.7	17.6	-3.1	-0.3
13	1131.7	1086.0	1017.8	883.7	673.8	418.3	188.7	16.5	-3.1	-3.2
14	1131.7	1086.0	1018.9	883.7	674.9	417.2	187.6	16.5	-3.1	-1.0
15	1131.7	1084.9	1021.2	884.8	674.9	416.2	186.6	15.5	-2.1	0.0
16	1132.9	1086.0	1022.3	883.7	674.9	417.2	187.6	16.5	-3.1	-4.5
17	1132.9	1087.2	1021.2	882.5	676.0	417.2	188.7	17.6	-1.0	-2.5
18	1135.1	1087.2	1023.5	883.7	677.1	417.2	188.7	16.5	-1.0	0.3
19	1134.0	1086.0	1024.6	883.7	678.2	417.2	188.7	17.6	-2.1	-1.4
20	1135.1	1086.0	1024.6	883.7	679.3	418.3	187.6	17.6	-2.1	-0.2

Appendix shows sample data only. All data is save in electronic form and is available on my computer.

APPENDIX H

TPS 333 DATASHEET

TPS 333 - Thermopile Detector Miniature Sensor Housing

Figure 1. Package Drawing

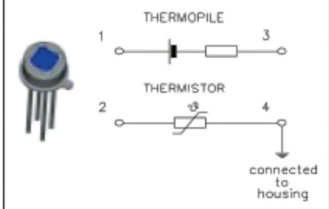

Figure 2.

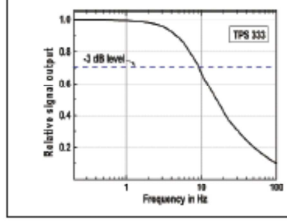

Figure 3.

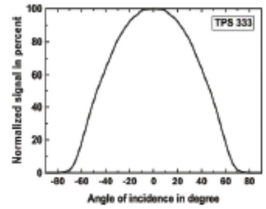

Figure 4. Top View Package Dimension

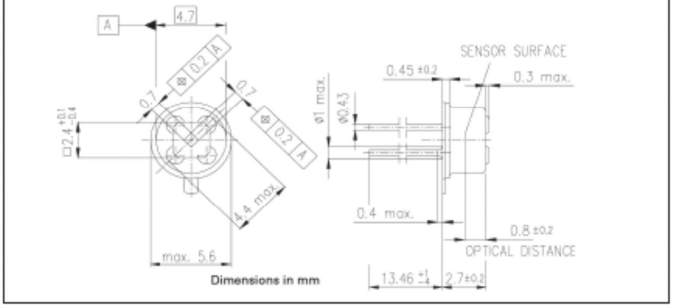

Figure 5. Bottom View

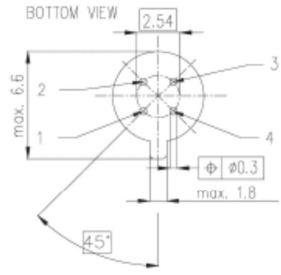

Table 1. TPS 333

Parameter		Typical	Units	Condition
Sensitive area		0.7 x 0.7	mm²	absorbing area
Window size		2.4 x 2.4	mm²	
DC sensitivity		35	V/W	500K BB 5 ... 14µm
Resistance		75	kΩ	
Noise		38	nV/√Hz	r.m.s. 300K
NEP		1.2	nW/√Hz	500K BB 5 ... 14µm
D*		0.6 x 10^8	cm√Hz/W	500K BB 5 ... 14µm
TC of sensitivity		0.02	%/K	
TC of resistance		0.02	%/K	
Time constant		25	ms	
Operating temperature		-40 to 100	°C	non permanent
Storage temperature		-40 to 100	°C	non permanent
Thermistor	resistance	100	kΩ	25°C
	beta	3964	K	25°C/100°C
Field of view		100	°	at 50% points

For more information e-mail us at opto@perkinelmer.com or visit our website at www.perkinelmer.com/optoelectronics
All values are nominal; specifications subject to change without notice.

North America:
PerkinElmer Optoelectronics
16800 Trans-Canada Highway
Kirkland, Quebec J7V 8P7 Canada
Toll Free: (877) 734-OPTO (6786)
Phone: +1-450-424-3300
Fax: +1-450-424-3411

Europe:
PerkinElmer Optoelectronics
Wenzel-Jaksch-Str. 31
D-65199 Wiesbaden, Germany
Phone: +49-611-492-430
Fax: +49-611-492-165

Asia:
PerkinElmer Optoelectronics
47 Ayer Rajah Crescent #06-12
Singapore 139947
Phone: +65-6770-4366
Fax: +65-6775-1008

PerkinElmer® precisely.

DS443-Rev A-0503